1153

TRANSPORTATION RESEARCH RECORD

Reinforced Layered Systems

TRANSPORTATION RESEARCH BOARD
NATIONAL RESEARCH COUNCIL
WASHINGTON, D.C. 1987

Transportation Research Record 1153
Price: $7.50
Typesetter: Marion L. Ross

modes
1 highway transportation
3 rail transportation
4 air transportation
5 other (bicycle, pipeline, pedestrian)

subject areas
21 facilities design
24 pavement design and performance
62 soil foundations
63 soil and rock mechanics

Transportation Research Board publications are available by ordering directly from TRB. They may also be obtained on a regular basis through organizational or individual affiliation with TRB; affiliates or library subscribers are eligible for substantial discounts. For further information, write to the Transportation Research Board, National Research Council, 2101 Constitution Avenue, N.W., Washington, D.C. 20418.

Printed in the United States of America

Library of Congress Cataloging-in-Publication Data
National Research Council. Transportation Research Board.

Reinforced layered systems.
p. cm.—(Transportation research record, ISSN 0361–1981 ; 1153)
ISBN 0-309-04660-2
1. Embankments—Design and construction. 2. Geotextiles. 3. Soil stabilization. I. National Research Council (U.S.). Transportation Research Board. II. Series.
TE7.H5 no. 1153
[TA760]
380.5 s—dc19
[624.1'62] 88-21112
CIP

Sponsorship of Transportation Research Record 1150

GROUP 2—DESIGN AND CONSTRUCTION OF TRANSPORTATION FACILITIES

Soil Mechanics Section
Raymond A. Forsyth, California Department of Transportation, chairman

Committee on Mechanics of Earth Masses and Layered Systems
Robert D. Stoll, Columbia University, chairman
S. S. Bandyopadhyay, Walter R. Barker, Richard D. Barksdale, Jerry C. Chang, J. M. Duncan, Kingsley Harrop-Williams, John S. Horvath, T. Kuppusamy, Zenon G. Kyfor, Michael S. Mamlouk, Gerald P. Raymond, Robert L. Schiffman, H. J. Siriwardane, Harry E. Stewart, Kenneth H. Stokoe II, Harvey E. Wahls, John L. Walkinshaw, T. H. Wu

Committee on Engineering Fabrics
Verne C. McGuffey, New York State Department of Transportation, chairman
Robert K. Barrett, Laurinda T. Bedingfield, Calvin G. Burgess, Robert G. Carroll, Jr., Steven M. Chrismer, Jerome A. Dimaggio, Graham Ruby Ford, S. S. Dave Guram, Curtis J. Hayes, Gary L. Hoffman, Robert D. Holtz, Thomas P. Hoover, Donald J. Janssen, James H. Keil, Thomas C. Kinney, Robert M. Koerner, Jim McKean, Gregory N. Richardson, Harry H. Ulery, Jr., Dennis B. Wedding, David C. Wyant

Neil F. Hawks, Transportation Research Board staff

Sponsorship is indicated by a footnote at the end of each paper. The organizational units, officers, and members are as of December 31, 1986.

Transportation Research Record 1153

The **Transportation Research Record** series consists of collections of papers on a given subject. Most of the papers in a Transportation Research Record were originally prepared for presentation at a TRB Annual Meeting. All papers (both Annual Meeting papers and those submitted solely for publication) have been reviewed and accepted for publication by TRB's peer review process according to procedures approved by a Report Review Committee consisting of members of the National Academy of Sciences, the National Academy of Engineering, and the Institute of Medicine.

The views expressed in these papers are those of the authors and do not necessarily reflect those of the sponsoring committee, the Transportation Research Board, the National Research Council, or the sponsors of TRB activities.

Transportation Research Records are issued irregularly; approximately 50 are released each year. Each is classified according to the modes and subject areas dealt with in the individual papers it contains. TRB publications are available on direct order from TRB, or they may be obtained on a regular basis through organizational or individual affiliation with TRB. Affiliates or library subscribers are eligible for substantial discounts. For further information, write to the Transportation Research Board, National Research Council, 2101 Constitution Avenue, N.W., Washington, D.C. 20418.

Contents

Foreword

This Record will be of interest to engineers involved in design and construction of reinforced layered systems. Laboratory and field investigations are described.

Vokas and Stoll use a continuum model to describe the response of a horizontally layered elastic system containing one or more reinforcing sheets located at any prescribed depth below the surface. The method of analysis and numerical results are presented.

Bathurst and Raymond tested large-scale models of a single tie/ballast system by repeating loading and compared the performance of geogrid-reinforced sections with that of an unreinforced section. The greatest influence on the performance of test sections was the compressibility of ballast support. The performance of reinforced model tests was related to cost-effectiveness of comparable configurations in track.

Duncan et al. report on the performance of a bank reinforced with a heavy steel mat, which was constructed to increase the height of a dike that failed during construction. Results of instrumentation monitoring showed acceptable performance of the embankment. Finite element and slope stability analyses were effective methods in determining the required reinforcements.

Bonaparte and Christopher review experience with design and construction of reinforced embankments over saturated clay foundations. The conditions under which the beneficial effects of reinforcement occur are described and design charts, figures, and construction aspects are presented.

Sakti and Das investigate the ultimate bearing capacity of a model strip foundation resting on a saturated soft clay internally reinforced with geotextile layers. They make recommendations on the depth of geotextile placement and ratio of the length of geotextile to the width of the foundation for maximum efficiency.

Reinforced Elastic Layered Systems

CONSTANTINE A. VOKAS AND ROBERT D. STOLL

A continuum model is used to describe the response of a horizontally layered elastic system containing one or more reinforcing sheets that may be located at any prescribed depth below the surface. The analysis is based on well-known equations for layered systems from the linear theory of elasticity. The effect of reinforcing is included by specifying the interlayer boundary conditions on the basis of an analysis that is similar to that used in the classical theory of thin plates. Numerical results are presented for the case of an axisymmetric load applied at the surface of a two-layered system with different combinations of elastic moduli and reinforcing stiffness. The results of these computations represent a limiting case that should be approached by more general models when nonlinear and inelastic effects are made small. Moreover, in many cases in which normal working loads are expected, the analysis will provide a good approximation for the trends that result from various changes in thickness and stiffness of the components.

For the last two decades the practice of reinforcing soil with tension-resistant materials has been widely implemented in geotechnical engineering. Even though examples of using reinforcing materials for strengthening soil foundations date back to the Roman Empire, it was not until Henri Vidal, a French architect and engineer, in the late 1950s, investigated the effects of reinforcement in soil with the aim of improving its mechanical properties that a new era in earth construction began. Reinforcement can take many forms, depending on the material used. Common forms are metallic sheets and meshes, bars, metallic or glass fiber strips, polymer grids, and high-modulus fabrics. The advent of new, stronger, and nondegradable synthetic textile materials and the development of modern synthetic polymer chemicals such as polyamides and polyesters, along with the ever-accelerating development of technical expertise, have led to new, more economical applications in civil engineering practice. Typical applications include construction of railroads, temporary and permanent roads, parking lots, storage-handling sites, and other facilities over poor subgrades; building of facilities of almost any nature over permafrost, muskeg, and other soils in cold weather regions; and construction of earth dams and embankments over compressible fine-grained or peat soils.

A considerable amount of research on reinforced soil systems has been undertaken by numerous universities and research establishments throughout the world over the last two decades, and there is an ever-increasing number of experimental investigations that have demonstrated the efficacy of tension-resistant inclusions in improving the response of reinforced soil systems. However, considering the widespread use of such systems, only a limited amount of theoretical work that describes the detailed mechanisms of the reinforced earth systems has been published. Moreover, many of these investigations are based on limit state theories or simple mechanical models that do not permit a complete description of the stress and displacement field of the system.

Three different approaches have been used to solve the problem of reinforced layered systems. The first is modeling of such systems by simple mechanical models. The distribution of stresses on top of the inclusion is computed by using either the Boussinesq solution for a semi-infinite halfspace *(1, 2)*, a probabilistic concept for the stress diffusion in particulate media *(3)*, or other approximate geometrical methods *(4–6)*. The inclusion is modeled as an elastic or viscoelastic material described mathematically either by a differential equation appropriate for a membrane or an equation derived from an assumed geometry of the deflected and stretched inclusion. The subgrade is represented either by a series of springs or by elastoplastic models, in which an elastic analysis based on a coefficient of subgrade reaction is coupled with a rigid-plastic analysis. Tensile stresses in the inclusion, vertical displacements on top of the subgrade, and other quantities are then computed by applying the equilibrium equations in the vertical and horizontal directions.

In a somewhat different approach, some authors have used continuum models to simulate the effects of horizontal reinforcement. Harrison and Gerrard *(7)* considered a series of equally spaced sheets occurring either in one, two, or three orthogonal sets and applied a theory defining an equivalent homogeneous material that can represent a sequence of alternating orthorhombic layers. Barvashov et al. *(8)* used an elastic solution for a layered system reinforced with a membrane but did not satisfy the equation of equilibrium for the inclusion in the vertical direction.

The third approach involves the use of the finite element method, employed with a varying degree of sophistication in modeling the soil layers and the inclusion at the interface. Examples of this approach include the work done by Barksdale et al. *(9)*, Al-Hussaini and Johnson *(10)*, Raad *(11)*, Andrawes et al. *(12)*, Chang and Forsyth *(13)*, Rowe *(14)*, and Salomone et al. *(15)*. Romstad et al. *(16)*, Shen et al. *(17)*, Herrmann and Al-Yassin *(18)*, and Naylor *(19)* combined the finite element method and the composite stress concept to model the properties of an orthorhombic material that is equivalent to a nonlinear soil reinforced by a set of thin strips.

The finite element approach is a powerful method and, depending on the degree of sophistication, is capable of describing almost any kind of reinforced layered system. Various kinds of inelastic behavior and nonlinearity can be incorporated into a finite element analysis, provided that a realistic set of constitutive equations can be defined for the soil and reinforc-

Department of Civil Engineering and Engineering Mechanics, Columbia University, New York, N.Y. 10027.

ing material. In addition, discontinuities in the displacement field (i.e., slip at the interfaces) and finite strains can also be accommodated. Nevertheless, certain problems require special care in the use of this powerful tool. The necessity of using a finite domain in the calculations and the heavy computational effort required can both lead to unrealistic results unless great care is exercised. Moreover, improperly posed constitutive equations can lead to instabilities, particularly when loading and unloading are not precisely defined. For these reasons it is always good practice to test a program for various limiting cases for which the analytical solution is known. Thus many solutions from the theory of elasticity have played an important role in the development and verification of different finite element codes in many areas of solid mechanics.

In this paper a continuum model that represents a horizontally layered system containing one or more reinforcing sheets located at any prescribed depths below the surface is described. The objective is to define a linear model that closely matches the geometry of real horizontally layered systems containing only a few discrete reinforcing sheets, as opposed to the many closely spaced sheets assumed in some prior investigations *(7)*. Moreover, discontinuities will be allowed both in the normal and tangential tractions across any of the discrete reinforcing sheets because this assumption is more realistic than the membrane analogy used in some previous work *(8)*. Both axisymmetric and plane strain loading on the surface of the layered system have been considered, and stresses and displacements have been calculated for a variety of different combinations of reinforcing stiffness, soil layer thickness, and relative rigidity of the soil layers. Because no interlayer slippage or nonlinearity of material properties is included, the solutions represent a limiting case that should be approached by more general models when the nonlinear and inelastic effects are made small. Furthermore, in cases for which stresses are the result of normal working loads so that inelastic effects are small, the results of the linear analysis should produce a good approximation to the trends that result from various changes in the thickness and stiffness of the different components.

THEORETICAL FORMULATION

Engineers have made extensive use of the theory of elasticity for the calculation of stresses and displacements in soil media. Among the most notable examples is Burmister's solution for layered systems *(20)*. His work has been used for many years as a basis for determining stresses and displacements in highway pavements. Although problems in the theory of elasticity are restricted to consideration of ideal materials and ideal boundary conditions, they have been found to be of practical use in studies of imperfectly elastic and somewhat nonhomogeneous materials, such as soils. The extent to which the computed results approximate the actual response of the system depends on how closely the conditions of the problem can be linearized in the analysis. The authors make no claim that such an approach is the best for estimating inclusion properties for final design, but they do believe that it is advantageous to have a theoretical yardstick to compare with other mathematical or empirical methods.

The system to be analyzed and the cylindrical coordinate system (r, θ, z) that is used are shown in Figures 1 and 2, respectively. The system may have an arbitrary number of horizontal layers, of which the lowermost one is considered to be of infinite extent in both the horizontal and vertical directions. The thickness of the individual layers and the physical properties of the material may vary from one layer to the next, but in any one layer the material is assumed to be homogeneous, isotropic, and linearly elastic. The modulus of elasticity and Poisson's ratio of the jth layer are E_j and ν_j, respectively. The depth to the jth interface is H_j. Any number of thin, linearly elastic, horizontal reinforcing inclusions may be introduced in the system, either at the interface of two adjacent layers or at any depth within a soil layer. The elastic constants of the inclusion are E_g and ν_g and its thickness is t_g. In the case in which an inclusion is introduced within a soil layer and not

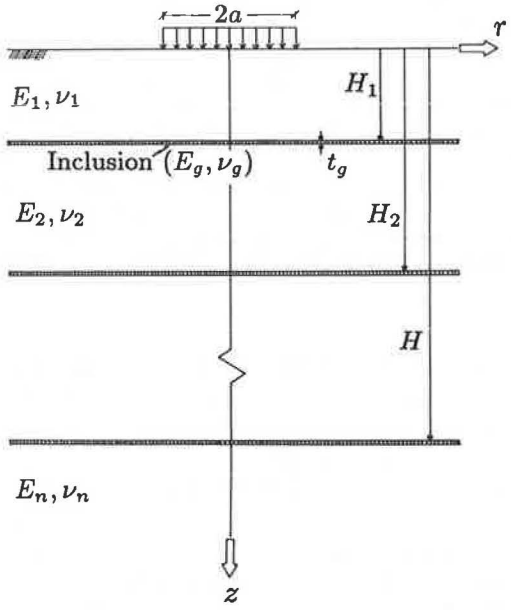

FIGURE 1 Reinforced layered elastic system.

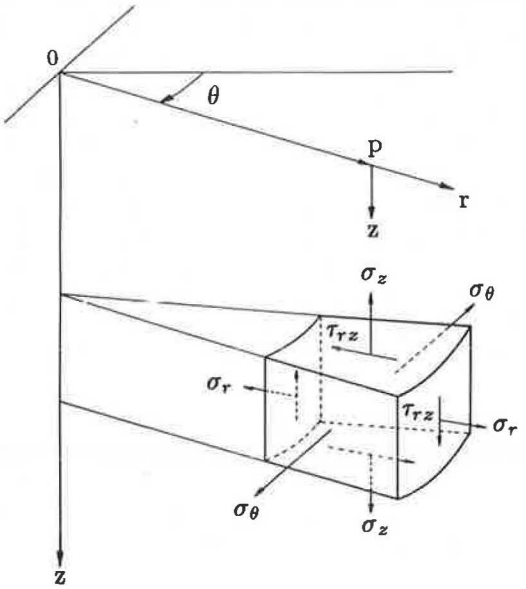

FIGURE 2 Axisymmetric coordinate system.

at an interface, the layer is subdivided into two distinct layers that have the same elastic constants, and the inclusion is introduced at their newly formed interface. It is assumed that there is no slippage between either surface of an inclusion and the adjacent soil strata. The method of analysis that is adopted is based on the classic solution of multilayer elastic systems *(20, 21)* but differs in the way the boundary conditions are handled to take into account the reinforcing action of the inclusions.

As in prior work on layered systems, a stress function ϕ_j that satisfies the governing differential equation

$$\nabla^4 \phi_j = 0 \tag{1}$$

is assumed for each of the layers. For systems with an axially symmetrical stress distribution

$$\nabla^4 = \left(\frac{\partial^2}{\partial r^2} + \frac{1}{r}\frac{\partial}{\partial r} + \frac{\partial^2}{\partial z^2} \right) \left(\frac{\partial^2}{\partial r^2} + \frac{1}{r}\frac{\partial}{\partial r} + \frac{\partial^2}{\partial z^2} \right) \tag{2}$$

in which r and z are the cylindrical coordinates in the radial and vertical directions, respectively. After the stress function is found, the stresses and displacements for each layer can be determined from the following equations:

$$(\sigma_r)_j = \frac{\partial}{\partial z}\left(\nu_j \nabla^2 \phi_j - \frac{\partial^2 \phi_j}{\partial r^2} \right) \tag{3a}$$

$$(\sigma_\theta)_j = \frac{\partial}{\partial z}\left(\nu_j \nabla^2 \phi_j - \frac{1}{r}\frac{\partial \phi_j}{\partial r} \right) \tag{3b}$$

$$(\sigma_z)_j = \frac{\partial}{\partial z}\left[(2 - \nu_j)\nabla^2 \phi_j - \frac{\partial^2 \phi_j}{\partial z^2} \right] \tag{3c}$$

$$(\tau_{rz})_j = \frac{\partial}{\partial r}\left[(1 - \nu_j)\nabla^2 \phi_j - \frac{\partial^2 \phi_j}{\partial z^2} \right] \tag{3d}$$

$$(u)_j = -\frac{1 + \nu_j}{E_j} \frac{\partial^2 \phi_j}{\partial r \partial z} \tag{3e}$$

$$(w)_j = \frac{1 + \nu_j}{E_j}\left[2(1 - \nu_j)\nabla^2 \phi_j - \frac{\partial^2 \phi_j}{\partial z^2} \right] \tag{3f}$$

where $(\sigma_z)_j$, $(\sigma_r)_j$, and $(\sigma_\theta)_j$ are the normal stresses, $(\tau_{rz})_j$ is the shear stress, and $(u)_j$ and $(w)_j$ are the displacements in the radial and vertical directions for the jth layer.

Because Equation 1 is a fourth-order differential equation, the determination of stresses and displacements requires four constants of integration that must be determined from the boundary and interface conditions. Let $\rho = r/H$ and $\zeta = z/H$ be the dimensionless cylindrical coordinates, in which H is the distance from the surface to the upper boundary of the lowest layer. Consider a layered system subjected to a normal pressure $p_m^*(\rho)$ and a horizontal shearing traction $\tau_m^*(\rho)$, to be referred to as basic loads, identified by asterisk superscripts and defined by the equations

$$p_m^*(\rho) = -p_m J_0(m\rho) \tag{4a}$$

and

$$\tau_m^*(\rho) = \tau_m J_1(m\rho) \tag{4b}$$

where p_m and τ_m are the maximum intensities of the applied load. J_0 is the Bessel function of the first kind of order zero and J_1 is the Bessel function of the first kind of order one; m is a continuous parameter that arises when a Hankel transform is used in the solution of Equation 1. The basis loads will be summed to approximate any prescribed distribution of axisymmetric surface tractions.

It can be easily verified by substitution that

$$\phi_j = \frac{H^3}{m^3 p_m}\left[A_{mj} e^{-m(\zeta_j - \zeta)} - B_{mj} e^{-m(\zeta - \zeta_{j-1})} + C_{mj}\, m\zeta e^{-m(\zeta_j - \zeta)} - D_{mj} m\zeta e^{-m(\zeta - \zeta_{j-1})} \right] J_0(m\rho) \tag{5}$$

is a stress function for the jth layer, which satisfies Equation 1; A_{mj}, B_{mj}, C_{mj}, and D_{mj} are the integration constants; and the subscript j refers to the quantities corresponding to the jth layer and varies from 1 to n. By substituting Equation 5 into Equations 3, expressions for the stress and displacement components for each layer can then be obtained.

As mentioned previously, four integration constants need to be evaluated for the determination of stresses and displacements for each layer. For a system composed of n layers, the $4n$ unknowns are obtained from the conditions at the boundaries and interfaces. They depend on the parameter m, the relative stiffnesses of both layers and inclusion, the Poisson's ratios of the materials involved, and the geometry of the system.

If the n-layer system bounded by the surface $\zeta = 0$ is loaded by a vertical stress p_m^* and a tangential traction τ_m^*, then the first two boundary conditions, which describe the surface loading, are

$$(\sigma_z^*)_1 = p_m^* \tag{6a}$$

and

$$(\tau_{rz}^*)_1 = \tau_m^* \tag{6b}$$

in which the asterisk indicates that these quantities correspond to the effect of the basic loads defined by Equations 4.

Two more boundary conditions result from the requirement that the displacements and stresses must vanish at infinite depth. It can be shown that the two integration constants for the lowermost layer ($j = n$) are

$$A_{mn} = C_{mn} = 0 \tag{7}$$

The situation at the $n - 1$ interfaces between the n layers gives rise to the remaining $4(n - 1)$ boundary conditions. It is assumed that there is continuous contact and no slip occurs between layers and inclusions. By denoting the radial and vertical displacements of the inclusion by $\hat{u}$ and $\hat{w}$, respectively, and neglecting all displacement gradients across the small thickness of the much stiffer inclusion, one obtains

$$(u^*)_j = (u^*)_{j+1} = \hat{u}^* \tag{8a}$$

and

$$(w^*)_j = (w^*)_{j+1} = \hat{w}^* \tag{8b}$$

at $\zeta = \zeta_j$, where ζ_j is the depth to the jth interface. This simplifying assumption greatly reduces the amount of computational effort required, while still allowing for different normal traction components on the top and bottom of the reinforcement.

The use of the equilibrium equations for the inclusion gives rise to the two last conditions. By applying the equilibrium equation in the radial direction and assuming plane stress conditions for the inclusion, the following expression is obtained:

$$\frac{d\hat{F}_r}{d\rho} + \frac{\hat{F}_r - \hat{F}_\theta}{\rho} = (\tau^*_{rz})_j - (\tau^*_{rz})_{j+1} \tag{9}$$

where $\hat{F}_r$ and $\hat{F}_\theta$ are the forces per unit length of section within the inclusion. When Hooke's law and the strain-displacement equations for the inclusion are used, expressions for the forces in the radial and tangential directions can be derived in terms of the vertical and radial displacements at the bottom of the upper layer ($\zeta = \zeta_j$). Equation 9 then becomes:

$$\frac{E_g \delta_g}{(1-\nu_g^2)} \left[\frac{d^2(u^*)_j}{d\rho^2} + \frac{d(u^*)_j}{\rho d\rho} - \frac{(u^*)_j}{\rho^2} \right] = (\tau^*_{rz})_j - (\tau^*_{rz})_{j+1} \tag{10}$$

in which the asterisk again identifies the effects due to the basic load; $\delta_g = t_g/H$ is the inclusion's dimensionless thickness. Similarly, by considering equilibrium in the vertical direction and assuming small displacements, one obtains the following equations:

$$\frac{d\hat{F}_{rz}}{d\rho} + \frac{\hat{F}_{rz}}{\rho} = (\sigma^*_z)_j - (\sigma^*_z)_{j+1} \tag{11}$$

The transverse shear force $\hat{F}_{rz}$ that is due to the flexing of the inclusion is derived by considering equilibrium of moments about the circumferential direction:

$$\frac{d\hat{M}_r}{d\rho} + \frac{\hat{M}_r - \hat{M}_\theta}{\rho} = \hat{F}_{rz} \tag{12}$$

By substituting the moment curvature equations in Equation 12, an expression for $\hat{F}_{rz}$ in terms of the displacements can be obtained. Then Equation 11 becomes

$$\frac{E_g \delta_g^3}{12(1-\nu_g^2)} \left[\frac{d^4(w^*)_j}{d\rho^4} + \frac{2}{\rho} \frac{d^3(w^*)_j}{d\rho^3} - \frac{1}{\rho^2} \frac{d^2(w^*)_j}{d\rho^2} + \frac{1}{\rho^3} \frac{d(w^*)_j}{d\rho} \right] = (\sigma^*_z)_j - (\sigma^*_z)_{j+1} \tag{13}$$

Equations 10 and 13, which are similar to the ones used in thin plate theory (22), are the two last expressions needed for the determination of the integration constants for each layer. It can be easily verified that in the case for which no tension-resistant inclusion exists at the interface, the two conditions for the rough interface result from the previous equations by setting $\delta_g = 0$. Substitution of the expressions for the stress and displacement components obtained previously into the boundary and interface conditions yields expressions for the $4n - 2$ unknown integration constants needed for the determination of the stress and displacement components for each layer.

To find the stresses and displacements due to a prescribed axisymmetric vertical or tangential load, p or τ, respectively, one uses a Hankel transform. These loads may be expressed in the form

$$p(\rho) = \int_0^\infty p_m J_0(m\rho)\, dm \tag{14a}$$

and

$$\tau(\rho) = \int_0^\infty \tau_m J_1(m\rho)\, dm \tag{14b}$$

where,

$$p_m = m \int_0^\infty p(s) s J_0(ms)\, ds \tag{15a}$$

and

$$\tau_m = m \int_0^\infty \tau(s) s J_1(ms)\, ds \tag{15b}$$

The integrals in Equations 15a and 15b are the Hankel transforms of the functions $p(\rho)$ and $\tau(\rho)$. The subscript m in p_m and τ_m denotes their dependence in the continuous parameter m of the Hankel transform. Recalling Equations 4, Equations 14 may also be written

$$p(\rho) = \int_0^\infty p^*_m(\rho)\, dm \tag{16a}$$

and

$$\tau(\rho) = \int_0^\infty \tau^*_m(\rho)\, dm \tag{16b}$$

As shown in Equations 16, the desired loading function is expressed as a linear combination of an infinity of other functions that have desirable mathematical properties. Accordingly, after denoting by S^*_m and U^*_m the generalized quantities that describe the effect on the stress and displacement components due to the basic loading p^*_m or τ^*_m, respectively, the effects S and U produced by the actual load p or τ are then expressed

$$S(\rho, \zeta) = \int_0^\infty S^*_m(\rho, \zeta)\, dm \tag{17a}$$

$$U(\rho, \zeta) = \int_0^\infty U^*_m(\rho, \zeta)\, dm \tag{17b}$$

NUMERICAL CALCULATION

The parameters affecting the behavior of the reinforced layered system are the moduli of elasticity and the Poisson's ratios of the layers and the inclusion, their respective thicknesses, and the geometrical distribution of the surface loading. In the analysis, the quantities describing the geometry of the problem are made dimensionless by dividing them by an arbitrary distance, taken here as the distance between the free surface and the upper boundary of the lowermost layer, H. The moduli of elasticity of the soil layers enter as a dimensionless ratio describing the relative rigidity of two adjacent layers. Another dimensionless factor, λ_G, is used in the presentation of results. This factor describes the relative stiffness of the inclusion with respect to the lowermost soil layer and is given by

$$\lambda_G = \frac{E_g t_g}{E_n H} \tag{18}$$

The determination of the stress and displacement components S and U, respectively, produced by the prescribed load at the surface, involves the numerical evaluation of the integrals given by Equations 17. To evaluate these integrals, one must determine the integration constants A_{mj}, B_{mj}, C_{mj}, and D_{mj}, which are functions of the Hankel transform parameter m. A Gaussian quadrature scheme of variable order (from 4 to 256) has been used for this purpose, with the order depending on the degree of accuracy desired. The domain of integration was divided into a finite number of intervals, bounded by the subsequent zeros of one of the two Bessel functions involved. The number of intervals depends on the rate of convergence of the integration. The integration constants were evaluated by solving the $4n - 2$ simultaneous equations obtained from the boundary conditions. To calculate a stress or displacement component at a point, one solves these equations $s \times N$ times, s being the point number of the Gaussian quadrature formula and N being the number of intervals. For a two-layer system, the numerical integration was greatly accelerated by one refinement. The six integration constants required for the complete description of the stress and displacement components were obtained in the form of explicit expressions by using MACSYMA, a symbolic manipulator program. The complete expressions obtained for the cases of either a normal or horizontal traction at the surface may be found in the literature *(23)*.

RESULTS AND CONCLUSION

Figures 3–5 show the effect of a reinforcing inclusion inserted at the interface of a two-layer system. Because of space restrictions and the large number of parameters involved, it is possible to present only a few typical cases to illustrate the response of the reinforced system. In the examples shown, a two-layer system is loaded by a uniformly distributed normal load p_0 covering a circular area of dimensionless radius α, equal to

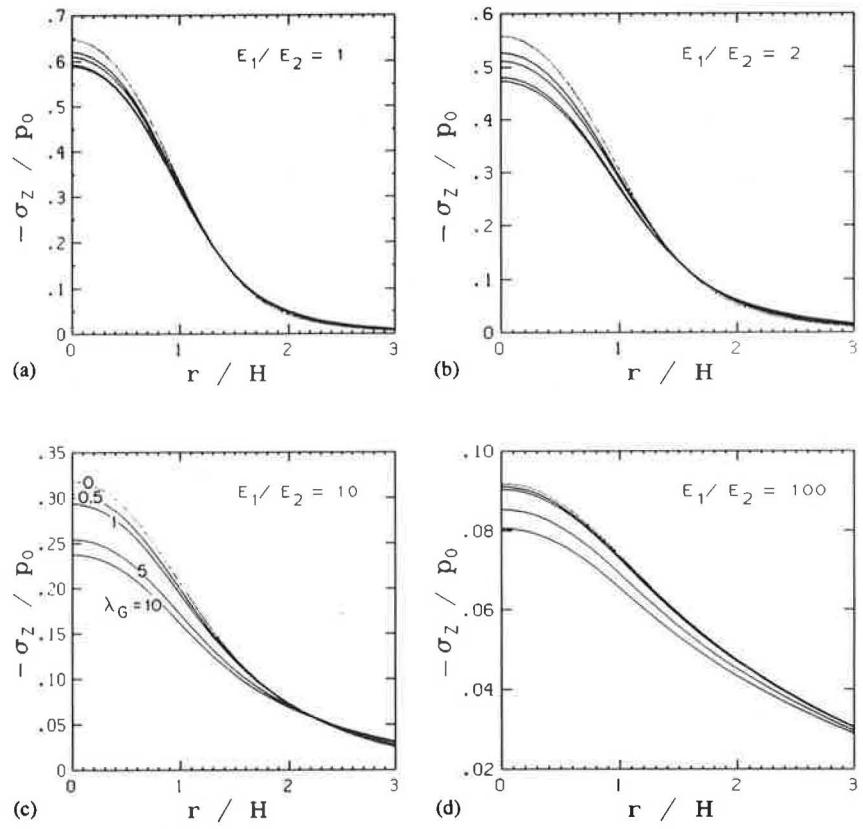

FIGURE 3 Vertical stress distribution on top of the subgrade for a reinforced two-layer system with varying reinforcement stiffnesses λ_G and different soil layer elastic modulus ratios E_1/E_2. $\alpha = 1$, $\nu_1 = \nu_2 = \nu_g = 0.25$. The curves corresponding to different values of λ_G in Figures 3a, 3b, and 3d follow the same order as in Figure 3c.

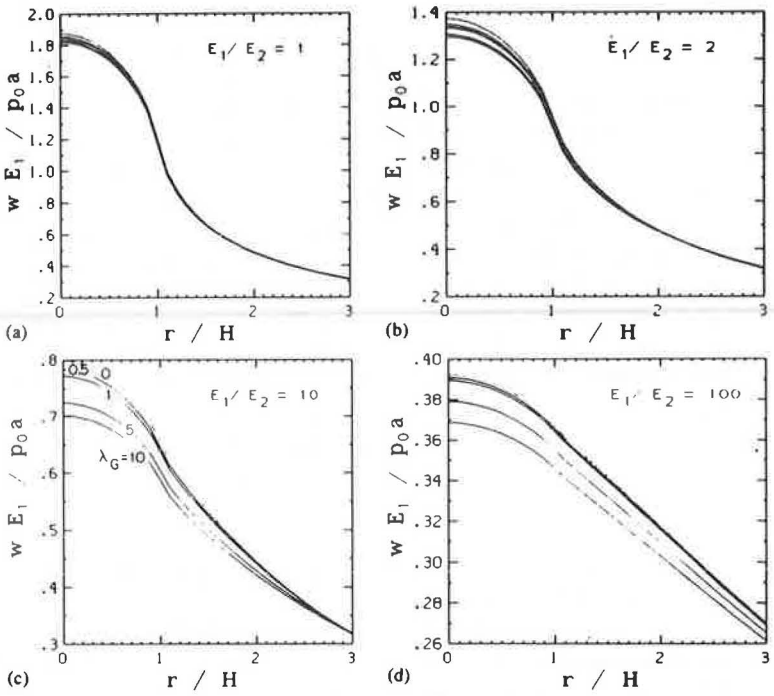

FIGURE 4 Vertical displacement at the free surface for a reinforced two-layer system with varying reinforcement stiffnesses λ_G and different soil layer elastic modulus ratios E_1/E_2. $\alpha = 1$, $\nu_1 = \nu_2 = \nu_g = 0.25$. The curves corresponding to different values of λ_G in Figures 4a, 4b, and 4d follow the same order as in Figure 4c.

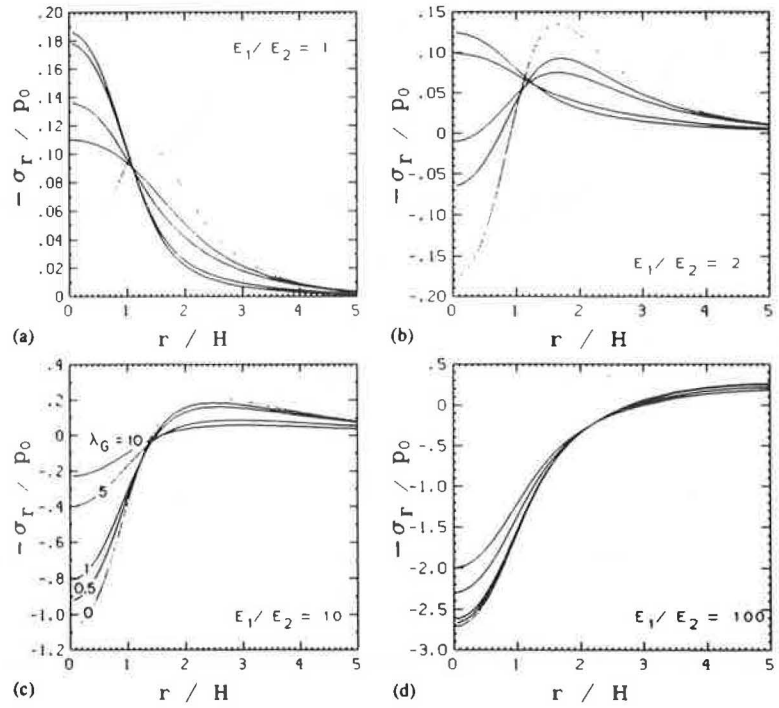

FIGURE 5 Radial stress distribution at the bottom of the top layer for a reinforced two-layer system with varying reinforcement stiffnesses λ_G and different soil layer elastic modulus ratios E_1/E_2. $\alpha = 1$, $\nu_1 = \nu_2 = \nu_g = 0.25$. The curves corresponding to different values of λ_G in Figures 5a, 5b, and 5d follow the same order as in Figure 5c.

the actual radius of the loaded area a divided by H, the distance between the free surface and the interface. In these examples the thickness of the upper layer is equal to the radius of the loaded area, and δ_g is taken equal to 0.01, 0.005, 0.001, and 0.0005. The Poisson ratios of the top and bottom layer and the inclusion are all taken equal to 0.25. Results are plotted for four different values of the ratio E_1/E_2 and for four values of λ_G, the relative stiffness of the inclusion given by Equation 18.

In Figures 3a–3d, the vertical stress on top of the lower layer is plotted as a function of distance away from the axis of symmetry and compared to the stress in an unreinforced ($\lambda_G = 0$) two-layer system. In all cases there is a decrease in the stress, especially out to a distance of about one radius from the axis of symmetry. The vertical displacements at the free surface are shown in Figures 4a–4d for the same combination of parameters. These figures show a favorable but relatively small decrease in settlement beneath the loaded area. A third set of figures (Figures 5a–5d) shows the radial stress at the bottom of the upper layer for the same two-layer system. The tendency for layered systems to develop tensile stresses in this region has always been a problem, and this set of figures shows the beneficial effect of reinforcing in alleviating this problem.

It is concluded that calculations based on the linear theory of elasticity can provide many insights into the effects produced by reinforcing of the type that is incorporated into layered systems, such as those used in pavement and railroad foundations. By using modern high-speed computers and an efficient computational scheme, one can economically study and compare many different cases. Moreover, the results of these computations represent an important limiting case for more involved and expensive calculations that attempt to include nonlinear effects and more detailed material models.

REFERENCES

1. J. D. Nieuwenhuis. Membranes and the Bearing Capacity of Roadbases. *Colloque International sur l'Emploi des Textiles en Geotechnique*, Vol. 1, Paris, April 1978, pp. 3–8.
2. J. B. Sellmeijer, C. J. Kenter, and C. Van Der Berg. Calculation Method for a Fabric Reinforced Road. In *Proc., 2nd International Conference on Geotextiles*, Vol. 2, 1982, pp. 393–398.
3. P. L. Bourdeau, M. L. Harr, and R. D. Holtz. Soil-Fabric Interaction—An Analytical Model. In *Proc., 2nd International Conference on Geotextiles*, Vol. 1, 1982, pp. 387–392.
4. J. P. Gourc, Y. Matichard, H. Perrier, and P. Delmas. Bearing Capacity of a Sand-Soft Subgrade System with Geotextile. In *Proc., 2nd International Conference on Geotextiles*, Vol. 2, 1982, pp. 411–416.
5. J. P. Giroud and L. Noiray. Design of Geotextile Reinforced Unpaved Roads. *Journal of the Geotechnical Engineering Division*, ASCE, Vol. 107, No. GT9, Sept. 1981, pp. 1233–1254.
6. V. D. Kasarnovsky, A. G. Polunovsky, and B. P. Brantman. Design of a Temporary Road Structure with the Use of a Textile Membrane. In *Proc., 2nd International Conference on Geotextiles*, Vol. 2, 1982, pp. 371–374.
7. W. J. Harrison and C. M. Gerrard. Elastic Theory Applied to Reinforced Earth. *Journal of the Geotechnical Engineering Division*, ASCE, Vol. 98, No. SM12, Dec. 1972, pp. 1325–1345.
8. V. A. Barvashov. Analysis of Stresses and Strains in Multi-Layered Soil Foundation Reinforced with Synthetic Fabrics. *Colloque International sur l'Emploi des Textiles en Geotechnique*, Vol. 1, Paris, April 1978, pp. 95–98.
9. R. Barksdale, Q. Robnett, J. Lai, and A. Zeevaert-Wolff. Experimental and Theoretical Behavior of Geotextile Reinforced Aggregate Soil Systems. In *Proc., 2nd International Conference on Geotextiles*, Vol. 2, 1982, pp. 375–380.
10. M. M. Al-Hussaini and L. D. Johnson. Numerical Analysis of Reinforced Earth Wall. *Symposium on Reinforced Earth*, ASCE Annual Convention, Pittsburgh, Pa., April 1978.
11. L. Raad. Reinforcement of Transportation Support Systems through Fabric Prestressing. In *Transportation Research Record 755*, TRB, National Research Council, Washington, D.C., 1980, pp. 49–51.
12. K. Z. Andrawes, A. McGown, R. F. Wilson-Fahmy, and M. M. Mashhour. The Finite Element Method of Analysis Applied to Soil-Geotextile Systems. In *Proc., 2nd International Conference on Geotextiles*, Vol. 3, 1982, pp. 695–700.
13. J. C. Chang and R. A. Forsyth. Finite Element Analysis on Reinforced Earth Wall. *Journal of the Geotechnical Engineering Division*, ASCE, Vol. 103, No. GT7, July 1977, pp. 711–724.
14. R. K. Rowe. Reinforced Embankments: Analysis and Design. *Journal of the Geotechnical Engineering Division*, ASCE, Vol. 110, No. GT2, Feb. 1977, pp. 231–246.
15. W. G. Salomone, R. D. Holtz, and W. D. Kovacs. A New Soil-Reinforcement Interaction Model. *Symposium on Reinforced Earth*, ASCE Annual Convention, Pittsburgh, Pa., April 1978.
16. K. W. Romstad, L. R. Herrmann, and C.-K. Shen. Integrated Study of Reinforced Earth. I: Theoretical Formulation. *Journal of the Geotechnical Engineering Division*, ASCE, Vol. 102, No. GT5, May 1976, pp. 457–471.
17. C.-K. Shen, K. M. Romstad, and L. R. Herrmann. Integrated Study of Reinforced Earth. II: Behavior and Design. *Journal of the Geotechnical Engineering Division*, ASCE, Vol. 102, No. GT6, June 1976, pp. 577–590.
18. L. R. Herrmann and Z. Al-Yassin. Numerical Analysis of Reinforced Soil Systems. In *Proc., Symposium on Reinforced Earth*, ASCE Annual Convention, Pittsburgh, Pa., April 1978.
19. D. J. Naylor. A Study of Reinforced Earth Wall Allowing Strip Slip. *Symposium on Reinforced Earth*, ASCE Annual Convention, Pittsburgh, Pa., April 1978.
20. D. M. Burmister. The General Theory of Stresses and Displacements in Layered Soil Systems. *Journal of Applied Physics*, Vol. 16, 1945, pp. 89–94, 126–127, 296–302.
21. M. R. Mehta and A. S. Veletsos. *Stresses and Displacements in Layered Systems*. Civil Engineering Studies, Structural Research Series, No. 178, University of Illinois, 1959.
22. L. H. Donnell. *Beams, Plates and Shells*. McGraw-Hill, New York, 1976.
23. C. A. Vokas. *Reinforced Layered Elastic Systems*. Ph.D. dissertation, Department of Civil Engineering and Engineering Mechanics, Columbia University, New York, May 1987.

Publication of this paper sponsored by Committee on Mechanics of Earth Masses and Layered Systems.

Geogrid Reinforcement of Ballasted Track

RICHARD J. BATHURST AND GERALD P. RAYMOND

Large-scale models comprising a single tie/ballast system were constructed over artificial subballast-subgrade supports having variable compressibility ranging from rigid to very flexible (with California bearing ratio of 1). Test configurations included a 0.45-m depth of crushed limestone ballast conforming to an American Railway Engineering Association (AREA) Grading No. 4. A 920-mm-long by 250-mm-wide by 150-mm-deep steel footing was used to model the bearing area of a typical tie. Each rail seat was subjected to a program of repeated loading equivalent to a cumulative axle tonnage of 2 to 20 million tonnes in track. The performance of test sections reinforced with a single layer of geogrid at variable depths below the footing (tie) was compared against unreinforced test configurations. The results showed that geogrid reinforcement in ballast over compressible ballast support can be effective in reducing the rate of permanent deformation associated with lateral ballast spreading. The optimum reinforcement depth-to-tie-width ratio was determined to be from 0.2 to 0.4 for the single-tie tests with compressible artificial supports. No performance benefit was observed for reinforced ballast sections over a rigid support. By far the greatest influence on the performance of test sections was the compressibility of the artificial supports used. Permanent deformations at a given tonnage increased dramatically with increased support compressibility both for reinforced and unreinforced tests. A preliminary attempt was made to relate the performance of reinforced model tests to the performance of comparable configurations in track.

Under repeated tie loading, railway ballast undergoes nonrecoverable vertical deformations, mostly due to ballast densification, aggregate degradation, and the lateral spread of ballast beneath the ties. A joint Queen's University and Royal Military College research program has been underway for several years to investigate the influence of track parameters on the performance of large-scale model tie/ballast systems and to investigate strategies to improve the performance of these systems. A companion paper *(1)* dealing with unreinforced single tie/ballast systems was presented by the authors at the Transportation Research Board 1987 annual meeting.

Earlier work has shown that the inclusion of open-grid polymer-based reinforcement (geogrid) in ballast may be a cost-effective method to reduce track settlements associated with lateral ballast spreading *(2)*. The current study reports recent additional work related to geogrid reinforcement of ballasted track.

R. J. Bathurst, Civil Engineering Department, Royal Military College of Canada, Kingston, Ontario, K7K 5L0 Canada. G. P. Raymond, Civil Engineering Department, Ellis Hall, Queen's University at Kingston, Ontario, K7L 3N6 Canada.

Large-scale models comprising a single tie/ballast system over artificial subballast-subgrade supports of variable compressibility, hereafter referred to as artificial support, were built and subjected to a program of repeated loading. The principal objectives of this investigation were to

1. Compare the performance of geogrid-reinforced and unreinforced ballast sections with respect to the rate at which permanent deformations are generated during repeated loading;
2. Examine the effect of ballast support compressibility on permanent deformation and elastic rebound for reinforced and unreinforced ballast test sections;
3. Establish a practical optimum depth of geogrid reinforcement below a tie; and
4. Relate laboratory test results to field applications.

The general test arrangement is shown in Figure 1. A 450-mm depth of ballast was confined within a rigid test box 3 m long by 1.5 m wide. Tests were performed with and without geogrid inclusions. For reinforced configurations, a single layer of geogrid was placed at a variable depth below the footing (tie) base.

A range of ballast support stiffnesses was incorporated into test sections. A perfectly rigid subgrade condition was simulated by placing ballast material directly over the concrete floor. For compressible ballast support models, rubber mats of variable stiffness were placed over the concrete floor.

A 920-mm-long (L = 920 mm) by 250-mm-wide (B = 250 mm) by 150-mm-deep steel footing was used to model the bearing area of a typical tie below the rail seat (i.e., one rail). The footing was placed within the ballast layer to a depth of 150 mm to simulate typical track structure. The footing was loaded by a computer-controlled closed-loop electrohydraulic actuator that applied a peak load of 85 kN at selected frequencies from 0.5 to 3 Hz.

TEST DETAILS

Ballast

Crushed limestone aggregate was used for all test configurations. The aggregate was screened close to an American Railway Engineering Association (AREA) No. 4 grading with a size distribution between about 10 mm (3/8 in.) and 50 mm (2 in.) *(3)*. AREA No. 4 gradation limits and mean particle size distribution for the test ballast are given on Figure 2. The ballast had a Los Angeles abrasion (LAA) value of 27 and a

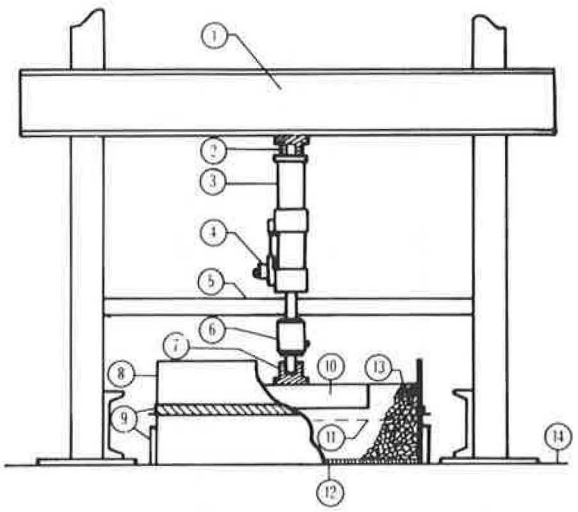

1 LOADING CROSS BEAMS (2 MC 460 x 63.5)
2 UPPER SWIVEL JOINT
3 MTS HYDRAULIC ACTUATOR / INTERNAL LVDT
4 SERVO CONTROL VALVE
5 ACTUATOR GUIDE & INSTRUMENTATION SUPPORT BEAM
6 LOAD CELL
7 LOWER SWIVEL JOINT
8 PLYWOOD BULKHEAD
9 BULKHEAD SUPPORTS
10 STEEL LOADING TIE (920 mm x 250mm x 150 mm)
11 GM1 GEOGRID
12 ARTIFICIAL SUPPORT
13 AREA #4 BALLAST
14 CONCRETE FLOOR

FIGURE 1 General test arrangement.

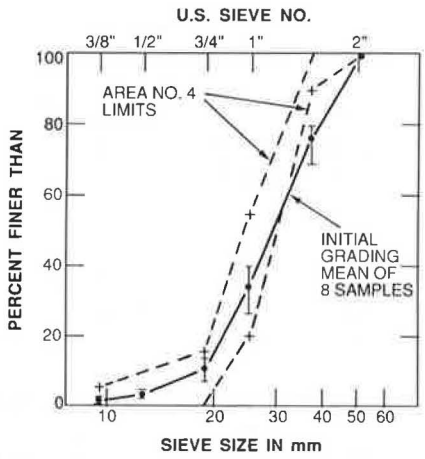

FIGURE 2 Ballast size distribution.

mill abrasion (*MA*) value of 8.5. The ballast depth below the footing was 300 mm, which corresponds to the minimum recommended depth for new construction according to the AREA *(3)*. The ballast was placed in 150-mm lifts and compacted by a vibrating plate tamper with a mass per unit area of 105 kg/m^2.

Geogrid Reinforcement

A high-density polyethylene polymer mesh was used for all reinforced tests (Tensar GM1 geogrid). The GM1 mesh consists of square openings with an aperture width of 46 mm and has identical mechanical properties in longitudinal and transverse directions.

A fresh sheet of geogrid was used for each test and was trimmed to fit without warping within the area of the ballast box. The geogrid was placed at depths D_r of 50, 100, 150, and 200 mm below the base of the footing.

Footing

Footing dimensions were selected to model one-half the total bearing area of a typical tie (i.e., the bearing area below one rail seat) as outlined in the AREA *Manual for Railway Engineering (3)*. When the AREA approach is used, the footing length L of 920 mm also corresponds to about the tamper influence distance along the tie on either side of each rail. The footing was constructed from a 3.15-mm-thick rectangular hollow steel section and was closed at the end to prevent aggregate infilling.

Ballast Support

Test configurations reported in this paper were constructed with artificial subgrades that had four different compressibilities. The purpose of the artificial subgrades was to model ballast support (i.e., subballast-subgrade formation at the subballast-ballast interface) having a range of stiffnesses.

A rigid subgrade condition was simulated by placing ballast directly over the laboratory concrete floor. This condition models a field situation in which track traverses exposed bedrock faces or chemically stabilized stiff subgrade conditions occur.

A flexible ballast support condition was modeled by using a closed-cell gum rubber mat. A subgrade modulus of 129 MN/m^3 was calculated for this material with a plate 762 mm in diameter and a maximum load of 85 kN. A California bearing ratio (*CBR*) value of 39 was determined for the same material by using the test procedure outlined in ASTM D 1883–73. This condition may be considered to simulate ballast support due to a granular subballast over a competent cohesive subgrade.

Very flexible ballast support conditions were modeled by using double layers of rubber mat materials. For example, a layer of gum rubber plus a layer of open-sheet neoprene rubber gave a subgrade modulus of 18 MN/m^3 and a *CBR* value of 1. A double layer of gum rubber increased the subgrade modulus to 62 MN/m^3 and gave a *CBR* value of 10. These low values indicate extreme compressibility that would tend to be avoided for the subballast-subgrade formation in a field situation. However, these weak artificial supports were used to clearly establish trends in ballast load-deformation behavior related to ballast support compressibility.

LOADING SYSTEM AND DATA ACQUISITION

Tie loadings were applied through an MTS closed-loop electrohydraulic actuator controlled by a DEC PDP11/34 computer.

The majority of tests reported in the current study were carried out in a load-controlled mode using a peak load of 85 kN and loading frequencies from 0.5 to 3 Hz. An 85-kN load (tie bearing pressure = 370 kPa) represents a typical magnitude of dynamic load felt by ballast directly beneath the tie for a track modulus between 14 and 85 MN/m per meter of rail *(4)*. The magnitude of permanent deformations generated in track is insensitive to the magnitude of loading frequency when low rates of loading are used *(5)*. A sinusoidal compressive repeated loading waveform was used in the testing program. This waveform is thought to approximate the loading pulse applied to railway ties under actual field conditions *(6)*.

A load cell and linear variable displacement transducer (LVDT) located above the actuator base were used to monitor footing loads and vertical footing displacements at all test stages. At programmed intervals, the load-deformation response of the footing during a loading cycle was taken, and at regular intervals the permanent deformation of the footing was recorded and stored by the computer.

TEST PROGRAM

Results from 15 tests have been used in the current study to provide data with which to compare the relative performance of reinforced and unreinforced tie, ballast, and support configurations. These test configurations are presented in Table 1. Tests were subjected to a maximum number of load repetitions that was equivalent to 2 to 20 million cumulative axle-tonnes in track. The equivalent axle-tonnage was calculated by summing the number of load repetitions and multiplying by twice the applied load. European railway experience has shown that for conventional main-line track, the settlement rate expressed as deformation per log cycle cumulative tonnage is usually constant after about 2 million tonnes *(7–9)*. In 1980, annual traffic of 10 to 60 million gross tonnes (MGT) was recorded for typical heavy branch-line and main-line track sections in Canada.

TABLE 1 SUMMARY OF TESTS

Test No.	Load Level (kN)	Support Condition (CBR)	Reinforcement Depth D_r (mm)
1	85	Rigid	Unreinforced
1A	85	Rigid	Unreinforced (repeat)
2	85	Rigid	50
3	85	Rigid	100
4	85	Rigid	150
5	85	39	Unreinforced
6	85	39	50
7	85	39	100
8	85	39	100 (repeat)
9	85	39	150
9A	85	39	200
10	85	1	Unreinforced
11	85	1	100
12	85	1	200
13	85	10	Unreinforced

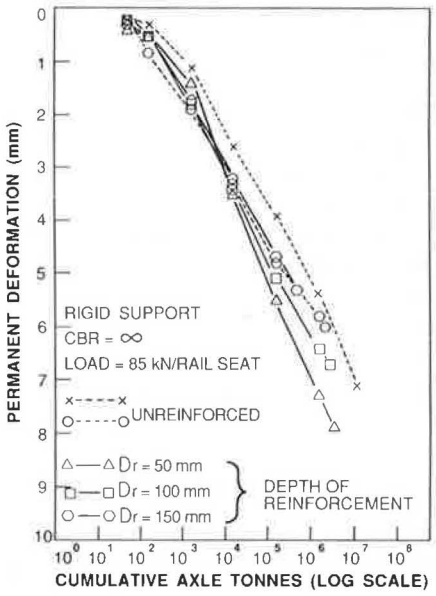

FIGURE 3 Accumulated permanent deformation (rigid support).

TEST RESULTS

Effect of Reinforcement on Permanent Deformations

A fundamental objective of this study was to determine the conditions under which geogrid reinforcement of railway ballast was effective in reducing the rate of development of permanent settlements below railway ties. Figures 3–5 show accumulated permanent deformations recorded for all tests as a function of equivalent cumulative axle tonnage. Permanent deformations shown on the figures are those measured at the base of the footing. A number of important observations can be made from these figures.

Figure 3 shows that the permanent settlements recorded after 1 to 10 MGT are small regardless of test configuration when the ballast is placed over a rigid support. The differences in accumulated settlements are probably caused by minor variations in ballast placement rather than the presence or absence of the reinforcement. Consequently, despite a small increase in recorded settlements for the reinforced configurations with respect to the control configurations at the end of the test of less than 2 mm, the performance difference is considered negligible.

In contrast, Figures 4 and 5 show a clear performance benefit due to the inclusion of geogrid at certain elevations within the ballast layer for tests constructed over a compressible ballast support. For comparative tests with a *CBR* = 39 support, permanent deformations were reduced for reinforcement depths D_r = 50, 100, and 150 mm below the tie. At D_r = 200 mm, the reinforced test showed greater settlement and larger settlement rates than the control test. However, the performance difference is probably within the range of test repeatability, and for practical purposes the D_r = 200 mm test over a *CBR* = 39 artificial support represents the limiting depth at which reinforcement is effective in these laboratory tests. The trend in

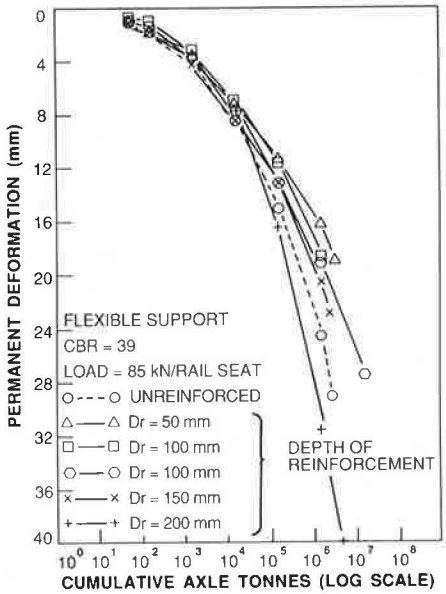

FIGURE 4 Accumulated permanent deformation (flexible support).

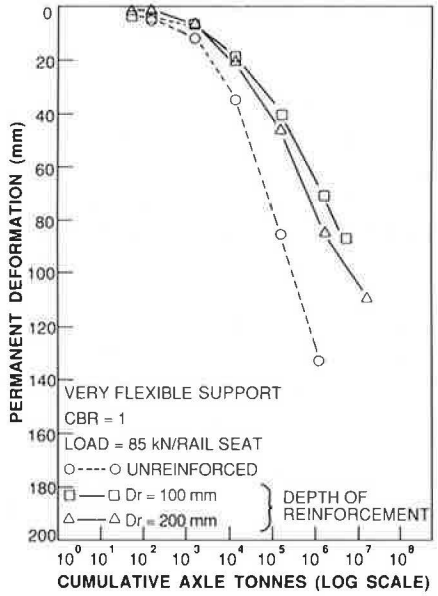

FIGURE 5 Accumulated permanent deformation (very flexible support).

reinforcement effect shown on the figure is similar to comparable small-scale tests built with compressible artificial subgrades *(10)*. For $D_r \cong 1$, there were marginally greater plastic settlements for the reinforced cases.

The *CBR* = 1 tests with reinforcement at D_r = 100 and 200 mm reduced permanent deformations more dramatically than the *CBR* = 39 tests. For example, at 2 million tonnes and D_r = 100 mm, the permanent deformations were reduced by about 20 percent for a *CBR* = 39 support condition. The same reinforcement depth and *CBR* = 1 support gave a 50 percent reduction. Taken together, the data shown on Figures 3–5 suggest that the ability of reinforced sections to reduce permanent deformations under repeated loading improves with increasing subballast-subgrade formation compressibility.

Effect of Ballast Support Compressibility on Permanent Deformations

The influence of ballast support compressibility on the permanent deformation response of control tests and tests with reinforcement at D_r = 100 mm is shown in Figure 6. The data show that as ballast support *CBR* $\rightarrow \infty$, the relationship between the magnitude of permanent deformation and the log number of cumulative tonnage becomes more linear. Linear semilogarithmic settlement trends have been observed in full-scale single-tie tests in which unreinforced ballast was placed over a firm subballast-subgrade formation *(11)* and by the European railways who have monitored conventional main-line track constructed over very competent subgrades *(7–9)*. In contrast, the deformation histories of the unreinforced and reinforced tests with very flexible artificial supports (*CBR* = 1 and 10) are distinctly nonlinear on a semilogarithmic plot. These data indicate that once some threshold tonnage is achieved for each support condition, the rate of track settlement per log cycle of cumulative tonnage increases. Similar nonlinear deformation-tonnage curves have been reported by the European railways for main-line track in need of ballast maintenance *(7–9)*.

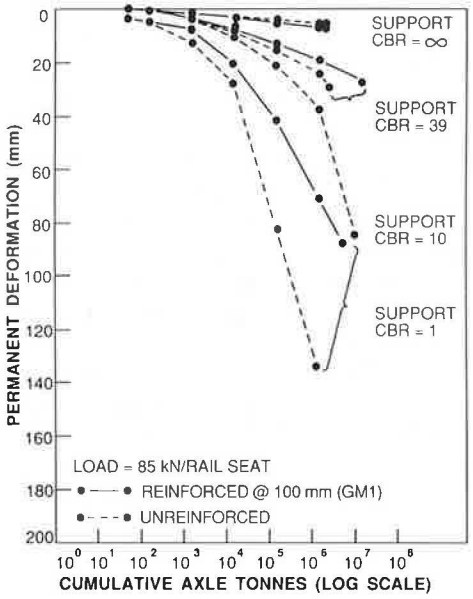

FIGURE 6 Influence of support compressibility on permanent deformations.

Elastic Rebound

Elastic rebound (unloading) is the difference between recoverable and nonrecoverable deformations associated with each load repetition and can be used to evaluate the resilience (elasticity) of track subjected to repeated loading. Figure 7 shows the range of elastic rebound recorded in the ballast-subgrade formation for 85-kN tests after 1,000 load applications. The data reveal that the magnitude of elastic rebound is sensitive to ballast support compressibility but relatively insensitive to the presence and depth of geogrid reinforcement.

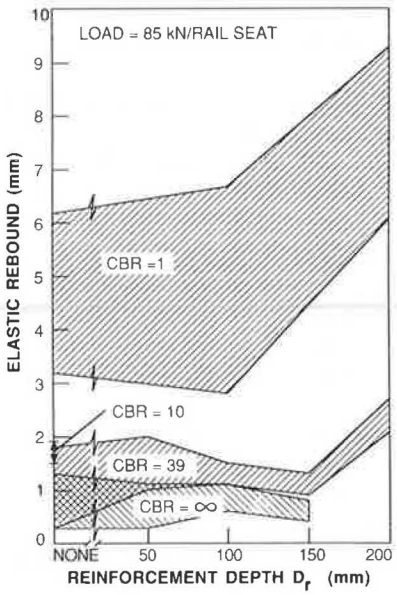

FIGURE 7 Elastic rebound.

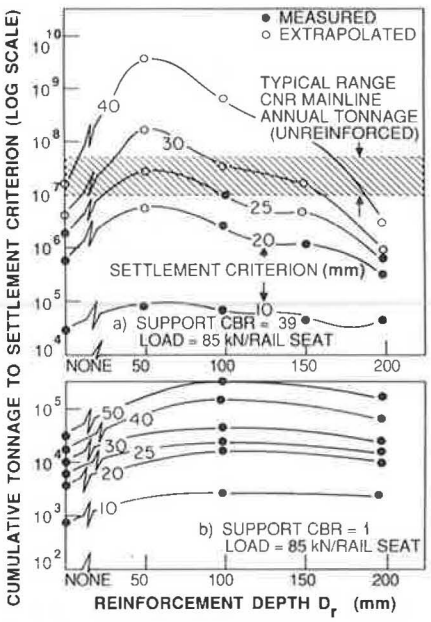

FIGURE 8 Optimum depth of reinforcement from single tie-ballast model tests.

Additional Observations

During excavation of reinforced-ballast sections, it was observed that numerous aggregate particles were tightly wedged into the grid apertures and could not be removed by hand. This observation is consistent with the concept of ballast-geogrid interlock as an important mechanism in resisting the lateral deformation of ballast under repeated loading. In addition, the geogrid was observed to form a well-pronounced depression bowl in nonrigid artificial support tests, consistent with the widely held belief that to mobilize the tensile and interlocking capacities of this material, large deformations in the surrounding aggregate are required. In the field, where ballast may be placed over low-CBR subballast-subgrade formations, the mobilization of the geogrid reinforcement may be even greater due to plastic deformation of the ballast support. Consequently, the relative improvements reported for reinforced configurations in this paper may actually be conservative.

Optimum Depth of Reinforcement

Figure 8 shows the equivalent tonnage required to achieve a given settlement criterion for all 85-kN tests with compressible-ballast support. Where necessary, settlements at large tonnages have been estimated by linearly extrapolating load-deformation results after 2 million tonnes. The mean settlement criterion adopted by a given railway to initiate mechanized maintenance may vary, but 40 or 50 mm may be considered a typical upper limit. Clearly, uniform settlement is not detrimental to track performance. However, track quality (expressed as the frequency of cross level, twist, and alignment defects) will deteriorate in direct proportion to mean settlement recorded at rail seat locations *(7–9)*.

The plots indicate that an optimum depth of reinforcement is in the range of 50 to 100 mm below the tie (i.e., D_r/B = 0.20 to 0.40). These results are consistent with the results of earlier small-scale model tests that examined the effect of reinforcement in sand layers over compressible artificial subgrades subjected to repeated loading *(10)*. In the small-scale tests the optimum ratio D_r/B was about 0.33, and the benefit due to the reinforcement was seen to decrease for D_r/B greater than this value.

Figure 9 shows the settlement rate expressed in millimeters per log cycle of accumulated tonnage after 2 million equivalent-axle-tonnes for 85-kN tests. The data show that the optimum depth for *CBR* = 39 tests is in the range of 50 to 100 mm but may be somewhat deeper for configurations with a subgrade *CBR* of 1. The figure also indicates that subballast-subgrade formation compressibility has a greater influence on the settlement rate than does the location of the reinforcement.

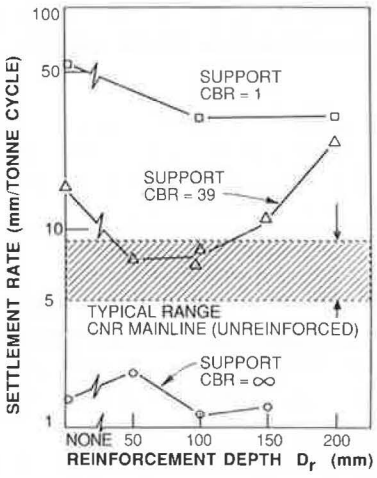

FIGURE 9 Railseat settlement rates after 2 MGT.

Implications for Track Design

Superimposed on Figure 8 is a range of typical Canadian National Railways (CNR) annual heavy branch-line and main-line tonnage *(12)*. This range shows that test configurations with *CBR* = 39 artificial support achieve settlement values after accumulated tonnages that are representative of annual traffic densities in CNR track. In contrast, the percentage reduction in permanent deformation for *CBR* = 1 tests is more dramatic, but the improvement is not meaningful because unacceptably high deformations would occur after only weeks of heavy branch-line or main-line traffic.

Superimposed on Figure 9 is the measured track settlement rate for a section of CNR conventional track after 2 million tonnes of main-line traffic *(12)*. Similar rates have been reported by the European railways for conventional track considered to be optimized *(7–9)*. Nevertheless, settlement rates in track constructed over poor subgrades or curved track have led to measured settlement rates as high as 26 mm per log cycle of accumulated tonnage *(7–9)*. On the basis of available field data, the *CBR* = 30 tests appear to give settlement rates that are reasonable for main-line track.

From practical considerations, a reinforcement depth between 50 and 100 mm is unsatisfactory because the tines for tamping equipment typically extend to between 100 and 150 mm below the base of the tie. However, a safer 200-mm depth of reinforcement may be effective in reducing settlements in actual track because the single-tie and rail seat model used in the current study may underestimate the optimum reinforcement depth. In the field, rolling loads are delivered over several ties; in addition, ballast spreading in the longitudinal track direction is more constrained. Qualitatively, these effects lead to an equivalent width B that is greater than the width of a single tie. If it is assumed that the experimentally determined optimum ratio D_r/B = 0.2 to 0.4 is valid, it is possible that a 200-mm depth of reinforcement in actual track will be as effective in reducing the rate of permanent deformation for ballasted track as indicated by the model tests with D_r/B 0.2 to 0.4. In addition, the use of a purely elastic artificial support may penalize the performance benefit that would otherwise occur for the comparable configuration in a field condition. Actual subballast-subgrade formations with low *CBR* values will generate additional plastic deformations that can assist to mobilize the inherent capacity of geogrids to resist lateral spreading of ballast. On the basis of the previous comments, much work remains to be done to calibrate the laboratory test results with the performance of actual reinforced-track structures in the field.

Nevertheless, if it is assumed that the model tests are conservative, the potential for increased maintenance cycle times can be appreciated from Figure 10, which shows that if reinforcement is placed at an effective depth in ballast over a *CBR* = 39 support, the tonnage saved after 20 to 30 mm of accumulated settlement is equivalent to 1 year of heavy CNR branch-line or main-line traffic. Alternatively, the potential benefit of reinforcement under the same conditions can be expressed as a 25 to 50 percent reduction in the rate of settlement after 2 million cumulative tonnes, as shown in Figure 9. For conditions under which permanent settlements greater than 30 mm are permitted, the semilogarithmic settlement trend in the test data can be extrapolated to predict even greater savings in terms of years between mechanized maintenance duties *(2)*.

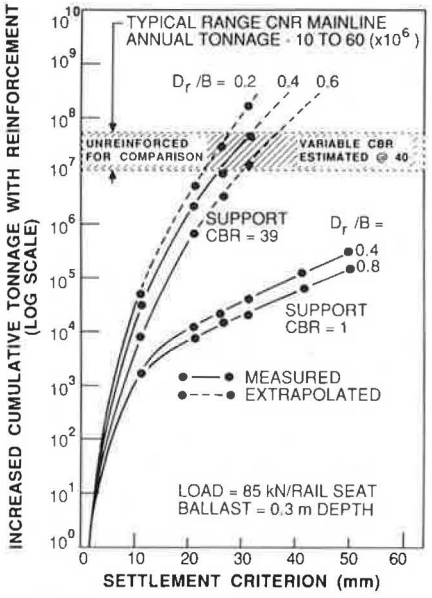

FIGURE 10 Cumulative tonnage saved from single tie-ballast tests.

The results of the current study indicate that there is a combination of criteria that must be met before ballast reinforcement can be considered a cost-effective method to improve track performance. If the track subballast-subgrade formation is too stiff, the performance difference between reinforced and unreinforced systems is negligible. Conversely, if the ballast support is too compressible, the reinforcing benefit is pronounced, but the maintenance cycle times remain uneconomically short (i.e., curves fall below the 10-MGT line in Figure 10). Figure 9 shows that even though reinforcement is a viable option to increase maintenance cycle times, a modest improvement in the quality of the subballast-subgrade formation may be equally effective. For new construction, the latter is likely more cost-effective, whereas on rehabilitation work restricted to the track ballast the former is probably the preferred approach.

CONCLUSIONS

The major conclusions that can be drawn from the current study and implications to track design are summarized as follows:

1. Test results showed that geogrid reinforcement in ballast can reduce the rate at which permanent (nonrecoverable) deformations are generated within ballast for track structure over compressible subballast-subgrade formations. Conversely, no performance benefit was observed for reinforced ballast sections constructed over a rigid subgrade.
2. By far the greatest influence on the generation of permanent deformations beneath the tie was the compressibility of the artificial support below the ballast. Increases in permanent deformation were proportional to increases in subgrade compressibility for both reinforced and unreinforced test sections.

3. As subballast-subgrade formation compressibility increases, the benefit derived from the geogrid reinforcement becomes more pronounced. Model tests showed that for reinforced ballast over a very flexible support the permanent deformation recorded after about 2 million tonnes was only 50 percent of that recorded for the same configuration without reinforcement.

4. The test results show that the experimentally determined optimum reinforcement depth-to-tie breadth ratio D_r/B is in the range 0.2 to 0.4 for ballast over a compressible ballast support. Tests with a $CBR = 39$ support and reinforcement at $D_r/B = 0.2$ to 0.6 resulted in tonnage savings equivalent to 1 year of heavy CNR branch-line or main-line track.

5. In actual track, the depth of reinforcement would be restricted to about 200 mm to avoid damage by the ballasting tines of reballasting equipment. Although this depth results in no performance benefit according to tests with a ballast support of $CBR = 39$, the model tests are considered conservative because the artificial supports used in the laboratory could not deform plastically. Consequently, geogrid at 200-mm depth in actual track would probably assist in reducing the rate of permanent deformation.

6. The inclusion of geogrid ballast reinforcement did not appear to alter the elastic rebound values in the large-scale test program. The most important factor affecting the magnitude of elastic rebound was ballast support compressibility. Increases in artificial subgrade compressibility resulted in a proportional increase in rebound deflection.

ACKNOWLEDGMENTS

The research reported in this paper was funded in part by the Tensar Corporation under a research contract awarded to the authors to investigate Geogrid-Reinforced Railway Ballast and Granular Bases and a National Scientific and Engineering Research Council (Canada) grant awarded to G. P. Raymond. The authors also would like to express their appreciation to research assistants T. A. Hawrysh and P. Hulley, who conducted the experiments.

REFERENCES

1. G. P. Raymond and R. J. Bathurst. Performance of Large-Scale Model Single Tie/Ballast Systems. In *Transportation Research Record 1131,* TRB, National Research Council, Washington, D.C., 1987, pp. 7–14.
2. R. J. Bathurst, G. P. Raymond, and P. M. Jarrett. Performance of Geogrid-Reinforced Ballast Railroad Track Support. In *Proc., 3rd International Conference on Geotextiles,* Vol. 1, Vienna, Austria, April 1986, pp. 43–48.
3. *Manual for Railway Engineering,* Vols. 1 and 2. American Railway Engineering Association, 1984.
4. G. P. Raymond. Track Support Must Be Right if Concrete Sleepers are to Survive. *Railway Gazette International,* Vol. 140, No. 7, July 1984, pp. 528–530.
5. D. H. Timmerman and T. H. Wu. Behaviour of Dry Sands Under Cyclic Loadings. *Journal of the Soil Mechanics and Foundations Division, ASCE,* Vol. 95, No. SM4, 1969, pp. 1097–1113.
6. D. L. Heath et al. Design of Conventional Rail Track Foundations. *Proc., Institute of Civil Engineers,* Vol. 51, London, 1972, pp. 251–267.
7. Description of Research Methods, Definitions. RP1. In *Question D117—Optimum Adaptation of Conventional Track to Future Traffic.* Office for Research and Experiments of the International Union of Railways, Oct. 1971.
8. Study of the Change in the Track Level as a Function of the Traffic and of the Track Components (First Results of Laboratory and Site Tests), RP2. In *Question D117—Optimum Adaptation of Conventional Track to Future Traffic.* Office for Research and Experiments of the International Union of Railways, April 1973.
9. Study of the Change in Track Geometry as a Function of Traffic. Additional Results, RP7. In *Question D117—Optimum Adaptation of Conventional Track to Future Traffic.* Office for Research and Experiments of the International Union of Railways, Oct. 1975.
10. G. P. Raymond and F. B. Hayden. *Effect of Reinforcement on Sand Overlying Bases of Different Compressibilities Subjected to Repeated Loading.* C.E. Research Report 79, Department of Civil Engineering, Queen's University, Kingston, Ontario, March 1983.
11. R. J. Bathurst. *The Performance of a Full-Scale Model Double-Width Railway Tie Under Repeated Loading.* M.Sc. thesis, Queen's University, Kingston, Ontario, 1978.
12. CN Rail Research Centre. *Predicting Requirements for Subballast Thickness Progress Report No. 3—Measurement of Railroad Track Loads, Roadbed Dynamic Deflections and Settlements, Period 1980–1982.* Transport Canada Report 4350E, March 1983.

Publication of this paper sponsored by Committee on Mechanics of Earth Masses and Layered Systems.

Design and Performance of a Reinforced Embankment for Mohicanville Dike No. 2 in Ohio

J. M. DUNCAN, V. R. SCHAEFER, L. W. FRANKS, AND S. A. COLLINS

Mohicanville Dike No. 2 is a rim dike on the Mohicanville Reservoir in Wayne County, Ohio. Constructed on a weak peat and clay foundation, the dike failed during construction and was 22 ft below its design height of 28 ft. Of a number of alternatives considered for raising the dike to its design height, construction of a reinforced embankment afforded the best combination of cost and reliability. Finite element and conventional limit equilibrium analyses were conducted to determine the reinforcing required for stability of the embankment. To achieve the factor of safety required for design, a reinforcing force of 30,000 lb/ft was required. A heavy steel mat was selected for the reinforcing material. (Although the steel reinforcement will probably corrode in time, it is only needed for the first few years of the embankment's life; after the foundation gains strength through consolidation, the reinforcement will no longer be required for stability.) The embankment was instrumented to measure reinforcement forces, settlements, horizontal movements, and pore pressures. Instrumentation studies have shown that the performance of the embankment is fully acceptable and that finite element and slope stability analyses provide an effective means for designing reinforced embankments and for anticipating their performance.

Mohicanville Dike No. 2 is a rim dike on the Mohicanville Reservoir in Wayne County, Ohio. Originally constructed by the U. S. Army Corps of Engineers in 1936, the dike is 28 ft high and about 1,800 ft long. The dike suffered a number of failures during construction and could not be raised above 12 ft owing to the weakness of the peat and clay foundation at the site. Subsequent settlement reduced the height of the dike to about 6 ft, and it was maintained at this height—about 22 ft below design grade—until its reconstruction in 1984 and 1985.

Alternatives for raising the dike to its design height were evaluated in the late 1970s by Law Engineering Testing Company working for the Huntington District of the Corps of Engineers to determine the most feasible method *(1)*. Because of the weakness of the foundation soils, construction of a conventional embankment was infeasible, no matter how flat the slopes. The depth of the peat and clay was so great (about 60 ft) that excavation of the weak materials was not economically feasible. Displacement of the soft foundation soils was considered but was rejected because of the large quantities of fill required and the uncertain quality of the resulting structure. Use of a concrete flood wall was considered but rejected because of the poor foundation support. Eventually it was decided that the best alternative for raising the dike would be construction of a reinforced embankment.

Use of a reinforced embankment as a permanent water-retaining structure is not common and may be unprecedented in the United States. However, the infeasibility of other solutions made this design necessary at Mohicanville. Furthermore, although the structure is permanent, the reinforcement will only be needed to improve stability during the first 10 years of its life. After that, the foundation will have gained sufficient strength by consolidation that the embankment will be stable without reinforcement.

The use of reinforcement to improve embankment stability is fairly new, and design procedures are still being developed. For Mohicanville, both finite element analyses and conventional equilibrium slope stability analyses were performed. A complete set of limit equilibrium analyses were performed by Law Engineering Testing Co. *(1)*, and finite element analyses were performed by the U.S. Army Engineers Waterways Experiment Station (WES) *(2)* in conjunction with the senior author. Finite element analyses were used to estimate the force in the reinforcing and the horizontal and vertical movements of the embankment. The limit equilibrium analyses were used to evaluate the factor of safety with respect to shear failure through the embankment and its foundation and to determine the amount of reinforcement required for stability.

Because of the unusual design concept and the importance of the structure, the Huntington District installed a large number of instruments in the embankment and the foundation to confirm that forces in the reinforcement, movements of the embankment, and pore pressures in the foundation were within acceptable limits during and following construction. The information derived from these instrumentation studies has been used to monitor construction progress and assess the accuracy of the finite element analyses and stability analyses, as explained subsequently.

After construction, a second finite element analysis was performed by Schaefer and Duncan *(3)* for the Huntington District. The purpose of this new analysis was to more closely represent the actual field conditions at the instrumented sections, including two layers of reinforcement as actually installed at the Sta. 9+00 cross section and slightly different foundation and embankment strengths than had been used in

J. M. Duncan, Department of Civil Engineering, Virginia Polytechnic Institute and State University, Blacksburg, Va. 24061. V. R. Schaefer, Department of Civil Engineering, University of New Mexico, Albuquerque, N. Mex. 87131. L. W. Franks, Huntington District, U.S. Army Corps of Engineers, 502 8th St., Huntington, W. Va. 25701. S. A. Collins, Federal Energy Management Administration, 1040 Austin Ave., Atlanta, Ga. 30307.

the original analyses performed by WES. These changes were found to have only small effects on the calculated results. Both the original WES analyses and the more recent analyses performed by Schaefer and Duncan *(3)* are in good agreement with the field measurements, indicating that finite element analyses combined with conventional limit equilibrium analyses provide a suitable basis for design of reinforced embankments on weak foundations.

PROPERTIES OF THE DIKE AND FOUNDATION

Mohicanville Dike is located on a glaciated plateau of glacial till in a moraine belt. The site contains a peat bog that developed in postglacial kettle holes *(4)*. The foundation soils consist of peat overlying soft clay, as shown in Figure 1. Soil properties were assessed through field vane shear tests and laboratory triaxial, consolidation, permeability, compaction, and classification tests *(1)*. A summary of the test results is shown in Table 1.

The foundation clay ranges in thickness from 10 to 60 ft and varies across the site from a silty clay to an organic clay. The shear strength of the clay where it has not been loaded by the old dike is small, due to the small unit weight of the overlying peat deposits. Typical undrained shear strength values range from 300 to 1,000 lb/ft^2, as shown in Figure 1. Stress-strain characteristics of the clay are shown in Figure 2a, consolidation test results in Figure 3.

The peat varies from fibrous near the ground surface to amorphous in the lower portions of the deposit, and is 16 to 20 ft thick in the virgin state. Where it was compressed under the weight of the old embankment, the thickness of the peat was reduced to 11 to 15 ft. Typical undrained shear strengths for the peat ranged from about 150 lb/ft^2 in the virgin state to about 500 lb/ft^2 where it was compressed under the old embankment, as shown in Figure 1. Stress-strain characteristics of the peat are shown in Figure 2b, consolidation characteristics in Figure 3.

The permeability of the peat was assessed by performing field and laboratory permeability tests. In Figure 4 the results are compared with values for California peats obtained by Weber *(5)*. For the California and the Mohicanville peats, the variations of permeability with consolidation pressure are similar. The line shown in Figure 4 was used in the finite element analyses to represent the variation of permeability with effective stress.

TABLE 1 SUMMARY OF SOIL PROPERTIES

Soil Property	Foundation Clay	Peat	Embankment Fill
Unified Classification	CL, CH, and OH	Pt	CL
Dry Unit Weight, pcf	OH: 40 to 84 CL-CH: 60 to 91	10 to 36	113 to 120
Water Content, %	OH: 37 to 67 CL-CH: 28 to 65	280 to 540	15 to 18
Liquid Limit	28 to 80	--	27 to 57
Plastic Limit	16 to 37	--	17 to 21
Plasticity Index	14 to 43	--	10 to 37
Specific Gravity	2.61 to 2.80	1.50	2.70 to 2.80
% Finer than			
#4	100	--	73 to 100
#10	100	--	60 to 95
#40	96	--	40 to 90
#200	90 to 95	--	25 to 80
2 micron	10 to 40	--	10 to 20
Undrained Shear Strength, psf	400 to 1000	200 to 500	3000 to 6000
O', degrees	25 to 29	17 to 32	32
c', psf	0 to 500	200 to 400	200
Permeability, ft/yr	0.1 to 10	see Figure 4	0.1 to 1

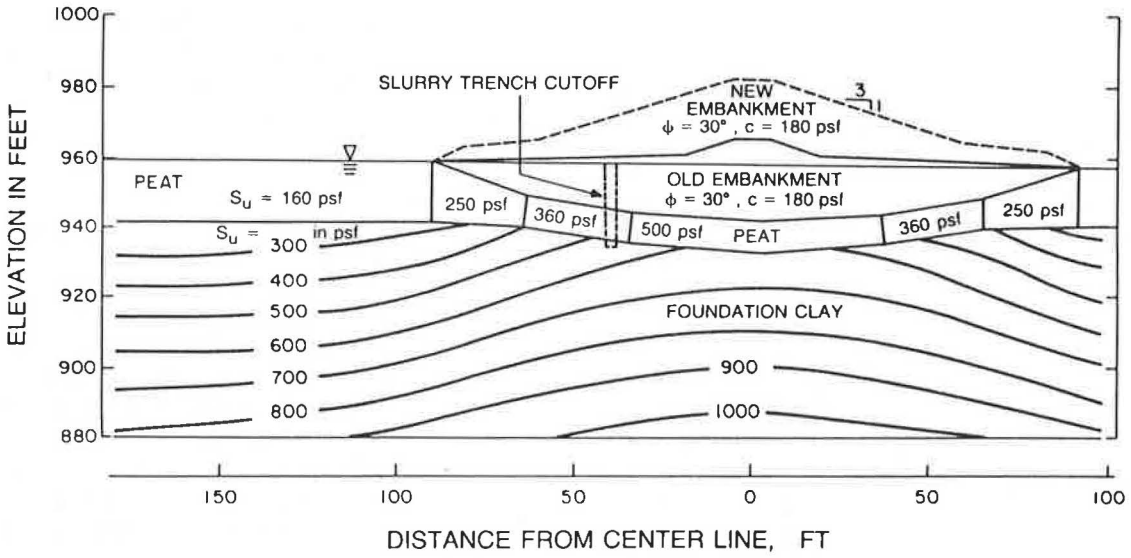

FIGURE 1 Typical cross section and undrained shear strengths [after Collins et al. *(1)*].

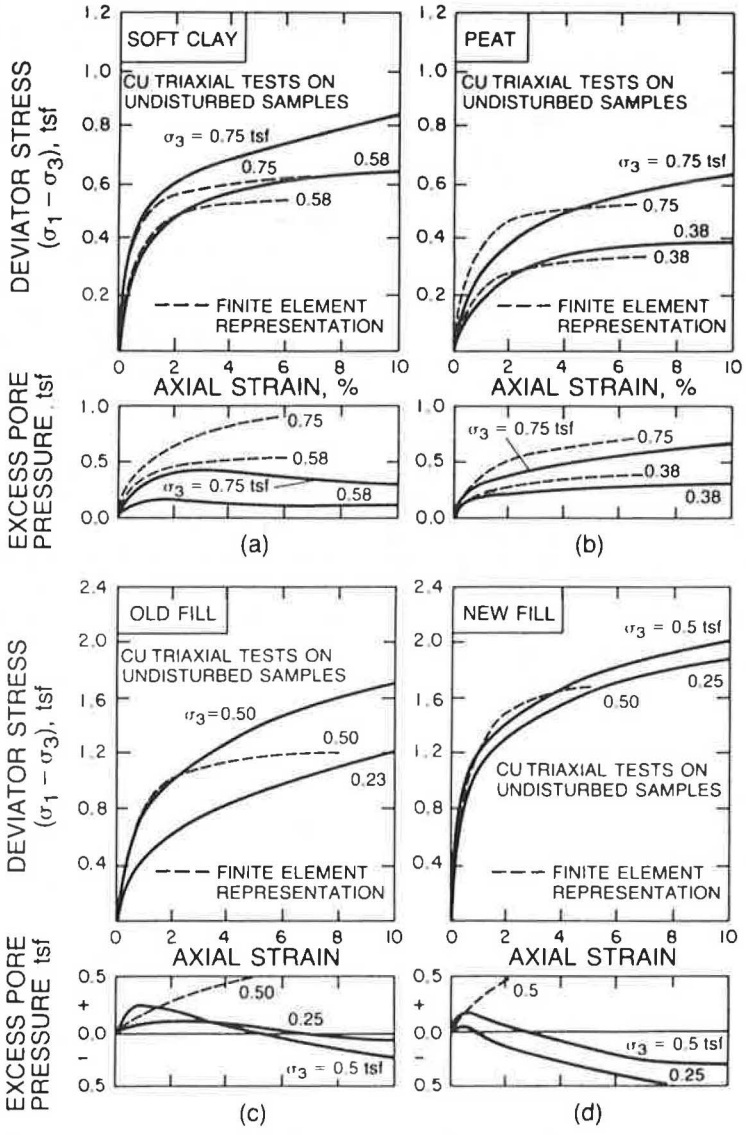

FIGURE 2 Stress-strain curves from consolidated undrained triaxial tests with pore pressure measurement.

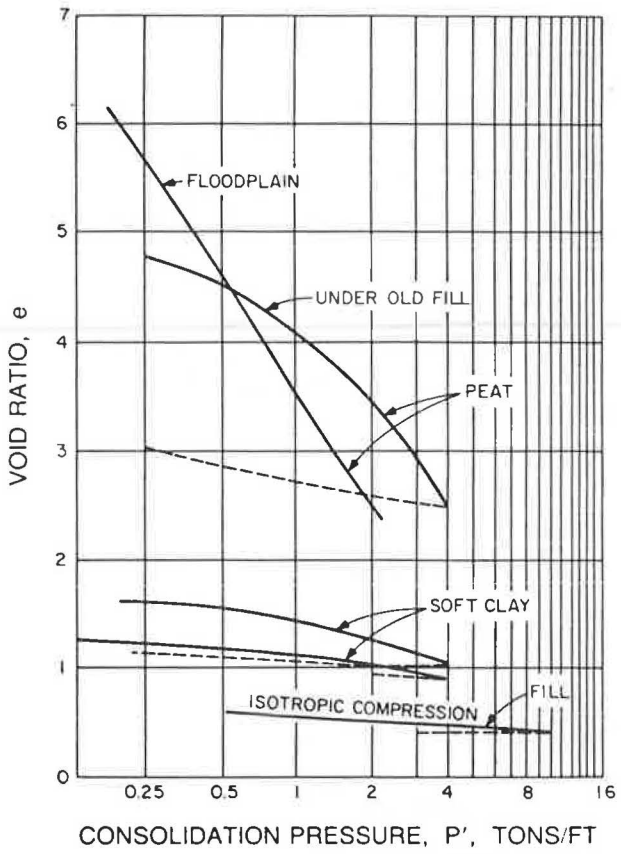

FIGURE 3 Consolidation curves for embankment and foundation soils.

Both the old and new embankment fill materials were derived from glacial tills in the surrounding uplands. The fill material grades as gravelly sandy clay with zones of gravelly clay. Pockets of poorly graded sand, silt, silty sand, and clayey gravel are also present. As it was compacted in the new embankment, the fill exhibits good shear strength characteristics and is quite ductile at the in-place water content of −2 to +2 percent with respect to optimum. The strength of the old fill is lower, especially in areas where previous failures occurred.

The stress-strain and strength characteristics of the old and new fill are shown in Figures 2c and 2d. The tests on the new fill were performed on block samples taken from the embankment after construction. The new fill exhibits higher strength and modulus than the old fill. Consolidation characteristics of the old fill are shown in Figure 3.

PROPERTIES OF THE REINFORCEMENT

The stability analyses performed for design by Law Engineering Testing Co. *(2)* indicated that a reinforcing force of about 30,000 lb per foot of embankment would be required to raise the factor of safety to a value of 1.3 at the end of construction, as required by Corps of Engineers design standards. The calculated distribution of reinforcing forces across the embankment required for a factor of safety equal to 1.3 is shown in Figure 5. The finite element analyses performed before construction *(2)* showed that a stiff reinforcing material would be required to achieve this amount of reinforcing force under working conditions.

To meet these requirements of stiffness and strength, a specially fabricated steel mesh was used. The mesh consists of No. 3 bars spaced 2 in. apart along the length of the dike, welded into a mesh with No. 2 bars parallel to the embankment axis, which are spaced on 6-in. centers. This mesh provides an ultimate reinforcement strength of 48,000 lb per foot of embankment.

The mesh was transported to the site in 8-ft-wide rolls and was unrolled at the site by the same machine used to roll it in the fabricating plant. When unrolled, the strips of mesh were cut into two pieces, each 8 ft wide and 160 ft long. These strips were dragged into position on the embankment with a bulldozer and end loader. The reinforcement extended 80 ft upstream and downstream from the centerline of the embankment between Station 3+00 and Station 14+00.

The reinforcing mat was placed at elevation 960 ft, approximately 4 ft above original ground elevation. In most areas, about 6 to 8 ft of old fill were excavated to reach this elevation before placement of the steel mesh. In one area where exceptionally large settlements occurred, additional fill had to be placed to increase the surface elevation to 960 ft before the steel mesh was placed. A second layer of reinforcing was placed at elevation 961 ft between Station 8+40 and Station 9+40 as an added precaution, because of the uncertain

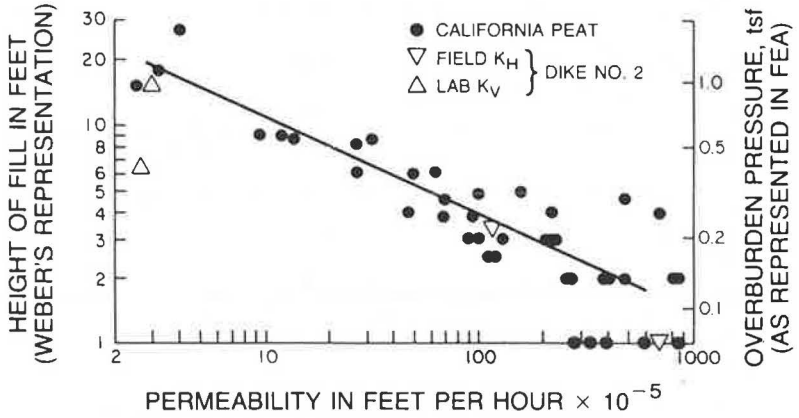

FIGURE 4 Variation of permeability with loading [after Collins et al. *(1)* and Weber *(5)*].

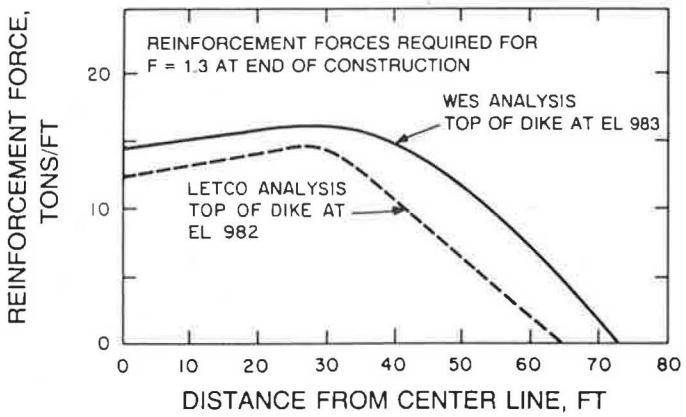

FIGURE 5 Distribution of required force from reinforcement to provide minim factor of safety of 1.3 [after Fowler et al. *(2)*].

foundation conditions in this area. Extensive failure occurred in this area in 1936 during the original construction, and a localized failure occurred in 1983 during construction of a slurry trench.

FIELD MEASUREMENTS

The dike, its foundation, and the reinforcement were instrumented extensively, as shown in Table 2. A total of 39 piezometers of three different types were used to measure foundation pore pressures. Some 13 inclinometers were installed to measure movements of the embankment and the foundation; 9 of these are vertical, and 4 are horizontal, placed just above the reinforcing mesh to determine settlements at this elevation. Also, 12 settlement plates were installed to measure vertical movements near the reinforcement level, and 25 surface monuments were installed to supplement the other measurements.

Strain gauges on the reinforcement provided a direct means for determining the force in the steel reinforcement throughout construction. Of 76 strain gauges installed on the reinforcing mesh, only 2 have failed, and the data appear to be consistent and reliable.

Reinforcement Forces

Values of reinforcement force measured at the embankment centerline at Stations 6+55 and 8+00 are shown in Figure 6, which covers the period from August to November, 1984. The force in the reinforcement increases as the embankment height increases. Between Points A and B in Figure 6, the reinforcing force increases approximately linearly with embankment height. In November, construction was halted for the winter and was not resumed until June 5, 1985. Placement of the first 3 or 4 ft of fill on the embankment after the winter shutdown induced little additional force in the steel. Aging of the recently compacted embankment fill over the winter may have caused the stiffness of the fill to increase sufficiently to affect its interaction with the reinforcement and the foundation. This possibility is currently under investigation through laboratory tests and finite element analysis. At more than 14 ft, as further fill was placed on the embankment the rate of increase of reinforcing force returned to that before the winter shutdown.

An interesting phenomenon is indicated by the data at Point C in Figure 6. At a constant embankment height of 19 ft, the reinforcement force increased by about 2 tons/ft over a period of 9 days. This increase in force is thought to be due to undrained creep in the foundation soils.

TABLE 2 INSTRUMENTATION AT MOHICANVILLE DIKE NO. 2

	Station						
Instrument	4+75	6+55	8+00	9+00	11+00	12+20	Total
Piezometers							
Open tube	1	3		4		1	9
Electric	1	2		3		1	7
Pneumatic	4	8		7		4	23
							39
Inclinometers							
Vertical	1	3		3	1	1	9
Horizontal	1	1		1		1	4
Strain gauges on steel	2	29	2	29 lower 10 upper	2	2	76
Settlement plates	3	3		3		3	12
Surface displacement monuments	5	5	5	5	5		25

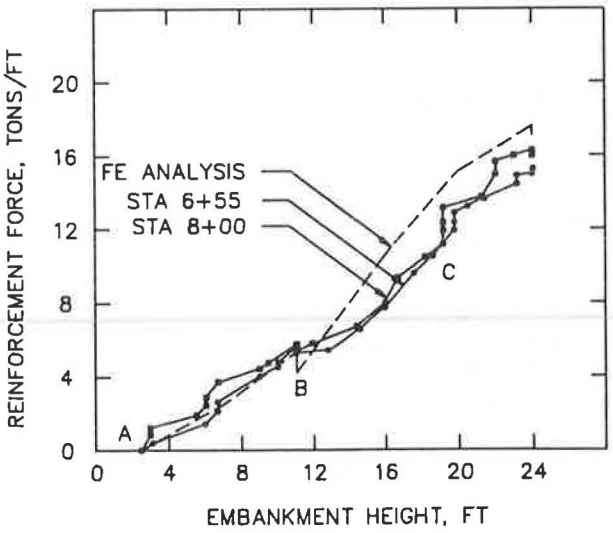

FIGURE 6 Centerline reinforcement forces versus embankment height for Stations 6+55 and 8+00.

Between Stations 8+40 and 9+40, two layers of reinforcement were used, spaced 1 ft apart vertically. This area is where the worst failures occurred during construction of the original embankment, where failure occurred in a wall of the slurry trench, and where the foundation conditions are most uncertain. The measurements of reinforcing force made in this area are shown in Figure 7. The lower layer of steel carries considerably greater force than the upper layer, although both have the same properties. The fraction of the total reinforcement force carried by the lower layer increases with increasing embankment height. After construction of the embankment was completed (Point *D* in Figure 7), the force in the lower layer of steel mesh increased slightly, whereas the force in the upper layer decreased by about 50 percent. Although many factors may be involved in this complex behavior, the most important factor appears to be that the effectiveness of embankment reinforcement is improved by placing it lower within the embankment,

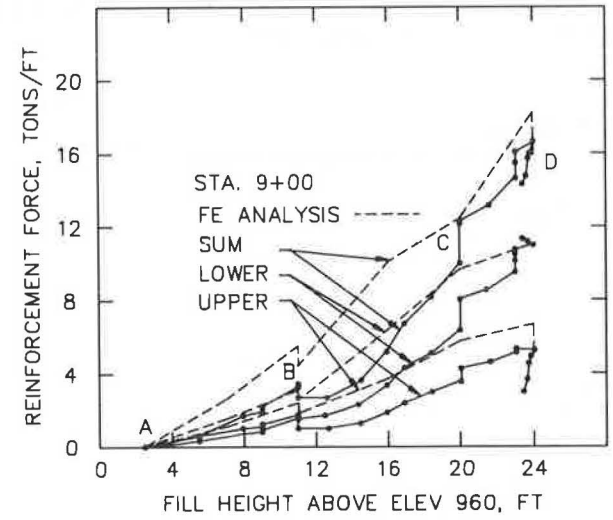

FIGURE 7 Centerline reinforcement forces versus embankment height for Station 9+00.

and the lower layer of steel mesh is thus in a position to be more effective than the upper layer.

Distributions of the reinforcement forces across the embankment at Station 6+55 are shown in Figure 8 for various times during construction. Throughout construction, the maximum force occurs at the center of the embankment, as would be expected. In the downstream portion of the embankment, the variations of force with distance from the centerline are smooth and regular, indicating that the measurements probably contain little scatter. In the upstream portion of the embankment, the reinforcement forces are more erratic and are believed to be influenced by the slurry trench cutoff wall, which was located 45 ft upstream from the centerline.

Pore Pressures

Values of pore pressure measured during construction are shown in Figure 9 for piezometers in the peat and in Figure 10 for piezometers in the foundation clay. In both the peat and the clay, the increase in pore pressure is greater beneath the center of the embankment than for the piezometers located upstream and downstream. Both in the peat and in the clay, the response for piezometers downstream from the center is slightly greater than for piezometers the same distance upstream. This difference may be due to the effect of the slurry trench cutoff, which is restricting drainage of the foundation soils. The cutoff is located 45 ft upstream from the embankment centerline and probably restricts lateral migration of high pore pressures from the center of the embankment in the upstream direction.

The rate of increase of pore pressures beneath the center of the embankment during construction was approximately 1 ft of increase in pressure head for each 1 ft of increase in embankment height. Because the moist unit weight of the embankment fill is approximately twice the unit weight of water, this response corresponds to a value of the pore pressure ratio r_u, approximately equal to 0.5 (r_u = change in pore pressure divided by change in overburden pressure). The pore pressures both in the peat and in the clay decreased appreciably during the winter shutdown (Point *B* in Figures 9 and 10.)

Settlements and Horizontal Movements

Settlements measured by a horizontal inclinometer located at Station 6+55 are shown in Figure 11. The settlement at the beginning of the second construction season was largest at the downstream toe, where approximately 0.5 ft of settlement occurred. Subsequently, during the second construction season, and after the end of construction, the settlements near the center of the embankment were greater than those that occurred upstream and downstream.

The pattern of settlements shown in Figure 11 may be due to two separate influences, both of which tended to cause the downstream settlements to be larger than the upstream settlements. One is the influence of the old fill. The upstream portion of the old dike at this station was considerably thicker than the downstream portion. This greater fill thickness would have the

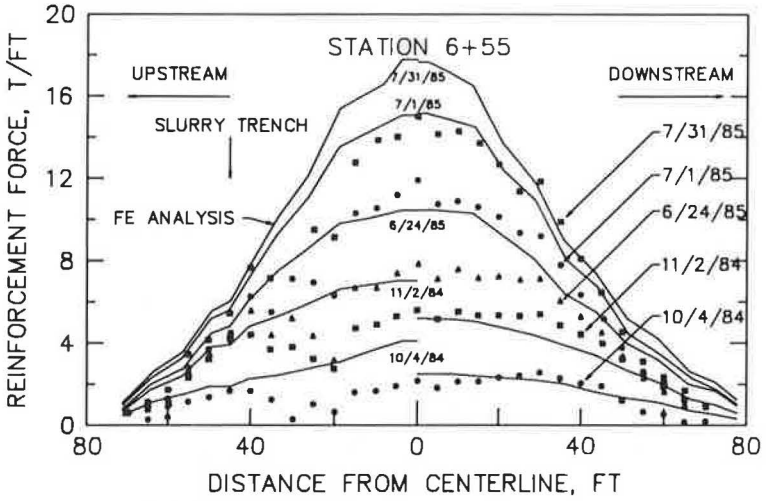

FIGURE 8 Reinforcement force distribution about the centerline for Station 6+55.

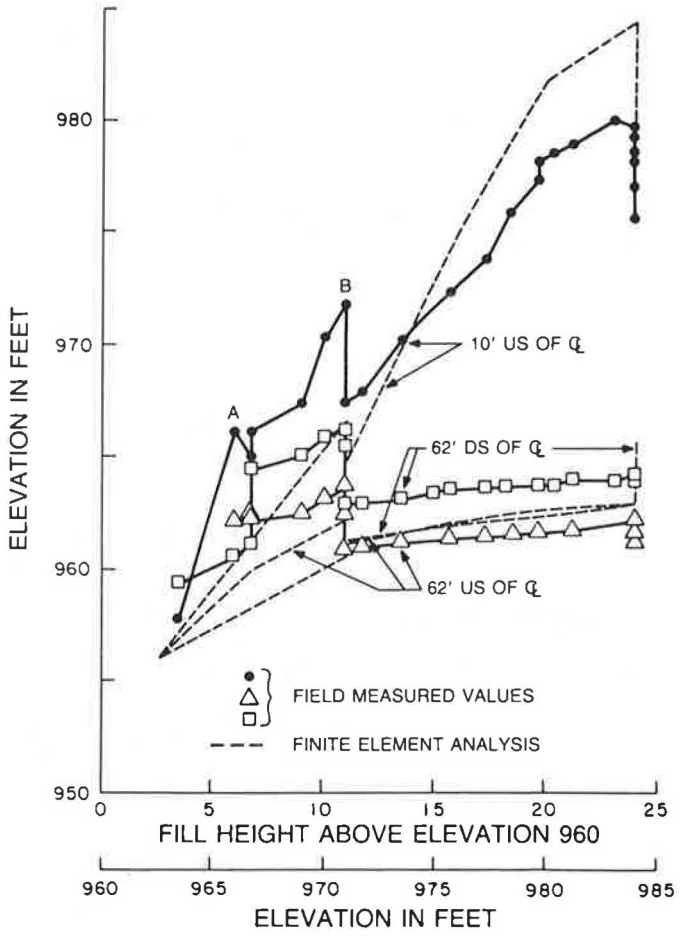

FIGURE 9 Piezometric levels in peat versus embankment height for Station 6+55.

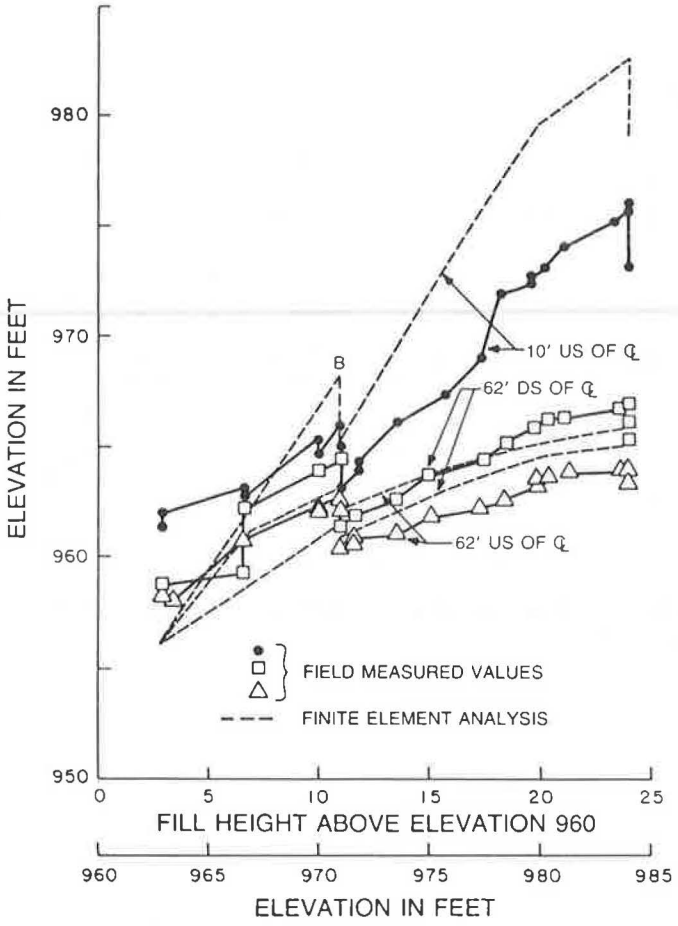

FIGURE 10 Piezometric levels in foundation clay versus embankment height for Station 6+55.

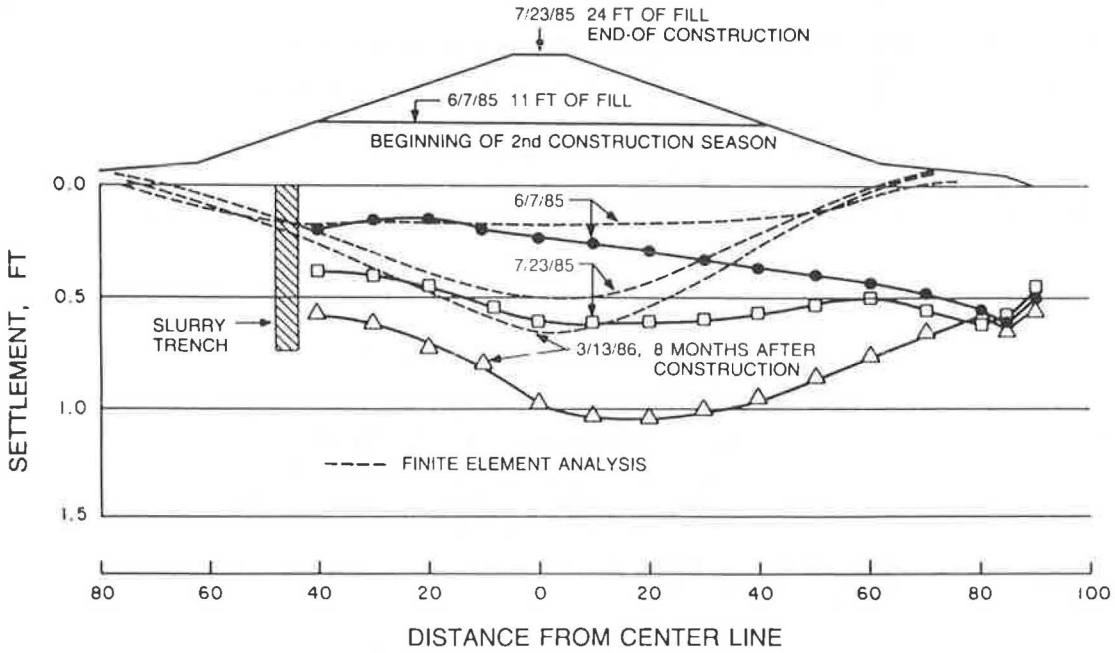

FIGURE 11 Settlement profile along Station 6+55.

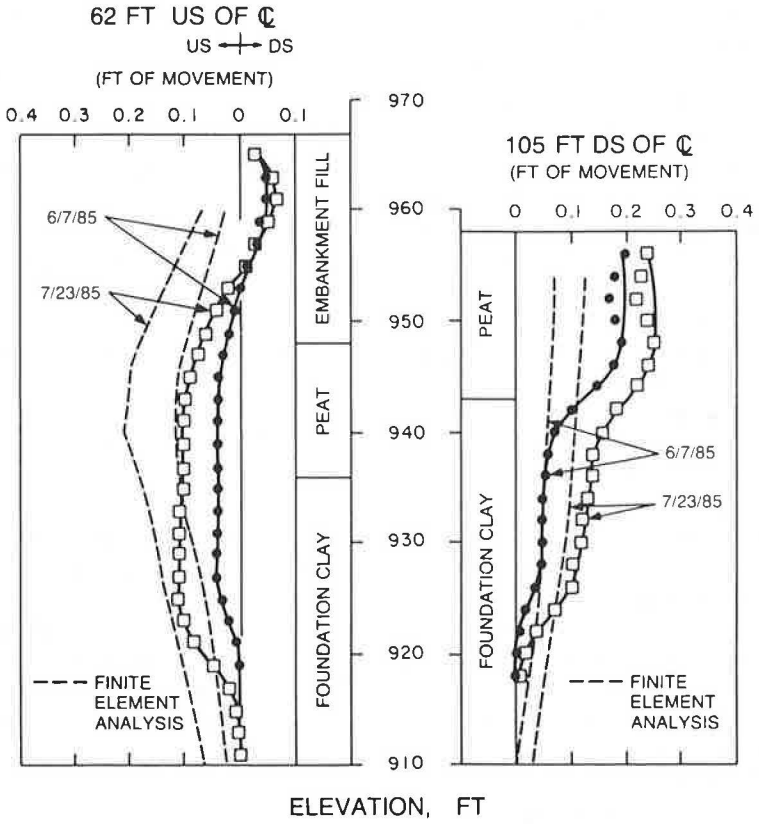

FIGURE 12 Movements of vertical inclinometers near embankment toes at Station 6+55.

effect of preconsolidating the upstream area more than the downstream area and would lead to smaller settlements upstream *(6)*.

A second influence is the slurry trench cutoff. This cutoff, by inhibiting drainage of the foundation soils in the upstream direction, may have effectively trapped pore pressures in the peat and clay beneath the upstream central portion of the embankment. As a result the settlements beneath the upstream portion of the embankment were smaller than those beneath the downstream portion. According to this explanation, the settlements upstream and downstream would become more nearly equal with time.

Horizontal movements measured near the upstream and downstream toes of the embankment at Station 6+55 are shown in Figure 12. The movements are small, the largest measured movement being less than 0.25 ft. In both cases, most of the shear deformations that give rise to the horizontal movements occur in the clay layer, within the depth interval between elevations of 915 and 930 ft. Also the movements at the level of the reinforcement are small, as expected. The measured movements at the elevation of the reinforcement are in fact less than 0.02 ft.

FINITE ELEMENT ANALYSES

As mentioned previously, finite element analyses were performed for design at WES *(2)*, and additional analyses were performed by Schaefer and Duncan *(3)* after construction, in connection with evaluation of the results of the instrumentation program. The same computer program was used in both analyses. The program, CON2D, was developed originally by Chang and Duncan *(7)* and was subsequently modified by Duncan et al. *(8)* and by Schaefer and Duncan *(2)*.

CON2D uses a modified form of the Cam Clay constitutive model and is capable of analyzing consolidation of soils as well as deformations under undrained and fully drained conditions. The stress-strain parameters used in the model can be evaluated using the results of conventional laboratory strength and consolidation tests. Reinforcing in embankments is modeled by bar elements with zero flexural stiffness, and slip between the reinforcement and the adjacent soils is modeled by special interface elements.

The degree of agreement between the actual stress-strain characteristics of the soil and those modeled by CON2D can be evaluated by using the parameters to calculate triaxial stress-strain curves, and comparing the computed stress-strain behavior with experimental results. Comparisons for the clay and peat from the foundation of Mohicanville Dike and for the old and new embankment fill are shown in Figure 2. The stress-strain curves are modeled accurately by the modified Cam Clay parameters used in the finite element analyses. The degree of agreement is not as good for the pore pressures, but the results shown in Figure 2 represent the best agreement that could be achieved within the constraints of the constitutive model. In selecting the parameters used in the analyses, emphasis was placed on matching the actual behavior of the soils in the small-strain range, because it was known that the actual strains would be small, provided that the design analyses were correct and the embankment remained stable. In the range of strains below 2

percent, the calculated pore pressure variations were in reasonable agreement with the measured values.

Results of the analyses performed by Schaefer and Duncan *(2)* are shown in Figures 6 through 12, together with measured values from the field instrumentation studies.

Reinforcement forces at the embankment centerline are shown in Figure 6. The calculated values are in good agreement with those measured during the first construction season. The calculated reduction in force during the winter shutdown due to consolidation of the foundation soils is considerably greater than the amount that actually occurred. After winter shutdown the calculated rate of increase in force was slightly greater than that measured. As explained previously, it is believed that the smaller rate of increase in reinforcement force after the winter shutdown may have been due to an increase in stiffness of the fill that resulted from aging during the shutdown period. This effect was not represented in the analyses presented here but will be considered in further studies.

Calculated and measured reinforcement forces at Station 9+00, where two layers of reinforcement were used, are shown in Figure 7. The calculated values are higher than the measured values through most of the embankment construction, and the difference is greatest during the first part of the second construction season. The calculated and measured values agree well in two respects. One is the decrease in reinforcing force during the shutdown period and during the period following construction. The other is the tendency for the upper layer of reinforcing to be less effective than the lower layer and for the force in the upper layer to decrease at a faster rate than that in the lower layer.

One aspect of the interaction between the reinforcing and the embankment was not modeled by the analyses. During a pause in the second construction season, the reinforcing force increased. As mentioned previously, this increase in force may have been due to undrained creep in the foundation. A similar increase near the end of construction may also have been due to creep effects. Because the modified Cam Clay model used in the analyses does not simulate creep effects, the finite element analyses do not simulate this aspect of the actual behavior. The field data indicate that after a period of 3 or 4 weeks the effects of creep die out, and the reinforcing force begins to decrease as the foundation soils consolidate.

Calculated distributions of reinforcing force across the embankment are compared to the measured values in Figure 8. The calculated distributions are discontinuous at the centerline because they were calculated by using two half-meshes rather than a whole mesh. It can be seen that the agreement is quite good overall, especially for the downstream half of the embankment. The behavior of the upstream half of the embankment was apparently affected to some degree by the slurry trench cutoff. Because the cutoff was represented in the analyses by only one element's width, its interaction with the foundation and the embankment and its effect on the behavior may not have been accurately reflected in the calculated results.

In Figures 9 and 10, calculated pore pressures are compared to the measured values. The calculated values are smaller than the measured values at the early stages and larger than the measured values at the later stages. These differences appear to be consistent with the differences between the calculated and measured laboratory test results, as shown in Figure 2 and discussed previously. The calculated amounts of decrease in pore pressure during shutdown periods and after construction are in good agreement with those measured, indicating that the consolidation characteristics of the foundation soils are reasonably accurately represented in the analyses.

The calculated settlements are compared with those measured in Figure 11. The agreement is not good at the early stages. As noted previously, the settlements at this time were strongly affected by the variations in preconsolidation pressure from upstream to downstream, and this detail of the initial conditions was not represented in the finite element analyses. The settlements that occurred during the second construction season and those that occurred after construction are in better agreement with the calculated values.

Calculated horizontal movements are compared with those measured near the toes of the embankment as shown in Figure 12. The calculated variations of horizontal movement with depth are much more uniform than the measured values. As mentioned previously, much of the measured lateral movement was caused by deformations of the soils between elevations of 915 and 930 ft, indicating existence of a soft or weak zone in this area. The fact that such a weak zone was not represented in the finite element analyses is probably responsible for the differences between the measured and the calculated horizontal movements.

CONCLUSIONS

The experience gained from design, construction, instrumentation, and analysis of the Mohicanville Dike has provided information of considerable value with regard to the behavior of reinforced embankments on weak peat and clay foundations.

The experience has shown that it is feasible to effectively stabilize an embankment on a weak foundation using a single layer of reinforcement near the base of the embankment. Because the Mohicanville Dike is 28 ft high, and the necessary improvement in safety factor was considerable (about 40 percent), the amount of reinforcing force required was large (about 30,000 lb per foot of length of embankment). A steel mat, specially fabricated for the job, proved to be an economical reinforcing material from the points of view of both initial cost and construction feasibility. Although the steel will probably corrode in time and its reinforcing capacity will decrease, the foundation soils will have consolidated and gained strength by that time, and the reinforcing will no longer be needed to maintain the stability of the embankment.

The instrumentation studies performed on the embankment during and following construction have provided valuable information regarding the accuracy of the finite element analyses and the limit equilibrium slope stability analyses used to design the embankment. Comparisons of the calculated and measured reinforcement forces indicate that the finite element analyses provide an effective means of estimating the amount of reinforcing force that would develop during construction and the rate at which the force would decrease after construction as the foundation soils consolidate. The measured movements of the embankments have been small, consistent with the expected behavior of an embankment that has a factor of safety equal to 1.3 at the end of construction. Thus the combination of finite

element analyses to estimate reinforcing forces and conventional limit equilibrium analyses to calculate a factor of safety appears to provide an effective approach for design of reinforced embankments on weak foundations.

ACKNOWLEDGMENTS

Many people have contributed to the design, construction, and evaluation of the performance of Mohicanville Dike No. 2. The writers wish to specifically acknowledge the contributions of James Coffman and Thomas Plummer of the Huntington District; Jack Fowler, Roy Leach, John Peters, and Ray Horz of WES; and George Sowers and David Wheeless of Law Engineering Testing Company; without whose efforts the design, construction, and instrumentation studies would not have been possible.

REFERENCES

1. S. A. Collins, W. Rogers, and G. F. Sowers. *Report of Embankment Reanalysis—Mohicanville Dikes.* Huntington District, U.S. Army Engineers, Huntington, W.Va., July 1982.
2. J. Fowler, R. E. Leach, J. F. Peters, and R. C. Horz. *Mohicanville Reinforced Dike No. 2 Design Memorandum.* Geotechnical Laboratory, U.S. Army Engineer Waterways Experiment Station, Vicksburg, Miss., Sept. 1983.
3. V. R. Schaefer and J. M. Duncan. *Evaluation of the Behavior of Mohicanville Dike No. 2.* Huntington District, U.S. Army Corps of Engineers, Huntington, W.Va., Nov. 1986.
4. G. W. White. *Glacial Geology of Wayne County, Ohio.* Ohio Geological Survey Report 62, 1967.
5. W. G. Weber, Jr. Performance of Embankments Constructed over Peat. *Journal of the Soil Mechanics and Foundations Division,* ASCE, Vol. 95, No. SM9, Jan. 1969, pp. 53–77.
6. S. A. Collins. *Analysis of Instrumentation and Evaluation of Embankment Performance: Mohicanville Dike No. 2.* Huntington District, U.S. Army Corps of Engineers, Huntington, W.Va., June 1986.
7. C-S. Chang and J. M. Duncan. Analysis of Consolidation of Earth and Rockfill Dams. Report TE 77-3. U.S. Army Engineers Waterways Experiment Station, Vicksburg, Miss., Sept. 1977.
8. J. M. Duncan, T. B. D'Orazio, C-S. Chang, K. S. Wong, and L. Namiq. *CON2D: A Finite Element Computer Program for Analysis of Consolidation.* Report UCB/GT/81-10. College of Engineering, University of California, Berkeley, 1981.

Publication of this paper sponsored by Committee on Mechanics of Earth Masses and Layered Systems.

Design and Construction of Reinforced Embankments Over Weak Foundations

RUDOLPH BONAPARTE AND BARRY R. CHRISTOPHER

Experience with design and construction of reinforced embankments over saturated clay foundations is reviewed. Reinforcement materials considered are geotextiles and geogrids. The effects of tensile reinforcement include increased embankment stiffness and reduced shear stress and strain magnitudes and plastic deformations in the foundation. Analysis results show that reinforcement reduces embankment settlement and lateral spreading due to undrained constant-volume distortion. The conditions under which these performance improvements are significant are described. Limit equilibrium design procedures are discussed. Available information indicates that modified classical stability procedures are suitable for relatively uniform clay foundations. Their applicability to peat foundations appears to be more limited. Aspects of limit equilibrium analyses specific to use of reinforcement are discussed. These include *(a)* effect of the reinforcement force, *(b)* orientation of reinforcement force, *(c)* selection of reinforcement force for design, and *(d)* reinforcement embedment length. Simple design charts and figures presented can be used to make a preliminary assessment of overall factors of safety against foundation bearing capacity and slip surface failures and lateral sliding of the embankment. Last, construction aspects are described.

Tensile reinforcing elements may be used to increase the stability of embankments constructed over weak foundations. In this type of application, horizontal strips or layers of reinforcement are placed on the natural soil or within the base of the embankment with the remainder of the embankment constructed in the conventional manner. Materials used as tensile reinforcement include steel strips, bars, or meshes *(1)*, geotextiles *(2–5)*, geogrids *(6, 7)*, and other materials. In this paper, the use of polymer-based reinforcing elements such as geotextiles and geogrids is addressed. The use of steel reinforcement is described by Duncan et al. in another paper in this Record.

Reinforced embankments over weak foundations typically fall into one of two categories *(8)*. The more common category consists of embankments, dikes, or levees constructed over soft, saturated silt, clay, or peat layers (Figure 1a). In this category, the reinforcement is typically placed with its strong direction perpendicular to the centerline of the embankment, and plane-strain conditions are assumed to prevail. Additional reinforcement with its strong direction oriented parallel to the centerline may also be required at the ends of the embankment.

The second category of reinforced embankment applications consists of those in which the foundation below the embankment is locally weak and the role of the reinforcement is to bridge over the weak zones or voids. These zones or voids may be caused by sinkholes, thawing ice, old stream beds, or pockets of silt, clay, or peat (Figure 1b). In this category of applications, tensile reinforcement may be required in more than one direction, and thus the strips or layers of reinforcing material may be placed with varied orientations with respect to the embankment centerline. Reinforcement design for the case of an embankment over a void has typically been based on the conservative assumption *(7, 9, 10)* that the reinforcement acts as a tensioned membrane supporting the full overburden pressure (Figure 2). The equations shown in Figure 2 are from Giroud *(9)*. T is the tensile force per unit width in the reinforcement; an approximate value for the reinforcement stiffness required to span a circular void of diameter b can be obtained by dividing K by 2. This second category of applications will not be discussed further.

MECHANISMS OF REINFORCEMENT FOR EMBANKMENTS OVER WEAK FOUNDATION LAYERS

The mechanism of reinforcement for an embankment constructed over a uniform deposit of saturated clay is to stiffen the base of the embankment and reduce shear stress magnitudes and plastic shear deformations in the foundation. This mechanism is illustrated in the results from a recent investigation by Low and Duncan *(11)*, who used finite element analyses that included nonlinear (hyperbolic) soil stress-strain behavior. Their analyses showed that tensile reinforcement placed at or near the base of an embankment increased the stiffness of the embankment fill. This increase was proportional to the tensile stiffness K (reinforcement tensile modulus multiplied by reinforcement cross sectional area per unit width) of the reinforcement. Only part of the mobilized tensile force went into stiffening the embankment fill. The rest of the tensile force was transferred from the stiff reinforced fill to the less stiff foundation soil below the reinforced zone. The average shear stress and strain levels in the foundation were thereby reduced.

The combined effects of increased fill stiffness and reduced shear stresses and strains in the foundation soil include reduced undrained (constant-volume) foundation distortion beneath the embankment as well as reduced embankment spreading and initial (undrained) embankment settlements. These effects are illustrated in Figure 3 for an embankment on a saturated clay foundation with an unreinforced factor of safety (FS) of just less than 1.0 and a ratio of foundation depth to crest width (D/B) equal to 0.36. [This D/B ratio and low unreinforced FS were selected to highlight the effect of reinforcement. A larger

R. Bonaparte, GeoServices Inc., Consulting Engineers, 5950 Live Oak Pkwy., Norcross, Ga. 30093. B. R. Christopher, STS Consultants Ltd., 11 Pfingsten Rd., Northbrook, Ill. 60062.

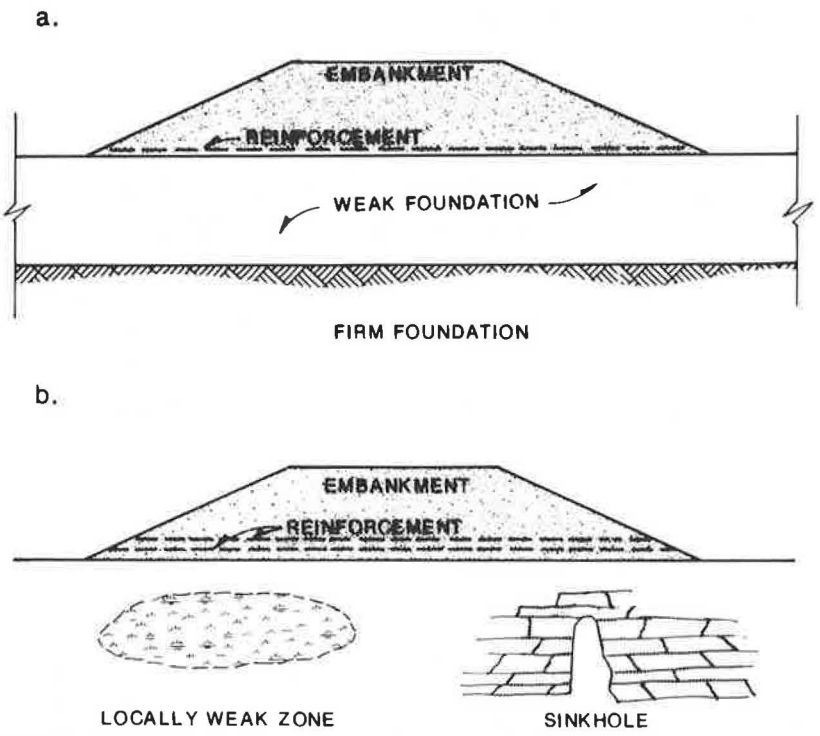

FIGURE 1 Embankments on weak foundations: (a) embankment on uniform weak foundation; (b) embankment on locally weak foundation with lenses of clay or peat, or with sinkholes.

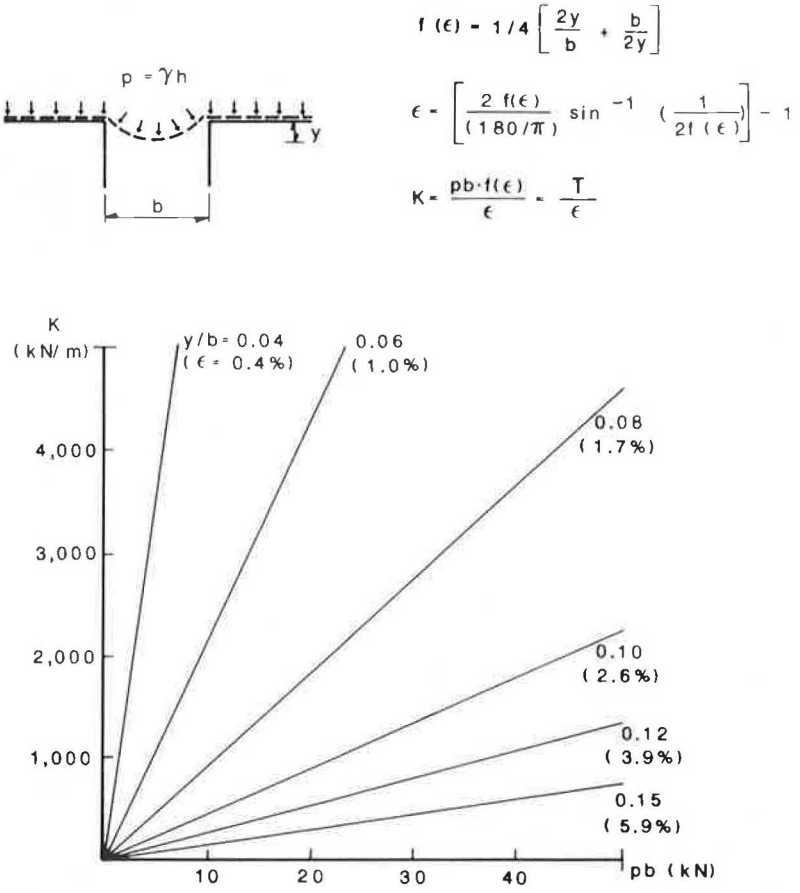

FIGURE 2 Tensioned membrane analysis of an embankment spanning an infinitely long void of width *b*.

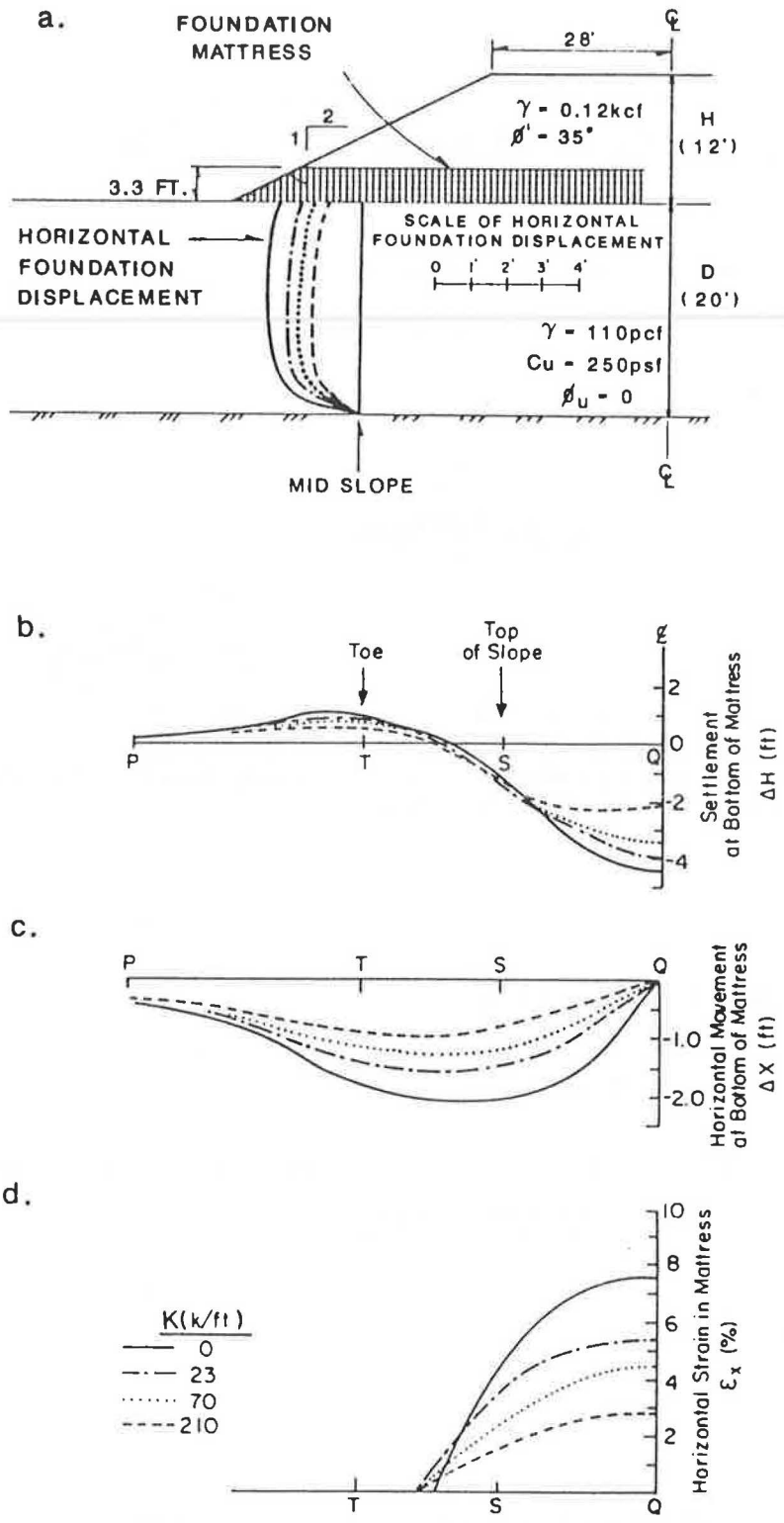

FIGURE 3 Behavior of embankments with varying reinforcement stiffnesses constructed over a uniform weak foundation layer.

unreinforced *FS* and larger or smaller *D/B* would show a smaller influence of the reinforcement. Rowe and Soderman *(12)* discuss the influence of *D/B*.] The results in Figure 3 were predicted by Low and Duncan *(11)*, who used nonlinear finite element analysis to analyze the embankment-foundation mattress system shown in the figure. The mattress consisted of a 1-m-thick geogrid-reinforced zone that was assumed to have uniform tensile stiffness. Low and Duncan *(11)* also showed that the influence of this mattress on embankment performance is roughly equivalent to that of a single layer of reinforcement of similar tensile stiffness located at the mid-height elevation of the mattress. On the basis of Low and Duncan's work, as well

as that of Rowe and his coworkers *(12–17)*, and others [summarized by Christopher and Holtz *(18)*], a number of general observations can be made with respect to the beneficial effects of reinforcement placed at or near the base of embankments built over weak foundation layers:

1. Tensile reinforcement reduces displacements beneath the embankment centerline and heave near the embankment toe caused by undrained, constant-volume deformation. Tensile reinforcement also reduces vertical and horizontal displacements in the embankment.
2. By reducing the magnitude of shear deformations at the foundation-embankment interface, reinforcement decreases the average shear stress and shear strain magnitudes and the extent of the plastic zone in the foundation.
3. The improvements described in embankment performance increase with increasing mobilized reinforcement force. For a given embankment, the mobilized reinforcement force increases with increasing reinforcement tensile stiffness and decreasing foundation soil modulus (strength). The performance improvements can be significant for embankments with unreinforced factors of safety less than one (Figure 3) but decrease for unreinforced *FS* values much above 1. All other factors being equal, the mobilized reinforcement force increases with increasing D/B, up to D/B approximately equal to 0.4. For deep deposits with D/B greater than about 0.8, the mobilized reinforcement force will be small *(12)*.
4. Tensile reinforcement may increase the height to which many types of embankments can be constructed without inducing a foundation failure. Alternatively, for a given embankment height, tensile reinforcement increases the factor of safety against foundation failure.
5. The reduction in shear stress and strain magnitudes in the foundation due to reinforcement is largest at shallow depths. A decrease in shear stress magnitude at shallow depths is important for sites at which a desiccated crust is underlain by saturated clay that exhibits a normally consolidated strength profile. In these cases, shear stresses will be reduced in the zone of minimum shear strength just below the crust and the failure surface will be forced deeper into stronger soil *(19, 20)*.

The reinforcement does nothing to increase the strength of the foundation soil. Therefore the foundation soil must have adequate strength to support the entire reinforced embankment. If the embankment is made very stiff through sufficient reinforcement, it may behave as a semirigid mat, and the critical failure mechanism becomes one of bearing capacity of the entire embankment. At that point, additional reinforcement will not further increase embankment stability. Also, reinforcement does not significantly reduce overall embankment settlement owing to consolidation of the foundation soil.

DESIGN OF REINFORCED EMBANKMENTS OVER WEAK FOUNDATION LAYERS

This section of the paper deals solely with the end-of-construction design of reinforced embankments over weak foundation layers. Locally weak foundations are not addressed. Primary emphasis is on uniform, purely cohesive foundation deposits, although some reference is made to peats. The reader is referred to the work of Rowe et al. for peats *(12–17)*.

Mechanisms of Failure

Published case studies *(11, 13, 16)* have shown that nonlinear finite element analyses can be used to evaluate the load-deformation response of embankments built over uniform weak foundations. However, the large majority of projects are designed using limit equilibrium procedures that evaluate a number of idealized failure mechanisms. The three failure mechanisms most often considered are *(18, 21, 22)*

- Overall bearing capacity failure of the foundation that may occur if the foundation is so weak that it cannot support the weight of the embankment;
- Lateral sliding of a portion of the embankment that may occur along the embankment-reinforcement interface, along the foundation-reinforcement interface, or along a shallow, weak seam or layer in the foundation soil; and
- Slip surface failure through the embankment and foundation.

Overall Bearing Capacity

A simplified analysis to use in calculating the factor of safety against bearing capacity failure is shown in Figure 4 [after Mandel and Salencon *(23, 24)*, originally published by Bonaparte et al. *(8)*]. Other bearing capacity analyses have also been discussed by Bonaparte et al. *(8)*.

If the embankment bearing capacity factor of safety is less than 1.0, the embankment cannot be constructed in the conventional manner without inducing foundation failure. Sometimes, however, embankments are built over very weak sites with bearing capacity factors of safety less than 1.0. In these cases, the fill sinks into the soft ground, displacing the foundation material. This displacement method of construction has its origins in nonreinforced embankment construction *(20)*. The displacement method is sometimes used with geotextile reinforcement to reduce the required fill volume. Geotextiles are beneficial in this case because they replace uncontained local failures of the embankment with more uniform sinking of the entire embankment. Under these circumstances, geotextile strains can be very large. Strains in excess of 30 percent have been measured *(4)*. Low-modulus, high-elongation geotextile products may be considered for displacement applications along with other design measures such as flat side slopes, berms, staged construction, and wick drains.

Lateral Embankment Sliding

A simplified analysis to use in calculating the factor of safety against failure due to lateral embankment sliding is shown in Figure 5. The important reinforcement properties for design against sliding are the soil reinforcement interface friction or adhesion characteristics, determined from direct shear tests and a limiting reinforcement tensile force per unit width, T (in kN/m); in Figure 1, $\lambda_1 \tan \phi'$ is the embankment fill-reinforcement interface friction, and λ_2 is the reinforcement-foundation interface adhesion. To control embankment cracking, T is usually

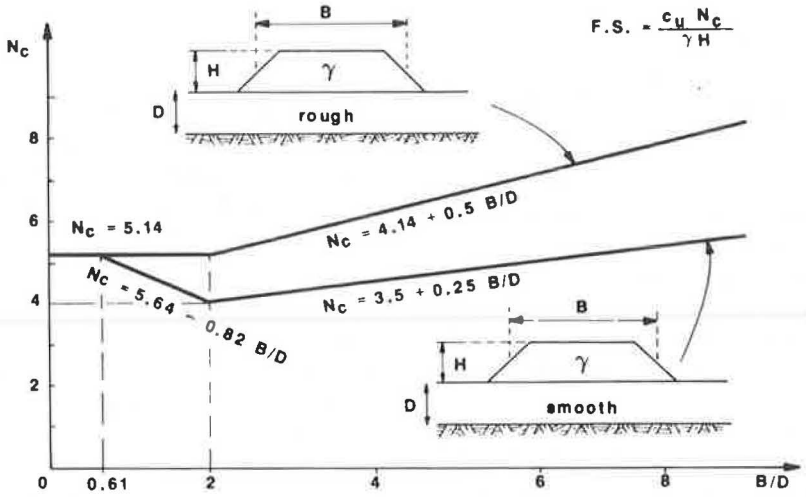

FIGURE 4 Bearing capacity failure of embankment.

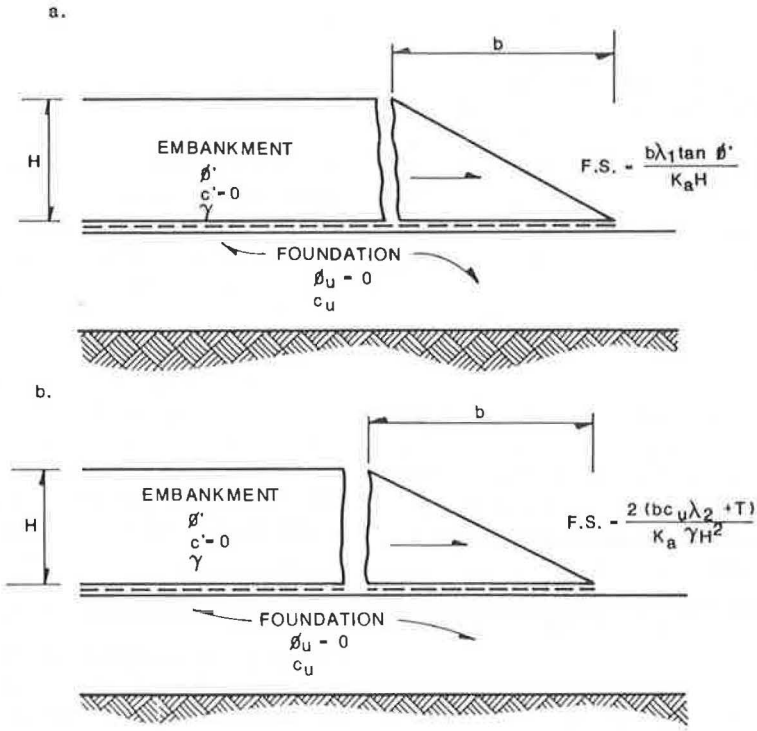

FIGURE 5 Lateral sliding of embankment: (a) embankment sliding over reinforcement; (b) reinforcement tensile rupture and embankment sliding over foundation soil.

selected on the basis of a limiting strain criterion. Bonaparte et al. *(8)* suggest a strain limit of not more than 5 percent for embankments constructed with cohesionless fill and not more than 2 percent for those constructed with cohesive fill.

Slip Surface Failure Through Embankment and Foundation

The reinforcement tensile force required to increase the factor of safety against slip surface failure through the embankment and foundation can be estimated by using modified classical limit equilibrium stability analyses. Usually it is assumed that the reinforcement provides a stabilizing tensile force at the location of its intersection with a considered slip surface. Although this approach is attractive because of its simplicity and connection to classical design, it involves a number of arbitrary assumptions whose verification through comparison with field performance or detailed numerical studies is lacking. Back-analyses suggest limited applicability of modified classical stability analyses to embankments over peat foundations *(14, 15)*. Back-analyses of embankments over relatively uniform saturated cohesive foundations appear to have given better results *(6, 11, 16)*.

Simplified design charts based on limit equilibrium analyses have been presented for embankments built on saturated clay foundations by Fowler *(25)*, Gourc *(26)*, Ingold *(27)*, and

Milligan and Busbridge *(28)*. Rowe and Soderman *(13, 17)* presented charts for peat foundations based on finite element analysis results. The charts prepared by Milligan and Busbridge *(28)*, shown in Figure 6, are conservative and useful. These charts show the required reinforcement force per unit width, T, to obtain a state of limit equilibrium (FS = 1). To obtain larger factors of safety, one uses the charts with factored soil strengths ($\tan \phi_f' = \tan \phi'/FS$; $C_{uf} = C_u/FS$). These charts were developed on the basis of *(a)* moment equilibrium along the critical circular arc through the foundation and Coulomb wedge through the embankment, and *(b)* horizontal force equilibrium along a critical multipart wedge. The latter equilibrium condition was found to control for ratios of foundation depth to embankment height of less than about 0.5. These charts are conservative (they overpredicted tensile force by 10 to 30 percent) when compared to computer solutions that use the stability analyses discussed subsequently. The charts are presented here as a simple means to obtain a preliminary indication of the influence of tensile reinforcement on a given design. Usually, however, real design problems require more detailed analyses using computer-based analyses, as presented later.

To include the influence of tensile reinforcement into limit equilibrium stability analyses requires assumptions regarding the

- Effect of the reinforcement force;
- Orientation of the reinforcement force at the location of the considered slip surface;
- Magnitude of the reinforcement force to ensure strain compatibility of the reinforced system at failure; and
- Reinforcement embedment length.

Effect of Reinforcement Force

The reinforcement force can be assumed to have one of two different effects on stability: *(a)* it can act as a boundary free-body tensile force that does not affect soil strength but that contributes to force and moment equilibrium; or *(b)* it can modify the strength of the embankment fill. The second effect can exist only if the reinforcement force is properly transmitted to the embankment fill.

The application of the reinforcement force as a boundary free-body tensile force that does not affect soil strength is shown in Figure 7a for the case of moment equilibrium along a circular slip surface. In Figure 7, M_T is the stabilizing moment due to the reinforcement force. This approach, which neglects any effect of the reinforcement force on soil strength, has been the one most commonly used in the past.

An approach assuming that the reinforcement force modifies soil strength is shown in Figure 7b for the case of moment equilibrium along a circular slip surface. In this approach, which was first proposed by Wager *(29)*, the reinforcement tensile force is decomposed into vector components normal and tangent to the slip surface. The component of force parallel to the slip surface is assumed to provide a pseudo-cohesion that acts in addition to any soil cohesion. The component of force normal to the slip surface is assumed to increase the normal stress acting on the soil and thereby increase its shearing resistance due to the frictional component of shear strength (which is assumed to be fully mobilized).

A comparison of the normalized stabilizing moment M_T/RT associated with the two different assumptions regarding the effect of the reinforcing force is shown in Figure 8a. The comparison is made for two different reinforcement

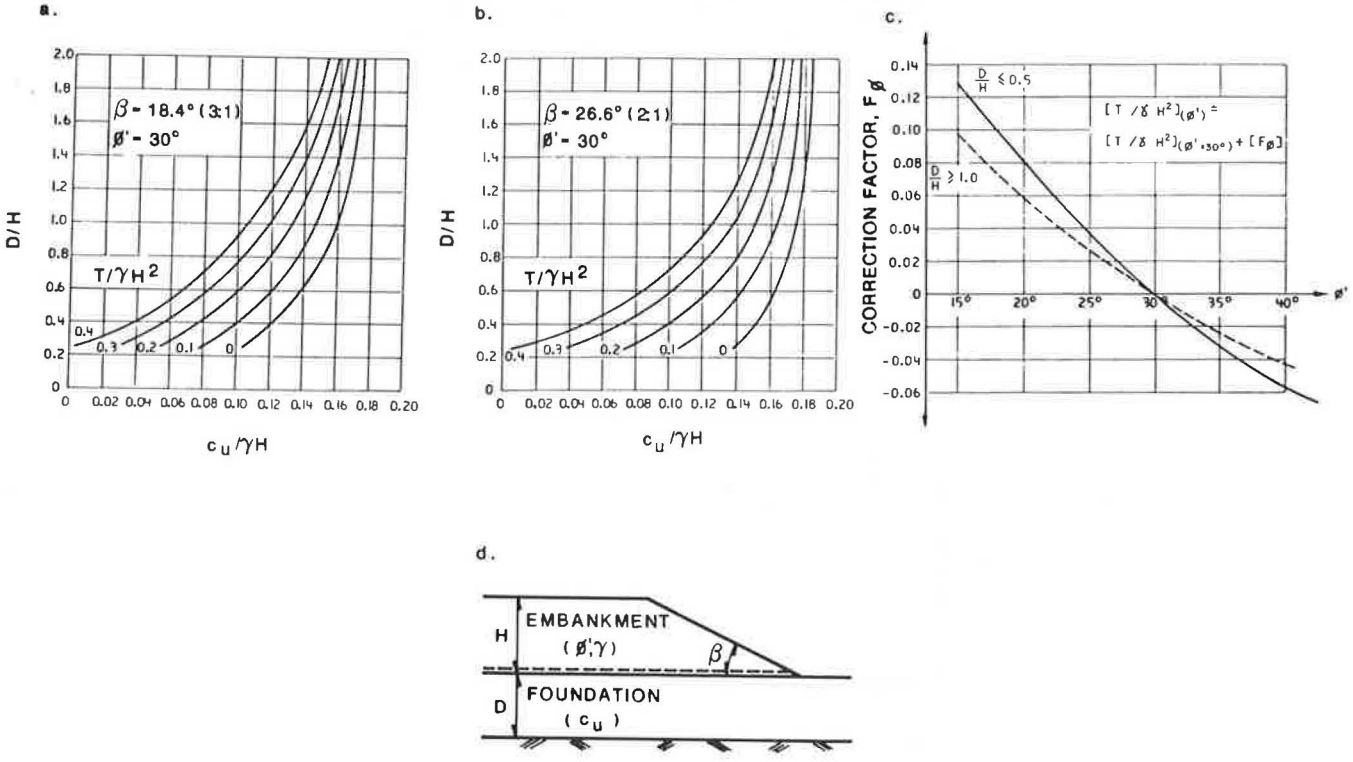

FIGURE 6 **Stability charts for the design of embankments on weak foundations [after Milligan and Busbridge *(27)*].**

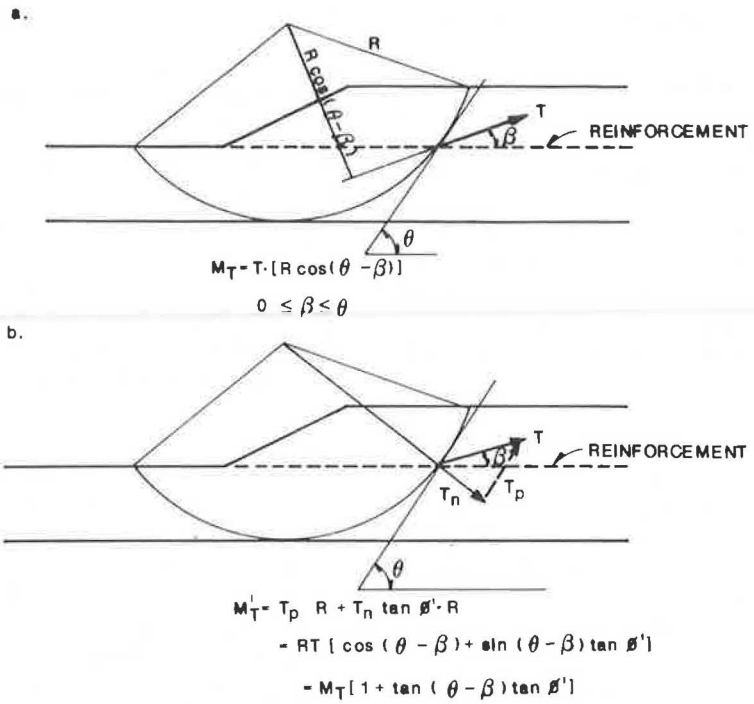

FIGURE 7 Effect of reinforcement force: (a) reinforcement force assumed to act as an independent free-body force that does not affect soil strength; or (b) reinforcement force assumed to increase soil strength.

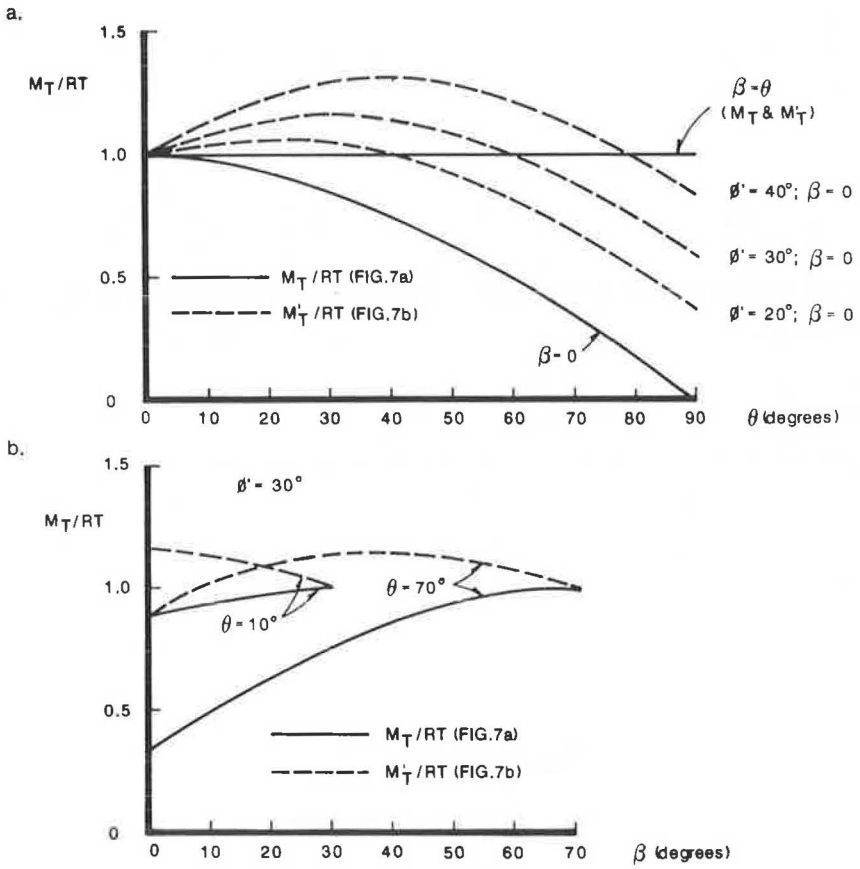

FIGURE 8 Stabilizing moments calculated using different assumptions from Figure 7: (a) comparison of moments calculated; (b) influence of reinforcement orientation.

orientations: horizontal ($\beta = 0$) and tangent to the slip surface ($\beta = \theta$). For the case of horizontal reinforcement and a granular fill with $\phi' = 30°$, the assumption that the reinforcement modifies the soil strength results in a larger stabilizing moment than that calculated under the assumption that the reinforcement acts as an independent force that does not affect soil strength. As the orientation of the reinforcement approaches the tangent to the slip surface (as β approaches θ), the stabilizing moments calculated by using the two assumptions converge.

Orientation of Reinforcement Force

The assumed orientation of the reinforcement force at its intersection with the slip surface has an effect on the results of force and moment equilibrium calculations. Almost all reinforcement is initially placed with a horizontal orientation. Most frequently, calculations are carried out by assuming that this initial orientation remains unchanged. It can also be assumed, however, that the initially horizontal strip or layer of flexible reinforcement bends because of large local displacements of the foundation soils at the onset of failure. The maximum possible amount of reinforcement reorientation would result in a reinforcement direction tangent to the slip surface. Fowler *(4, 25)*, for instance, assumed parallel reinforcement orientation. Reinforcement orientations between the two extreme values ($0 < \beta < \theta$ in Figure 7) would theoretically be possible.

A comparison of stabilizing moments calculated by using different reinforcement orientations is shown in Figure 8b for two different values of the angle θ. The influence of reinforcement orientation on the magnitude of the stabilizing moment is obvious. This influence is larger for large values of θ.

The practical significance of the effects shown in Figure 8 can be seen in Figure 9, which shows the influence of reinforcement orientation on the calculated factor of safety for a range of typical conditions. In Figure 9, the reinforcement is assumed to act as an independent free-body force that does not influence soil strength (Figure 7a). The calculated factor of safety was obtained by using Bishop's modified method (*30*, hereafter called BMM) of stability analysis and the reinforcement effect shown in Figure 7a. The figure shows the larger factor of safety computed based on tangential reinforcement orientation (FS_T) versus that based on horizontal reinforcement orientation (FS_H). Figure 10 shows the combined influences of the depth of the critical slip circle (foundation depth for the case analyzed) and reinforcement orientation for the embankment shown in Figure 9 and $T = 67$ kN/m (6,000 lb/ft).

Discussion of Effect and Orientation of Reinforcement Force

The differences in factor of safety associated with the different assumptions regarding the effect and orientation of the reinforcement force are important because often the role of the reinforcement is to provide short-term stability of the embankment-foundation system. It is not uncommon for the unreinforced factor of safety to be less than 1.0 and the reinforced end-of-construction (undrained) factor of safety to be only slightly greater than 1.0 (1.1 to 1.2). Thus the engineer may be using reinforcement to provide relatively small increments in factor of safety. The sensitivity of the results shown in Figures 7–9 makes selection of reasonable assumptions critical if analyses are to provide reasonable results. The review of available information that follows is intended to help the design engineer select reasonable assumptions.

The approach shown in Figure 7b of assuming that the reinforcement modifies soil strength is applicable to direct shear tests on reinforced sand specimens *(31)* and may be considered for structures in which the entire soil mass is strengthened with regularly spaced multiple layers of reinforcement *(8)*. On the basis of the authors' experiences, some strength gain may be considered for low embankments with multiple layers of reinforcement. For a single layer of reinforcement, however, this approach is uncertain because the application of the normal force is localized near the embankment-foundation interface. As previously discussed, some of the reinforcement force is transmitted to the foundation and is not available to strengthen the embankment fill. Therefore, for a single layer of reinforcement the reinforcement tensile force should be modeled as a boundary free-body force that does not affect soil strength (Figure 7a).

Evidence for selection of a reinforcement orientation is skimpy. Rowe and Soderman *(16)* used an analysis based on BMM to predict the height at which a geotextile-reinforced sand embankment would fail. The embankment, located at Almere, Netherlands *(3)*, was constructed over a 3.0- to 4.5-m-thick clay-peat deposit. The tensile force in the reinforcement at failure was estimated from field strain measurements. Rowe and Soderman *(12)* found that the factors of safety obtained with horizontal and tangential reinforcement orientation bounded the actual value of 1.0. Subsequently, Low and Duncan *(11)* also used a BMM analysis with both horizontal and tangential reinforcement orientation *(32)* and obtained results similar to those of Rowe and Soderman. On the basis of the back-analyses of the Almere test fill, Low and Duncan suggested that for low-sensitivity saturated clay foundations, the end-of-construction factor of safety could be approximated by averaging those obtained by using BMM with horizontal and tangential reinforcement orientation. Rowe and Soderman *(12)* suggest that for D/B less than about 0.4 the factor of safety could be calculated by using BMM along with a reinforcement moment arm equal to the average of those for horizontal and tangential orientation. For D/B greater than about 0.4, they conservatively suggest horizontal orientation.

Busbridge et al. *(6)* used an analysis based on BMM to predict the performance of both a reinforced and an unreinforced embankment built over highly sensitive Champlain Sea clay in eastern Canada. The soil conditions at the site on which the test embankments were built are well documented *(23)*. An analysis of the failure of the unreinforced embankment was used to calibrate the input parameters for analyses of the reinforced structure. On the basis of a horizontal reinforcement orientation and the actual failure height of the embankment, the analyses predicted a tensile force in the two layers of geogrid reinforcement at failure of 123 kN/m (8,400 lb/ft). According to Busbridge et al. *(6)*, "cracking noises were heard in the embankment moments before failure, and this is inferred to indicate tensile breakage of the geogrids." On the basis of constant strain-rate testing by McGown et al. *(34)* on the

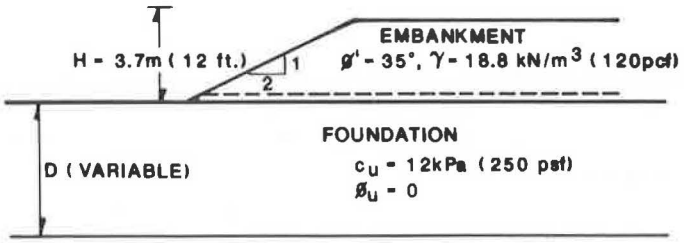

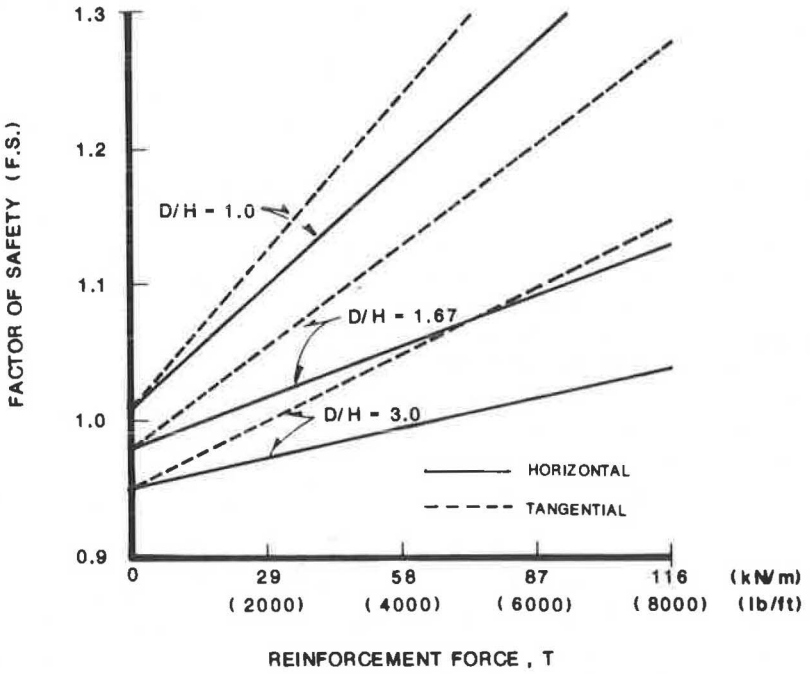

FIGURE 9 Influence of assumed reinforcement orientation on calculated factor of safety for typical embankment reinforcement application.

geogrid product used in the field trials, the range of possible break loads for two layers of reinforcement are estimated to be 110 to 140 kN/m (7,500 to 9,600 lb/ft). Using the same location and radius of the critical circle found by Busbridge et al. *(6)*, and a tangential reinforcement orientation, the authors calculated a reinforcement force at a factor of safety of 1.0 equal to approximately 60 kN/m (4,100 lb/ft), which is too low. On the basis of this result, for brittle, strain-sensitive foundations, a horizontal reinforcement orientation would appear to be appropriate.

Reinforcement Tensile Force at Failure

Selection of a limiting value of reinforcement tensile force is a key step preceding stability calculations. The magnitude of this force should depend on the deformation at failure of the embankment-foundation system and on the force-elongation behavior of the reinforcement, including reinforcement creep. Determination of the force-elongation relationship for geotextile and geogrid reinforcement is discussed in detail elsewhere *(8, 18, 35, 36)*. Reinforcement elongation due to deformation of the embankment-foundation system is discussed next.

In an embankment application, reinforcement elongation may be induced as a result of the following *(8)*:

- Placement of reinforcement and establishment of construction working pad;
- Undrained constant-volume distortion of the foundation soil during and after embankment construction;
- Localized embankment deformations associated with the development of a slip surface at the onset of failure; and
- Settlement due to consolidation of the foundation soil.

For relatively stiff reinforcement [secant tensile stiffnesses of at least 250 kN/m (17,000 lb/ft) at a strain of 2 percent], strains due to reinforcement placement and establishment of a construction working pad would be expected to be small, certainly not more than 1 or 2 percent. These small strains are in contrast to the large strains that have been observed when lightweight nonwoven geotextiles have been used with foundation displacement construction methods. The latter construction alternative is not considered here.

The tensile strain in reinforcement due to undrained constant-volume distortion has been investigated by using nonlinear finite element analyses by Boutrup and Holtz *(37)*, Rowe

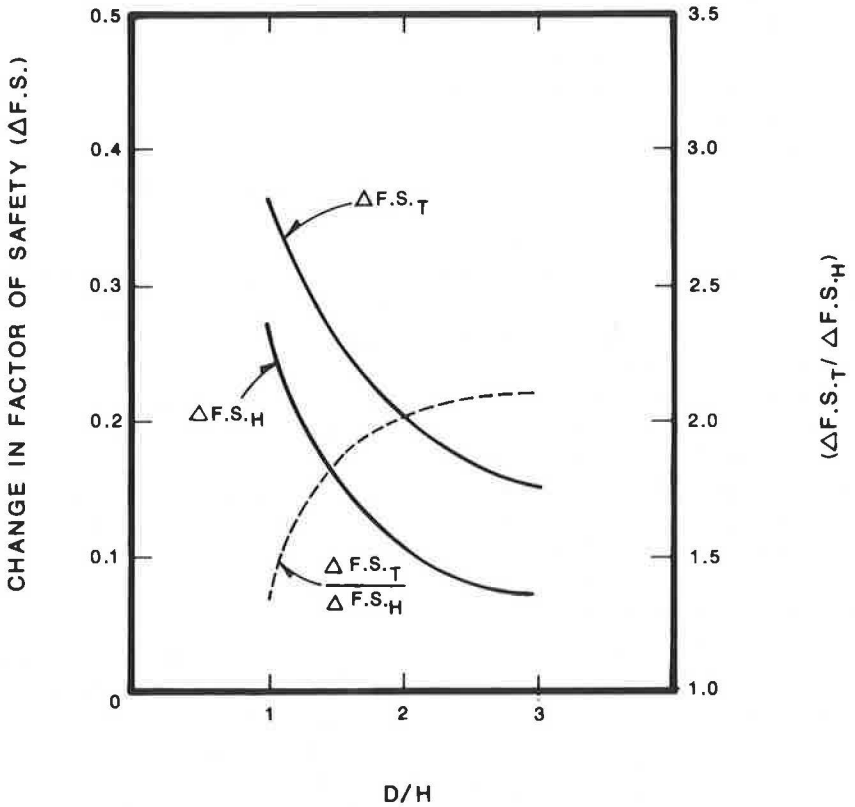

FIGURE 10 Comparison of changes in factor of safety for reinforcement with horizontal (ΔFS_H) and tangential (ΔFS_T) orientation for embankment shown in Figure 9.

and Soderman *(12)*, and Low and Duncan *(33)*. For a given embankment height and geometry, the mobilized reinforcement strain was found to be primarily dependent on the foundation stiffness and depth and on the reinforcement stiffness. The reinforcement strain varied between about 1 and 8 percent.

Field data from the fills constructed by Busbridge et al. *(6)* indicated prefailure reinforcement strains in the range 0 to 2 percent for the relatively stiff conditions (geogrid reinforcement and sensitive brittle foundation clay) existing in their tests. Tavenas et al. *(38)* analyzed available data for embankments on sensitive clay foundations and found that for end-of-construction conditions and factors of safety in the range 1.2 to 1.3, maximum lateral strains in the foundation were only a few percent for embankments with maximum vertical settlements of up to 10 percent of the embankment height.

Fowler *(4)* estimated approximately 4 percent reinforcement strain on the basis of field displacement measurements for a flat-sided (10H:1V) dike built over very weak, nonsensitive foundation clays located in an intertidal zone adjacent to Mobile Harbor. The design factor of safety for this case was in the range 1.1 to 1.2. The reinforcement was a 730-g/m^2 woven geotextile. The recorded reinforcement strain at incipient failure in the Almere test fill was approximately 4 to 6 percent *(3)*. At Almere, the foundation soils were clays and peats, and the reinforcement was a 450 g/m^2 woven geotextile. Barsvary et al. *(2)* and Rowe et al. *(14)* report reinforcement strains on the order of 20 percent for a 1.5-m embankment built over a 6- to 7-m-thick peat deposit with an initial average water content of 445 percent by weight. The unreinforced factor of safety for this embankment was estimated to be 1.15. In this case, a 225-g/m^2 woven geotextile was used, and although it enabled staged embankment construction, settlements were large, approaching 80 percent of the total height of fill. A 730-g/m^2 woven geotextile was used over a more compressible section of the same site where the peat had an average water content of 785 percent by weight. The unreinforced factor of safety for the embankment was estimated to be about 1.05. Settlements were again large. Maximum recorded reinforcement strains were on the order of 4 percent.

A number of references exist that describe reinforcement rupture *(3, 6, 7)*. At the onset of failure, reinforcement strains may become large in the vicinity of the failure surface. The additional reinforcement tensile force generated by this elongation may or may not restore stability, depending on the stiffness of the reinforcement and on the strain-softening characteristics of the foundation. Because most foundations are at least slightly strain softening, the reinforcement tensile force increase associated with this increment of strain should probably be neglected.

Foundation consolidation does not usually result in significant lateral embankment deformation. Consolidation also leads to a strengthening of the foundation soil and a decreased need for reinforcement. Therefore, reinforcement strains induced by consolidation are usually not significant from a design standpoint. A few exceptions to this conclusion do exist, and in these cases the time-dependent reinforcement force-strain response should be considered. Exceptions include embankments over

peat bogs or other deposits with nonuniform thicknesses that may result in large localized reinforcement strains.

On the basis of this discussion and review of available information for highly sensitive, brittle clay foundations, the reinforcement tensile force for design against slip surface foundation failure should be based on a limiting strain of not more than 2 to 3 percent. Limiting strains of not more than 4 to 6 percent should be considered for medium- to low-sensitivity clay foundations. If the foundation soils are nonsensitive and plastic, the reinforcing force should be based on limiting strains of not more than 10 percent.

Two additional factors that should be considered in selecting a reinforcement tensile force for design are *(a)* the strain to limit lateral embankment deformations to an acceptable level, and *(b)* the strain to limit creep rupture of the reinforcement. The first factor may be important if cohesive embankment fills are used. In this case, the primary benefit of reinforcement may be to prevent embankment cracking *(11)*. To prevent cracking, mobilized reinforcement strains should be small, as noted in the previous discussion. The second factor may become important if the anticipated reinforcement strains are larger than the strain that would result in reinforcement creep.

Reinforcement Embedment Length

The previous discussion was concerned with selection of a maximum reinforcement force under the embankment. This maximum force can only be generated if the reinforcement has adequate embedment beyond the failure surface. The embedment length required to mobilize a given reinforcement tensile force is dependent on the embankment-reinforcement bond, the foundation-reinforcement bond, or both, as well as on the embankment overburden pressure. For most new embankment construction, embedment length requirements are automatically satisfied by spanning the reinforcement from toe to toe. A length check should be made, however, for embankment-widening or embankment-raising projects when reinforcement lengths are limited, when the reinforcement does not span the entire embankment, or when very stiff [K greater than about 1,000 kN/m (68,000 lb/ft)] reinforcement is used.

An embedded geotextile or geogrid resists pullout through friction and adhesion on its upper and lower surfaces, and by passive resistance developed by elements perpendicular to the direction of reinforcement. Average interface friction and adhesion coefficients can be defined from the results of direct shear or pullout tests for geotextiles and pullout tests for geogrids. These average coefficients take into account both soil reinforcement friction and adhesion, as well as the passive resistances of regularly spaced, repetitive, perpendicular elements *(8)*. Interface parameters should be measured with soils representative of the embankment fill and the foundation, with test configurations as close as possible to conditions in the field.

Once the interface parameters have been defined, a profile of available reinforcement force *(22)* can be developed for any given embankment cross section. The available reinforcement force will be the lesser of the force available based on an embedment length analysis and the limit reinforcement tensile force based on the embankment deformation evaluation described in the last section. Near the edge of the embankment, reinforcement pullout or sliding will control the maximum available force. Under the center of the embankment, the limit reinforcement tensile force will control.

Longitudinal Reinforcement Force

The preceding discussion was directed solely at reinforcement forces and strains in the direction perpendicular to the embankment centerline. Reinforcement forces and strains can also be developed parallel to the embankment centerline. The potential for longitudinal reinforcement forces and strains may occur *(a)* during construction over very weak sites prone to mud waving; *(b)* at the ends of an embankment; and *(c)* owing to differential settlements and bending of embankments built over nonuniform foundation conditions. Barsvary et al. *(2)* measured reinforcement strains on the order of 8 percent under an embankment built over a peat bog that had variable depth. When these conditions prevail, longitudinal reinforcement forces and strains should be considered during design.

Other Factors

The discussion has focused on reinforcement aspects of limit equilibrium analyses of reinforced embankments. It should be remembered that other factors affect the stability of unreinforced and reinforced embankments alike. The geotechnical literature relating to unreinforced embankment stability should be consulted to evaluate these other factors, which include *(a)* foundation strength details, including the presence of a crust, strength changes with depth, or thin seams of silts and fine sands; *(b)* embankment fill properties, including undrained embankment cohesion; *(c)* embankment cracking, which may be reduced in a reinforced embankment compared to an unreinforced embankment; *(d)* progressive failure effects; and *(e)* time-dependent foundation changes, including creep and consolidation.

CONSTRUCTION OF EMBANKMENTS OVER WEAK FOUNDATIONS

Selection and implementation of appropriate construction procedures is of critical importance for reinforced embankments over weak foundations, for at least two reasons: *(a)* a potential exists for embankment failure during construction if construction sequencing and procedures are not carefully planned; and *(b)* because often only one layer of reinforcement is used, improper installation- or construction-related material damage could result in embankment failure because there is no redundancy in the reinforcement system.

Site Access and Construction Equipment

Procedures to prevent failures into very weak foundations during construction have been mostly concerned with the placement of woven geotextiles *(4, 18, 39)* because these were the first synthetic reinforcing materials used in this application. Light construction equipment is recommended so as not to disturb the ground surface (which might consist of a desiccated crust or vegetative mat) or, worse, induce bearing capacity failure of the foundation. Haliburton et al. *(40)* and Fowler *(4)*

reported that small, wide-tracked dozers with maximum ground pressures on the order of 17 kPa (2.5 psi) are suitable for spreading as little as 0.3 m (1 ft) of sand fill over geotextiles resting on saturated cohesive foundation soils with undrained shear strengths in the range of approximately 2 to 7 kPa (50 to 150 lb/ft^2). During the early stages of construction, haul roads for delivering embankment fill may require special design. Alternatively, partially loaded dump trucks can be used. Design criteria for reinforced haul roads were summarized by Christopher and Holtz *(18)*.

Site Preparation

Site preparation generally depends on the strength of the foundations soil and the presence of a desiccated crust or vegetative mat. As previously noted, care should be taken not to disrupt any crust or mat covering the site. Site preparation must be compatible with the survivability (ability to survive the construction process with minimum damage) and workability (ease of placement, sewing, joining, etc.) characteristics of the reinforcing material. Christopher and Holtz *(18)* provide guidelines for geotextile selection on the basis of survivability and workability criteria that depend on subgrade conditions, construction equipment, and type of cover or backfill material.

[A different approach to reinforcement survivability has been used by geogrid manufacturers. They have recommended reducing a product's reinforcement force for design by a site damage factor that accounts for possible material damage resulting from the construction operation *(8, 11)*. These factors are determined from tension tests on product specimens that have been subjected to field installation placement and fill compaction procedures.]

On sites that can support light construction equipment, a thin granular working table is often constructed before placement of the reinforcement. If the foundation cannot support construction equipment, geotextile reinforcement will usually be placed directly on the subgrade. With geogrid reinforcement, a lightweight geotextile separator is often placed on the subgrade, and the reinforcement is then placed on top of the separator, either before or after the first soil lift. The geotextile separator is usually ignored in stability calculations. Occasionally a lightweight (100 to 150 g/m^2) geotextile separator will be used to facilitate construction of a working pad before placement of heavyweight (typically 500 to 1,000 g/m^2) geotextile reinforcement. This procedure finds use when stumps and pointed brush that cannot be removed owing to site conditions might diminish the performance of the reinforcement *(18)*. With peat foundations, Rowe et al. *(15)* suggest placement of the reinforcement directly on the root mat.

Reinforcement Placement Procedures

Placement procedures for geotextiles have been reviewed in a number of references *(4, 18, 21, 39)*. All recommend that geotextile seams be sewn and not overlapped. Ideally, sewn seams should be as strong as the geotextile itself. Practically, seam strengths rarely exceed two-thirds of the geotextile strength, even with high strength thread and double sewn overlap seams *(18)*. Seam strengths must meet reinforcement design strength requirements as the seam strength represents the minimum strength or weak link of the reinforcement system. Lock-stitching has been recommended to preclude seam unraveling. Polypropylene, polyester, polyamide (nylon), and polyaramide (Kevlar) threads are used. To avoid the risk of overstressing seams, geotextiles are usually unrolled with their machine direction perpendicular to the centerline of the embankment. Field labor can be minimized by prefabricating multiwidth geotextile panels at the manufacturing plant or in a staging area.

Geogrid placement procedures differ somewhat from those used for geotextiles. Geogrid rolls tend to be smaller than geotextile rolls, and wind does not hinder placement. Overlapping procedures depend on geogrid type. Geogrid products that are strong in one direction only (uniaxial) are unrolled perpendicular to the embankment centerline, and adjacent strips are usually butted. No mechanical connection is used between strips except for occasional metal hog rings or stakes to hold the grid alignment during fill placement. This procedure works well when plane strain conditions prevail and when a good working pad is available. Otherwise, a second layer of uniaxial grid will be required, oriented parallel to the embankment centerline.

Geogrid products that are strong in two directions (biaxial) may be unrolled parallel or perpendicular to the embankment centerline. If the open area of the grid is large (greater than 60 to 70 percent) and its aperture size permits anchorage by the fill material, adjacent rolls can be overlapped without mechanical connection. Overlap widths should be based on pullout test results. For applications that require mechanical connections, polymer dowel bars, braid, and metal hog rings have been used to form the connections. All of these mechanical connection procedures are relatively labor-intensive. Connection strengths of 80 to 90 percent of the material strength can be achieved. Connection strengths must meet reinforcement design strength requirements. Often a combination of geogrid overlap and mechanical connection is used, and the connection strength is assumed equal to the geogrid strength.

Fill Placement Procedures

It is important that the reinforcement be placed without wrinkles or folds to allow mobilization of the reinforcement tensile force with a minimum amount of deformation. During fill placement, it may be necessary to pull wrinkles or folds out of the reinforcement manually to keep it taut. Hog rings, steel pins, and stakes can be used to hold geogrids in place during fill spreading. For sites that can support construction equipment [with undrained shear strengths greater than about 15 kPa (300 lb/ft^2)], Christopher and Holtz *(18)* suggest that fill be pushed from the center of the embankment forward and out towards the edges of the embankment. This is sometimes called the inverted-U fill placement procedure because of the shape of the front edge of the fill in plan view.

Fill placement procedures become critical for sites underlain by foundation soils with undrained shear strengths less than about 10 kPa (200 lb/ft^2) if construction related failures are to be avoided. Fill placement procedures for very weak inorganic clays were developed by Haliburton and have been described in detail in a number of references *(4, 18, 21, 40)*. They consist of building access roads and starter embankments along the longitudinal edges of the main embankment to pretension the reinforcement. Interior fill sections are placed after the reinforcement is pretensioned. In this way, fill placement proceeds in a

U shape that is just the opposite of the procedure prescribed for stronger sites. A mud wave will typically form inside the U. Fill dumping, spreading, and initial lift thickness need to be carefully managed during placement of the initial layer of fill to avoid localized bearing capacity failures. The lift thickness for the first lift should be the minimum required to support construction traffic and can be based on haul road design procedures.

SUMMARY

The goal of this paper is to give the design engineer an understanding of the ways in which geotextile and geogrid reinforcement improve the performance of embankments over weak foundations and to provide practical guidance in the use of limit equilibrium analyses for design. To achieve the latter goal, the available literature was reviewed and coupled with the authors' personal experiences. The literature review indicated that modified classical limit equilibrium procedures may be used to evaluate the end-of-construction factor of safety of embankments over saturated clay foundations. The procedures appear to be less reliable in predicting performance over peat deposits, however. Further, it was suggested that the reinforcement force be included as a boundary free-body force in the equilibrium calculations. Guidance was provided on the appropriate direction and magnitude of the reinforcement force to use in calculations. The reinforcement force magnitude was largely dependent on the deformation of the embankment foundation system at failure. Reinforcement strains induced by these deformations are in the range of 1 to 10 percent. Construction procedures that have been successfully used in the past were also reviewed.

ACKNOWLEDGMENTS

This paper was written while the first author was employed by the Tensar Corporation, Morrow, Ga. Its support is gratefully acknowledged. The authors also would like to thank G. R. Schmertmann and J. P. Giroud for reviewing a draft of the paper. Special thanks are due to Barbara Hutcheson and Doris Campbell, who typed the paper, and to Rick Komada, who drafted the figures.

REFERENCES

1. J. Fowler, J. Peters, and L. Franks. Influence of Reinforcement Modulus on Design and Construction of Mohicanville Dike No. 2. *Proc., Third International Conference on Geotextiles*, Vienna, Vol. 1, 1986, pp. 267–271.
2. A. K. Barsvary, M. D. MacLean, and C. B. H. Cragg. Instrumented Case Histories of Fabric Reinforced Embankments Over Peat Deposits. *Proc., Second International Conference on Geotextiles*, Las Vegas, Nev., Vol. 3, 1982, pp. 647–652.
3. J. Brackel, M. Coppins, A. C. Maagdenberg, and P. Risseeuw. Stability of Slopes Constructed with Polyester Reinforcing Fabric, Test Section at Almere-Holland. *Proc., Second International Conference on Geotextiles*, Las Vegas, Nev., Vol. 3, 1982, pp. 727–732.
4. J. Fowler. *Design, Construction, and Analysis of Fabric-Reinforced Embankment Test Section at Pinto-Pass, Mobile, Alabama.* Technical Report EL-81-8, Waterways Experiment Station, U.S. Army Corps of Engineers, Vicksburg, Miss., 1981.
5. J. Hannon. Fabric Support Embankment Over Bay Mud. *Proc., Second International Conference on Geotextiles*, Las Vegas, Nev., Vol. 3, 1982, pp. 653–658.
6. J. R. Busbridge, P. Chan, V. Milligan, P. R. LaRochelle, and L. D. Lefebvre. *The Effect of Geogrid Reinforcement on the Stability of Embankments on a Soft Sensitive Champlain Clay Deposit.* Report to Canadian Transportation Development Center, Golder Associates, and Ontario and Université Laval, Quebec, March 1985.
7. J. E. Fluet, B. R. Christopher, and A. R. Slaters. Geosynthetic Stress-Strain Response Under Embankment Loading Conditions. *Proc., Third International Conference on Geotextiles*, Vienna, Vol. 1, 1986, pp. 175–180.
8. R. Bonaparte, R. D. Holtz, and J. P. Giroud. Soil Reinforcement Design Using Geotextiles and Geogrids. *ASTM Symposium Geotextile Testing and the Design Engineer*, Los Angeles, Calif., July 1985.
9. J. P. Giroud. Designing with Geotextiles. *Materiaux et Constructions*, Vol. 14, No. 82, 1981, pp. 257–272.
10. T. C. Kinney. *Tensile Reinforcement of Road Embankments on Polygonal Ground by Geotextiles and Related Materials.* Interim Report to State of Alaska, Department of Transportation and Public Facilities, Fairbanks, Alaska, March 1986.
11. B. K. Low and J. M. Duncan. *Analysis of the Behavior of Reinforced Embankments on Weak Foundations.* Report VPI/CE-GT-85-11, Virginia Polytechnic Institute, Blacksburg, October 1985.
12. R. K. Rowe and K. L. Soderman. An Approximate Method for Estimating the Stability of Geotextile Reinforced Embankments. *Canadian Geotechnical Journal*, Vol. 22, No. 3, 1985, pp. 392–398.
13. R. K. Rowe. Reinforced Embankments: Analysis and Design. *Journal of Geotechnical Engineering Division*, ASCE, Vol. 110, No. GT2, 1984, pp. 231–246.
14. R. K. Rowe, M. D. MacLean, and A. K. Barsvary. The Observed Behavior of a Geotextile-Reinforced Embankment Constructed on Peat. *Canadian Geotechnical Journal*, Vol. 21, No. 2, 1984, pp. 289–304.
15. R. K. Rowe, M. D. MacLean, and K. L. Soderman. Analysis of a Geotextile-Reinforced Embankment Constructed on Peat. *Canadian Geotechnical Journal*, Vol. 21, No. 3, 1984, pp. 563–576.
16. R. K. Rowe and K. L. Soderman. Comparison of Predicted and Observed Behavior of Two Test Embankments. *Geotextiles and Geomembranes*, Vol. 1, No. 2, 1984, pp. 143–160.
17. R. K. Rowe and K. L. Soderman. Geotextile Reinforcement of Embankments on Peat. *Geotextiles and Geomembranes*, Vol. 2, No. 4, 1985, pp. 277–298.
18. B. R. Christopher and R. D. Holtz. *Geotextile Engineering Manual.* FHWA, U.S. Department of Transportation, 1985.
19. V. Milligan and P. LaRochelle. Design Methods for Embankment Over Weak Soils. *Proc., Symposium on Polymer Grid Reinforcement in Civil Engineering*, Institution of Civil Engineers, London, 1984, pp. 95–102.
20. K. Terzaghi and R. B. Peck. *Soil Mechanics in Engineering Practice*, John Wiley and Sons, New York, 1967.
21. J. Fowler and T. A. Haliburton. Design and Construction of Fabric Reinforced Embankments. *The Use of Geotextiles for Soil Improvements*, Preprint 80-177, ASCE Convention, Portland, Oreg., 1980, pp. 89–118.
22. R. A. Jewell. A Limit Equilibrium Design Method for Reinforced Embankments on Soft Foundations. *Proc., Second International Conference on Geotextiles*, Las Vegas, Nev., Vol. 3, 1982, pp. 671–676.
23. J. Mandel and J. Salencon. Force portante d'un sol sur une assise rigide. *Proc., Seventh International Conference on Soil Mechanics and Foundation Engineering*, Mexico City, Vol. 2, 1969, pp. 157–164.
24. J. Mandel and J. Salencon. Force portante d'un sol sur assise rigide: Etude théorique. *Géotechnique*, Vol. 22, No. 1, 1967, pp. 79–93.
25. J. Fowler. Theoretical Design Considerations for Fabric-Reinforced Embankments. *Proc., Second International Conference on Geotextiles*, Las Vegas, Nev., 1982, pp. 665–670.

26. J. P. Gourc. *Quelques Aspects du Comportement des Géotextiles en Mécanique des Sols*. Ph.D. thesis. University of Grenoble, Grenoble, France, 1982.
27. T. S. Ingold. An Analytical Study of Geotextile Reinforced Embankments. *Proc., Second International Conference on Geotextiles*, Las Vegas, Nev., Vol. 3, 1982, pp. 683–688.
28. V. Milligan and J. R. Busbridge. *Guidelines for the Use of Tensar Geogrids in Reinforcement of Fills Over Weak Foundations*. Golder Associates Report to the Tensar Corporation, Mississauga, Ontario, 1983.
29. O. Wager. *Building of a Site Road Over a Bog at Kilanda, Alvsborg County, Sweden*. Report to the Swedish State Power Board, Boras, Sweden, 1981.
30. A. W. Bishop. The Use of the Slip Surface in the Stability Analysis of Slopes. *Géotechnique*, Vol. 5, No. 1, 1955, pp. 7–17.
31. R. A. Jewell. *Some Effects of Reinforcement on the Mechanical Behavior of Soil*. Ph.D. thesis, University of Cambridge, Cambridge, U.K., 1980.
32. J. M. Duncan, B. K. Low, and V. R. Schafer. *STABGM: A Computer Program for Slope Stability Analysis of Reinforced Embankments and Slopes*. Geotechnical Engineering Report, Virginia Polytechnic Institute, Blacksburg, September 1985.
33. P. LaRochelle, B. Trak, F. Tavenas, and M. Roy. Failure of a Test Embankment on a Sensitive Champlain Clay Deposit. *Canadian Geotechnical Journal*, Vol. 11, No. 1, 1974.
34. A. McGown, K. Z. Andrawes, K. C. Yeo, and D. D. DuBois. The Load-Strain-Time Behavior of Tensas Geogrids. *Proc., Symposium on Polymer Grid Reinforcement in Civil Engineering*, Institution of Civil Engineers, London, 1984, pp. 11–17.
35. R. A. Jewell. Material Properties for the Design of Geotextile Reinforced Slopes. *Geotextiles and Geomembranes Journal*, Vol. 2, No. 2, 1985, pp. 83–109.
36. A. McGown, N. Paine, and D. D. Dubois. Use of Geogrid Properties in Limit Equilibrium Analysis. *Proc., Symposium on Polymer Grid Reinforcement in Civil Engineering*, Institution of Civil Engineers, London, 1984, pp. 11–17.
37. E. Boutrup and R. D. Holtz. Analysis of Embankments on Soft Ground Reinforced with Geotextiles. *Proc., Eighth European Conference on Soil Mechanics and Foundation Engineering*, Helsinki, Vol. 2, 1983, pp. 469–472.
38. F. Tavenas, C. Mieussens, and F. Bourges. Lateral Displacements in Clay Foundations Under Embankments. *Canadian Geotechnical Journal*, Vol. 16, No. 3, 1979.
39. R. D. Holtz. Soil Reinforcement with Geotextiles. *Third NTI International Geotechnical Seminar*, Nanyang Technological Institute, Singapore, 1985, pp. 55–74.
40. T. A. Haliburton, J. D. Lawmaster, and V. E. McGuffey. *Use of Engineering Fabrics in Transportation Related Applications*. FHWA, U.S. Department of Transportation, 1982.

Publication of this paper sponsored by Committee on Mechanics of Earth Masses and Layered Systems.

Model Tests for Strip Foundation on Clay Reinforced with Geotextile Layers

JONI P. SAKTI AND BRAJA M. DAS

The ultimate bearing capacity of a model strip foundation resting on a saturated soft clay internally reinforced with geotextile layers has been investigated in the laboratory. The geotextile used for the study was heat-bonded nonwoven polypropylene. On the basis of the present test results, geotextile layers placed under a foundation within a depth equal to the width of the foundation have some influence on the increase of the short-term ultimate bearing capacity. For maximum efficiency, the first layer of geotextile should be placed at a depth of about 0.4 times the width of the foundation. The minimum length of the reinforcing geotextile layers for maximum efficiency appears to be about four times the width of the foundation.

Shallow foundations constructed over soft saturated clay layers have low ultimate bearing capacity. They also undergo large elastic settlements. One of the possibilities for increasing the short-term bearing capacity of a shallow foundation is by reinforcing the clay under the foundation by means of geotextile layers (Figure 1). A review of the existing literature shows that relatively little is known at this time about how to quantify the parameters involved in estimating the increase of immediate load bearing capacity of shallow foundations resting on saturated clayey soil ($\phi = 0$ condition) internally reinforced with geotextile layers. The purpose of this paper is to present the experimental results of some small-scale laboratory bearing capacity tests on model strip foundations resting on clay reinforced with geotextiles.

LABORATORY MODEL TEST PROCEDURES

The laboratory bearing capacity tests were conducted in a clayey soil that had 100 percent passing No. 10 U.S. sieve (2.0 mm opening), 86 percent passing No. 40 U.S. sieve (0.425 mm opening), and 62 percent passing No. 200 U.S. sieve (0.075 mm opening). The liquid and plastic limits of the soil were 35 and 24 percent, respectively. A large amount of soil was brought to the laboratory and pulverized well. The soil was then mixed with a desired amount of water and transferred to several plastic bags that were sealed and stored in a moist curing room for about 1 week before use. The average moisture content during the actual model tests was 25.1 percent.

J. P. Sakti, Department of Civil Engineering, Ohio State University, Columbus, Ohio 43210. B. M. Das, Department of Civil Engineering, University of Texas at El Paso, El Paso, Tex. 79968.

The model foundation used for the laboratory tests was 76.2 mm wide, 228.6 mm long, and 9.5 mm thick. It was cut from an aluminum plate. The model test box was 652 mm long, 76.2 mm wide, and 610 mm high. The sides of the box were heavily braced to avoid lateral yielding during soil compaction and during testing. The inside of the test box was polished to avoid friction between edges of the model foundation and the box. The geotextile used in the laboratory tests was Mirafi 140N, a heat-bonded nonwoven type with polypropylene geotextile. Typical average properties of the geotextile as given by the supplier were as follows: grab tensile strength = 534 N (ASTM D–1682–64); grab tensile elongation = 55 percent; burst strength = 1,440 kN/m^2 (ASTM D–3786–80).

To conduct the model tests in the laboratory, the moist soil was compacted in 25- to 51-mm-thick layers in the test box up to the desired height. Geotextile layers of various lengths L with widths equal to the width of the test box were laid in the clay soil during the compaction. After completion of the compaction process, the model footing was centrally placed at the top of the clay. Load to the foundation was applied by means of a hydraulic jack. The load on the model footing was measured with a proving ring, and the corresponding deflection was obtained from a dial gauge. Figure 2 shows a schematic diagram of the experimental setup.

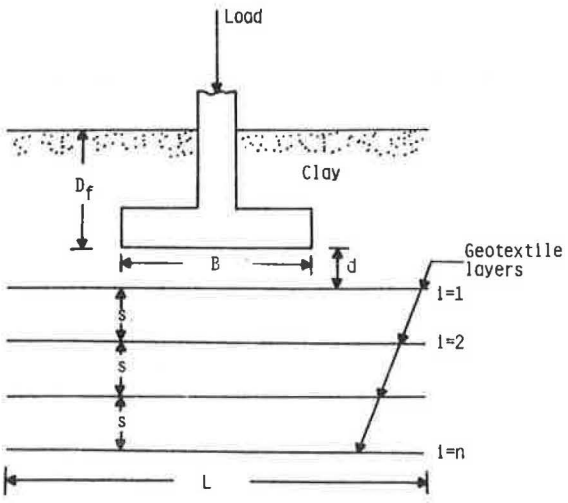

FIGURE 1 Shallow foundation on clay internally reinforced with geotextile layers.

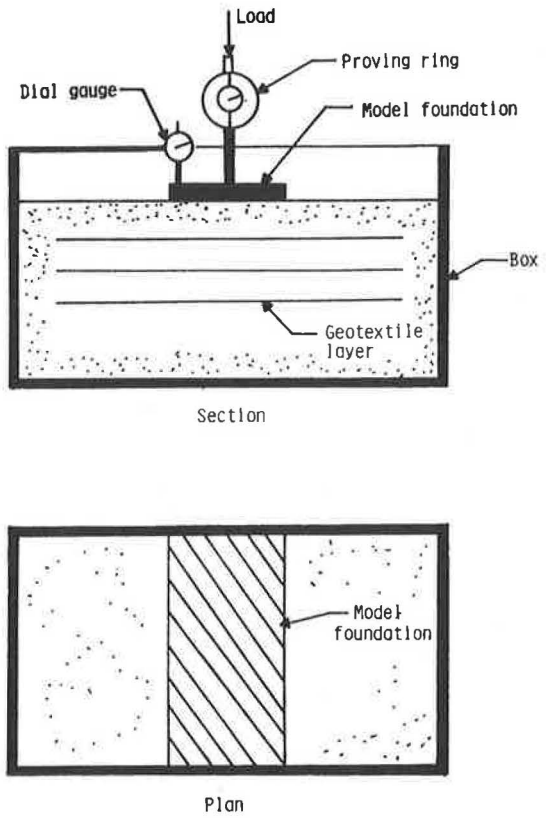

FIGURE 2 Schematic diagram of laboratory test arrangement.

SEQUENCE OF MODEL TESTS AND PARAMETERS STUDIED

All model tests conducted under this program were of the plane-strain type. Table 1 presents the sequence of experiments and other details of the tests. All tests except Test 2 were conducted with the moist clay medium, which had an average undrained shear strength of 22.5 kN/m^2 at an average moisture content of 25.1 percent and degree of saturation of about 96 percent. Test 2 was conducted on the compacted clay at a moisture content of 21.8 percent with an average undrained shear strength of 29 kN/m^2. The average degree of saturation of the clay for this test was 94.8 percent.

The model tests were conducted to evaluate the following: (a) the increase in the ultimate bearing capacity of foundations due to geotextile reinforcement and the optimum placement of geotextile layers for obtaining the maximum efficiency; (b) the settlement of foundations at ultimate load with and without geotextile reinforcement; and (c) the optimum length of geotextile layers to mobilize the ultimate bearing capacity.

The laboratory test results and the evaluation of the above factors are given in the following section.

EXPERIMENTAL RESULTS

Bearing Capacity of Reinforced Clay

Figure 3 shows the average plot of load versus displacement for the model foundation as observed in the laboratory for Tests 1 and 2, which were conducted in compacted clay without geotextile reinforcements. As seen from Figure 3, the nature of failure is of local shear type. The ultimate loads for the tests were determined in a manner suggested by Vesic *(1)*. The ultimate load was defined as the point at which the load-displacement plot became practically linear. For surface foundations ($D_f = 0$) in clay for the $\phi = 0$ condition,

$$Q_u = c_u N_c A \tag{1}$$

where

Q_u = ultimate load,
N_c = bearing capacity factor,
A = area of the model foundation, and
c_u = undrained shear strength of clay.

So

$$N_c = \frac{Q_u}{AC_u} \tag{2}$$

For Tests 1 and 2, the ultimate loads Q_u were 2,180 and 2,758 N, respectively. By using the proper values of c_u and A, the values of N_c were determined to be 5.57 and 5.46, respectively. These values are in the general range predicted by Prandtl *(2)* and Terzaghi *(3)*. The ultimate load occurred at a settlement of 16 to 18 percent of the width of the foundation.

Bearing Capacity of Clay with Geotextile Reinforcement

Model Tests 3 through 26 were conducted on clay with geotextile reinforcements that had length L equal to 10 times the footing width B (Table 1). Figure 4 shows typical plots of load versus displacement for Tests 8–12. For comparison purposes, the average relationship between load and displacement for Test 1 (on clay without reinforcement) has also been plotted in Figure 4. In general, for a given settlement, the load-carrying capacity of the model foundation increased when the geotextile reinforcement in the clay was introduced. The ultimate loads for all tests (Tests 1 and 3–26) as determined in the manner suggested by Vesic *(1)* have been compiled and are shown in Figure 5 for various combinations of d/B, s/B, and n (definitions of d, s, and n are given in Table 1). For given values of d/B and s/B, the magnitude of Q_u increased with n up to a maximum value $Q_{u(\max)}$ and remained constant thereafter. Binquet and Lee *(4)* have introduced the concept of bearing capacity ratio *(BCR)*, defined as

$$BCR = \frac{Q_{u(\text{reinforced})}}{Q_{u(\text{unreinforced})}} \tag{3}$$

In Figure 5, the scale of BCR is shown on the ordinate on the right hand side. The variation of the maximum bearing capacity ratio, $BCR_{(\max)}$, for different values of d/B and s/B as determined from Figure 5 is shown in Figure 6. The following

TABLE 1 SEQUENCE OF LABORATORY TESTS

Test No.	Depth of model foundation, D_f	d/B	Number of geotextile layers, n	s/B	L/B	Remarks
1	0	--	0	--	--	c_u=22.5 kN/m^2--test on clay alone γ=20.13 kN/m^3
2	0	--	0	--	--	c_u=29 kN/m^2--test on clay alone γ=20.76 kN/m^3
3	0	0.25	1	0.33	10	c_u=22.5 kN/m^2
4	0	0.25	2	0.33	10	
5	0	0.25	3	0.33	10	γ=20.13 kN/m^3
6	0	0.25	4	0.33	10	
7	0	0.25	5	0.33	10	
8	0	0.33	1	0.33	10	c_u=22.5 kN/m^2
9	0	0.33	2	0.33	10	
10	0	0.33	3	0.33	10	γ=20.13 kN/m^3
11	0	0.33	4	0.33	10	
12	0	0.33	5	0.33	10	
13	0	0.67	1	0.33	10	c_u=22.5 kN/m^2
14	0	0.67	2	0.33	10	
15	0	0.67	3	0.33	10	γ=20.13 kN/m^3
16	0	0.67	4	0.33	10	
17	0	1.00	1	0.33	10	c_u=22.5 kN/m^2
18	0	1.00	2	0.33	10	
19	0	1.00	3	0.33	10	γ=20.13 kN/m^3
20	0	0.67	1	0.67	10	c_u=22.5 kN/m^2
21	0	0.67	2	0.67	10	
22	0	0.67	3	0.67	10	γ=20.13 kN/m^3
23	0	0.67	4	0.67	10	
24	0	1.00	1	1.00	10	c_u=22.5 kN/m^2
25	0	1.00	2	1.00	10	
26	0	1.00	3	1.00	10	γ=20.13 kN/m^3
27	0	0.33	4	0.33	2	c_u=22.5 kN/m^2
28	0	0.33	4	0.33	3	
29	0	0.33	4	0.33	4	γ=20.13 kN/m^3
30	0	0.33	4	0.33	5	
31	0	0.33	4	0.33	6	
32	0	0.33	4	0.33	8	

B=foundation width
L=length of geotextile layer (Fig. 1)
d=distance between the bottom of the foundation and the first geotextile layer (Fig. 1)
s=spacing between geotextile layers (Fig. 1)
γ=moist unit weight
c_u=undrained shear strength

Note: Average moisture content-25.1%; average degree of saturation=96%

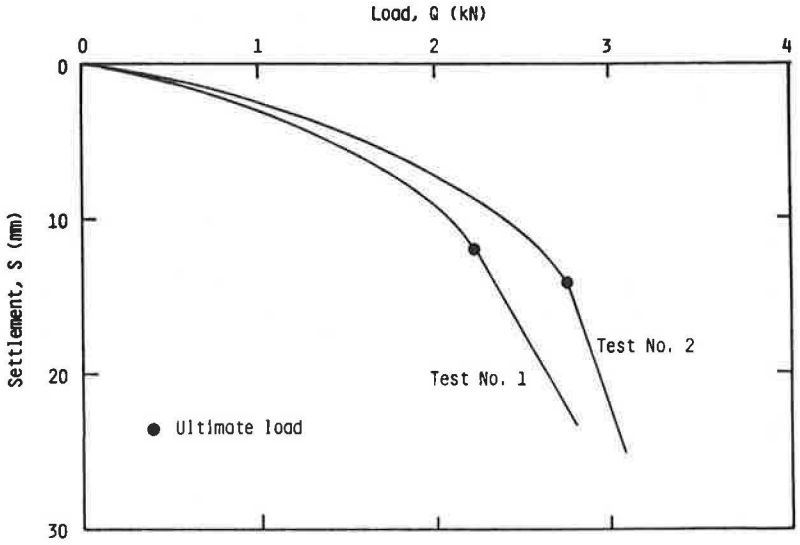

FIGURE 3 Average load-displacement diagram for Tests No. 1 and 2.

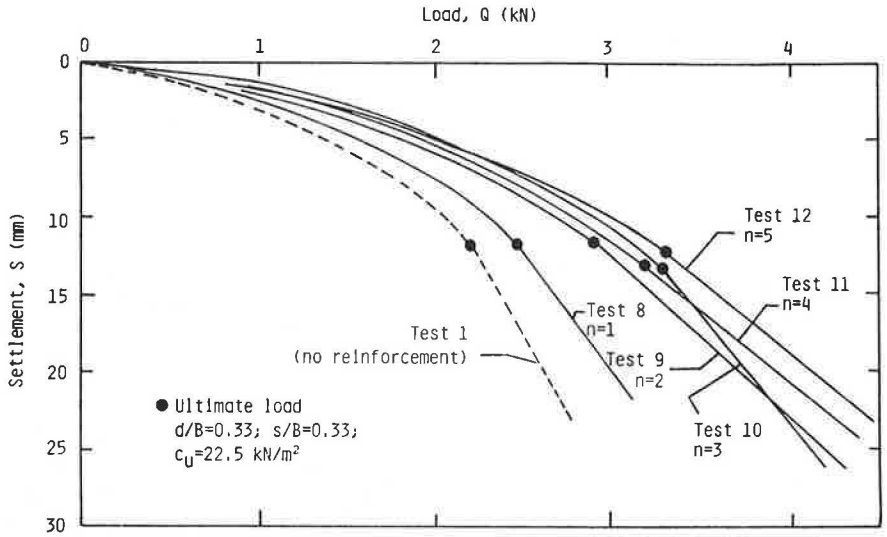

FIGURE 4 Typical load-displacement diagrams for foundation on clay internally reinforced with geotextile.

general observations can be made from the data shown in Figures 5 and 6:

1. For a given number of geotextile reinforcement layers, the maximum value of $BCR_{(max)}$ is obtained when d/B is about 0.35 to 0.4.
2. For a given number n of geotextile reinforcement layers and a given s/B, the magnitude of $BCR_{(max)}$ decreases with increasing d/B. However, when $d/B = 1.0$, $BCR_{(max)}$ is also approximately equal to 1.0.
3. The preceding statement implies that geotextile reinforcements placed below a depth equal to B do not create an increase in the ultimate bearing capacity. Thus

$$D_{\text{eff}} \cong B = d + s(n_{cr} - 1) \tag{4}$$

where

D_{eff} = effective depth (i.e., the depth below the foundation beyond which the placement of geotextile reinforcement does not have any effect on bearing capacity) and

n_{cr} = critical number of layers of geotextiles beyond which any increase does not contribute to the bearing capacity increase.

So

$$n_{cr} = \frac{B - d}{s} + 1 \tag{5}$$

However, for most effective design, $d \cong 0.4B$.

$$n_{cr} = \frac{0.6B}{s} + 1 \tag{6}$$

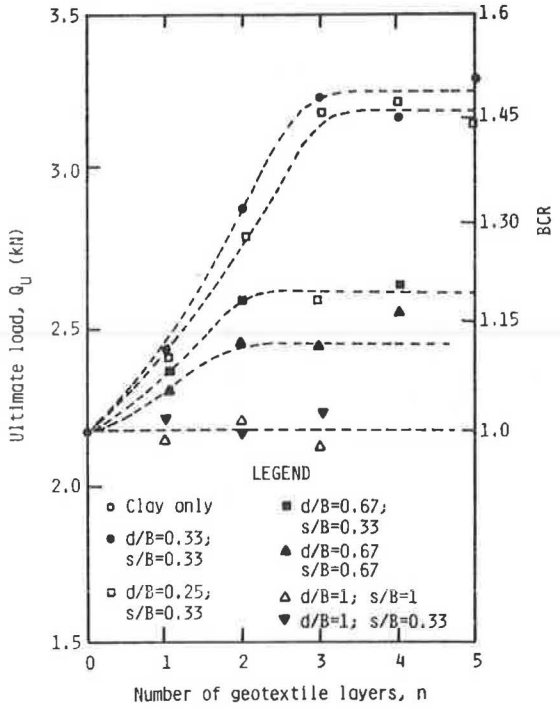

FIGURE 5 Variation of Q_u and *BCR* with *s/B*, *d/B*, and *n*.

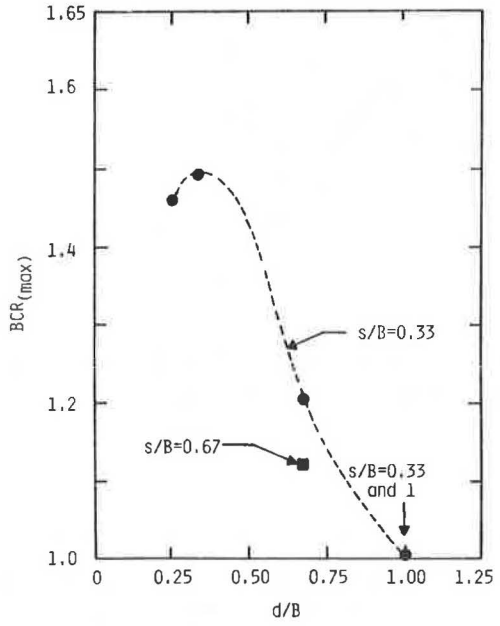

FIGURE 6 Variation of BCR_{max}.

Settlement at Ultimate Load

For all the tests conducted under this study, the settlements at ultimate load (with or without geotextile reinforcement) were in a range of 14 to 18 percent, with an average of 16 percent of the foundation width. The load versus displacement relationships shown in Figure 4 are typical for all tests conducted under this program. However, for all tests with geotextile reinforcements, the slope of the load-displacement diagrams (i.e., $\Delta S/\Delta Q$) was somewhat smaller than that observed for tests on unreinforced clay, or

$$\left(\frac{\Delta S}{\Delta Q}\right)_{\text{reinforced}} < \left(\frac{\Delta S}{\Delta Q}\right)_{\text{unreinforced}} \quad (7)$$

Length of Geotextile Reinforcement Layers

Tests 28–32 (Table 1) were conducted to determine the optimum length L of geotextile layers to be used as reinforcements to mobilize the maximum bearing capacity ratio. The tests were conducted with similar values of c_u, d/B, and s/B. A nondimensional relationship between *BCR* and L/B for these tests is shown in Figure 7. The magnitude of *BCR* increases with L/B and reaches a maximum value at about L/B between 3 and 4. For $L/B > 4$, the magnitude of *BCR* remains practically constant.

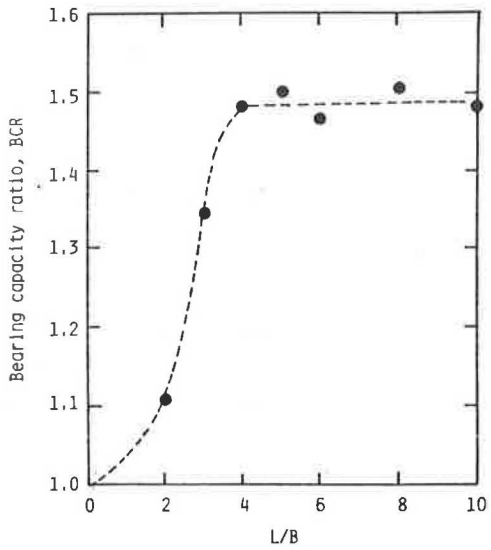

FIGURE 7 Variation of *BCR* with *L/B* (Tests No. 11, 27–32; $n = 4$, $s/B = 0.33$, and $d/B = 0.33$).

CONCLUSIONS

The results of a number of laboratory model tests for evaluation of the ultimate bearing capacity of a strip surface foundation resting on a nearly saturated clay layer reinforced with several layers of geotextiles have been presented. On the basis of the present study, the following conclusions can be drawn:

1. Inclusion of geotextile layers in saturated or nearly saturated clays increases the ultimate bearing capacity of foundations under undrained conditions.
2. The most beneficial effect of geotextile reinforcement on the bearing capacity is realized when the first layer is placed at a depth (d/B) of about 0.35 to 0.4 below the bottom of the foundation.
3. Reinforcements placed below a depth B measured from the bottom of the foundation do not have any influence on the ultimate bearing capacity of a foundation.

4. The most effective number of geotextile reinforcement layers (for $d < B$) can be obtained from Equation 6.

5. Geotextile reinforcements do not have much influence on the foundation settlement at ultimate load. For the present tests, the ultimate load occurred at a settlement of about $0.16B$ to $0.18B$, which is large.

6. The most effective length of geotextile layer obtained from these tests is about $4B$. However, this may change depending on the type of geotextile used. More research needs to be done in this area.

7. The results presented in this paper are based entirely on laboratory model tests. The applicability of the findings in this study to the field conditions needs to be confirmed by large-scale tests. Hence, caution must be exercised in using the present results for field design.

REFERENCES

1. A. S. Vesic. Analysis of Ultimate Loads on Shallow Foundation. *Journal of the Soil Mechanics and Foundations Division*, ASCE, Vol. 99, No. SM1, 1973, pp. 45–73.
2. L. Prandtl. Über die Eindringungstestigkeit (Harte) Plastischer Baustoffe und die Festigkeit von Schneiden. *Zeitschrift für Angewandte Mathematik und Mechanik*, Vol. 1, No. 1, 1921, pp. 15–20.
3. K. Terzaghi. *Theoretical Soil Mechanics*. John Wiley and Sons, New York, 1943.
4. J. Binquet and K. L. Lee. Bearing Capacity Tests on Reinforced Earth Mass. *Journal of the Geotechnical Engineering Division*, ASCE, Vol. 101, No. GT12, 1975, pp. 1241–1255.

Publication of this paper sponsored by Committee on Engineering Fabrics.